Uppsala Dissertations from
the Faculty of Science and Technology
55

PETER S. HAMMERSTEIN

Stochastic Resonance and Noise-Assisted Signal Transfer

On Coupling-Effects of Stochastic Resonators and Spectral Optimization of Fluctuations in Random Network Switches

ACTA UNIVERSITATIS UPSALIENSIS
UPPSALA 2004

ACTA UNIVERSITATIS UPSALIENSIS
Uppsala Dissertations from
the Faculty of Science and Technology
55

PETER S. HAMMERSTEIN

Stochastic Resonance and Noise-Assisted Signal Transfer

On Coupling-Effects of Stochastic Resonators and Spectral Optimization of Fluctuations in Random Network Switches

UPPSALA
UNIVERSITET

Dissertation for the Degree of Doctor of Philosophy presented at Uppsala University in 2004

Abstract

Hammerstein P. 2004: Stochastic Resonance and Noise-Assisted Signal Transfer. On Coupling-Effects of Stochastic Resonators and Spectral Optimization of Fluctuations in Random Network Switches. Acta Universitatis Upsaliensis. *Uppsala Dissertations from the Faculty of Science and Technology* 55. 117 pp. Uppsala. ISBN 91-554-5968-4.

Recent research shows that noise or random fluctuations must not always be destructive in Nature by degrading system performance. On the contrary, in nonlinear systems they can synchronize systems or enhance the quality of signal transmission. The latter possibility is reported in this thesis.

The phenomenon of *stochastic resonance* (SR) is presented and illustrated by an example of a ferromagnetically coupled spin chain, described by the Glauber's stochastic Ising spin model. It is demonstrated that an optimal strength of the next-neighbor interaction is able to improve the SR-effect. A similar mechanism has further been studied, both numerically and analytically, on the stochastic nonlinear dynamics of a ferromagnetic stripe domain in an inhomogeneous thin film. SR and its dependence on the domain stiffness, which is due to the exchange interaction, are presented. Experimental parameters for potential verification on Bi-doped epitaxial garnet-ferrite films are proposed.

Further-on, a nonlinear model of a junction in neuronal and road structures is studied using various types of noise (stochastic processes) to generate the incoming traffic. It is shown that random fluctuations are able to enhance signal transmission, whereby the zero crossings of colored ($1/f^k$) Gaussian noise is superior to Poissonian noise and, in certain cases, to deterministic, periodic traffic too. Optimal traffic for $k \approx 1$ has been found. In case of Gaussian $1/f^k$ noise modulated periodic input, noise-assisted traffic can be observed as well and demonstrate how random fluctuations can enhance the signal traffic efficiency in a network. The effect of an optimal k has finally been applied to a data package network switch, whereby a stochastic data scheduling algorithm is proposed and investigated numerically and analytically.

Peter Hammerstein, Department of Engineering Sciences, The Ångström Laboratory, Uppsala University, Box 534, SE-751 21, Uppsala, Sweden.

ISSN 1104-2516 ISBN 91-554-5968-4
Printed in Sweden by Elanders Gotab, Stockholm 2004
Distributor: Uppsala University Library, Box 510, SE-751 20 Uppsala, Sweden.
www.uu.se, acta@ub.uu.se

God not only play dice, but
sometimes throws them,
where they cannot be seen.
(Stephen Hawking)

List of Publications

Licentiate Thesis:

The Benefits of Noise: Stochastic Resonance and Noise Assisted Signal Transfer
Peter S. Hammerstein
Licentiate Thesis, Uppsala University (2002).

Journal papers:

I. **Stochastic Resonance in Ferromagnetic Domain Motion**
P.S. Ruszczynski[1], L. Schimansky-Geier, and I. Dikshtein,
Eur. Phys. J. B **14**, 569 (2000).

II. **Noise Enhanced Efficiency of Ordered Traffic**
P.S. Ruszczynski[1] and L.B. Kish,
Phys. Lett. A **267**, 187 (2000).

III. **Noise-Assisted Traffic of Spikes through Neuronal Junctions**
P.S. Ruszczynski[1], L.B. Kish, and S. Bezrukov,
Chaos **11**, 581 (2001).

IV. **Spectral Optimization of Computer Network Traffic in a Stochastic Data Packet Scheduling Algorithm Triggered by $1/f^k$ Noise**
P. Hammerstein and A. Ramanujam,
submitted , (2003).

[1]now: Hammerstein

Articles in conference proceedings:

V. Symbolic Representation of Neuronal State Space Dynamics
K. Stiefel , P. St. Ruszczynski[2] and R. Lakatos,
in *Student Papers of the Complex Systems Summer School 2001*, (Santa Fe Institute, U.S.A., 2001).

VI. Fluctuations of Cars and Neural Spikes at Junctions
P.S. Ruszczynski[2], L.B. Kish, and S. Bezrukov,
in *Proceedings of the 16th International Conference on Noise in Physical Systems and 1/f Fluctuations ICNF 2001*, Gainesville, Florida, U.S.A., edited by G. Bosman, (World Scientific, Singapore, 2001).

[2]now: Hammerstein

Contents

Chapter 1

INTRODUCTION

Most of the processes occurring in Nature share two properties: they are *nonlinear* and they are affected by *stochastic noise*. Scientists usually seek to neglect those facts because the theoretical modeling and description can get rather complicated. A linear, deterministic theory is preferred instead and often sufficient. But a lot of features and phenomena can not be captured by that.

Due to the enormous increase of computational power and the development of new physical fields, the treatment of stochastic, nonlinear systems became easier to handle and, hence, very popular. Special attention has been paid to effects where the stochastic noise, or fluctuations, do *not* degrade the performance of a system as it is often the case, but instead provides a useful and necessary tool to perform signal detection, enhance signal transmission, synchronize systems, form patterns and structures, etc. This can be the case if the system has nonlinear characteristics.

Nonlinearity means that the underlying dynamic (differential) equations are nonlinear in the independent variable, i.e., their typical solutions can not be expressed as a linear combination of elementary solutions. The branch of physics studying those systems is called *Complex Systems*, *Nonlinear Dynamics* or *Dynamical Systems*. The next section provides a brief overview over this branch.

Stochasticity means that random fluctuations can occur biasing the system in a probabilistic manner. Noise affects all kind of natural systems, often deteriorating the predictability of the future system state. The study of noise in physical, chemical and biological systems has been performed in branches like *Non-equilibrium*

Statistical Physics (Mechanics) and *(Applied) Stochastic Processes*.

The present treatise considers stochastic effects in nonlinear systems as a model of noise in physical and other systems.

In the following, short introductions are given to both fields, Complex Systems Theory and Stochastic Processes. Since the presented work focuses mainly on details of stochastic processes, the reader may consider the next Sec. 1.1 as an interesting trip into a modern discipline of physics, describing the more profound framework the presented phenomena should be seen in context to.

1.1 Complex Systems Theory

The study of complex systems (which not necessarily have to be complicated) can mainly be divided in

1. the analysis of problems continuous in time and/or space, i.e.,
   - nonlinear (partial) differential equations and
2. the analysis of problems discrete in time and/or space, e.g.,
   - discrete mappings, (complex[1]) number iterations
   - cellular automata.

Complex hereby does not necessarily mean that the systems have a very high number of degrees of freedom. Complex is rather meant as a distinction from simple systems which can sufficiently be described by linear mathematics. An overview on literature (journals, conference proceedings, textbooks and important papers) on this topic can be found in a Resource Letter at [1].

1.1.1 Continuous cases

The study of nonlinear differential equations arouse more than a century ago with problems of oscillations in classical mechanics and electric circuits (Duffing oscillator [2], van der Pol's equation [3]).

[1]Here, complex is meant in the mathematical sense as a linear combination of real and imaginary numbers, in contrast to *"complex"* in the physical terminology of complex systems.

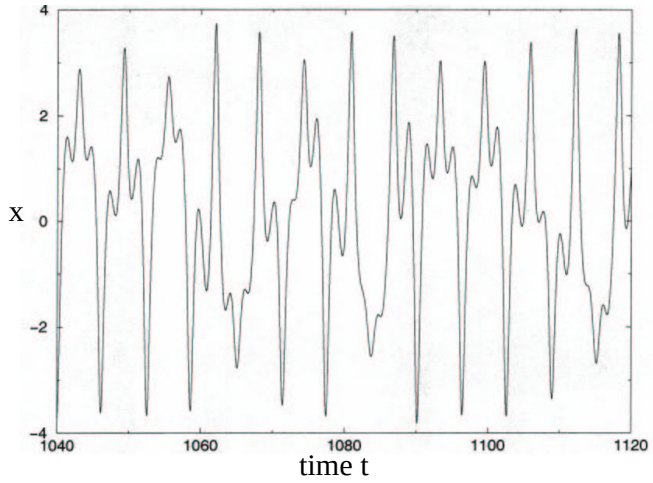

Figure 1.1: Chaotic oscillation: Simulation of the location X as a function of time of the nonlinear Duffing oscillator.

Driven and damped oscillation equations in various nonlinear potentials exhibited qualitatively new kinds of solutions, such as a dependence between amplitude and frequency of the oscillations. The analysis of the evolution of the trajectories in the state (phase) space discovered a topology which is more complex and exhibits new qualitatively distinct features than in simpler linear problems. An example for chaotic oscillation is given in Fig. 1.1.

Since a differential equation of n-th order can always be expressed as a system of n coupled differential equations of 1st order, n is called the dimension of the state space.

Coupled ordinary linear differential equations already exhibit a number of interesting behavior of the movement of the trajectories, such as stable and unstable fix-points (nodes) and stable and unstable foci, where the trajectory will be attracted (spiral in towards the fixpoint) or repelled (spiral away from the fixpoint).

Others, so called saddles (hyperbolic points) attract/repel trajectories depending on their initial condition. In that case there is always one trajectory separating those regions and therefore called the separatrix. There may exist other singular points too, so called centers (elliptic points), where the trajectories follow closed ellipses around them. Those points are neither attractive nor repulsive. Which of the above mentioned behaviors eventuate depends on the

dimensions and parameters of the system determining the signs and values of the (complex) eigenvalues.

Since the stability analysis of nonlinear solutions can (often) be carried out by a linearization around the singular points, results for the linear problems can be of use for the general nonlinear case as well.

However, in the case of nonlinearities one can observe phase transitions of the first and second kind in only one dimensional problems, e.g., by studying a single nonlinear differential equation of first order. An example is the kinetic description of an autocatalytic reaction. In two dimensions *bifurcations* can occur. Bifurcations are qualitative changes of the topology of the state space, caused by parameter variation (see Fig. 1.3). For example, a stable focus can become unstable (Hopf-bifurcation).

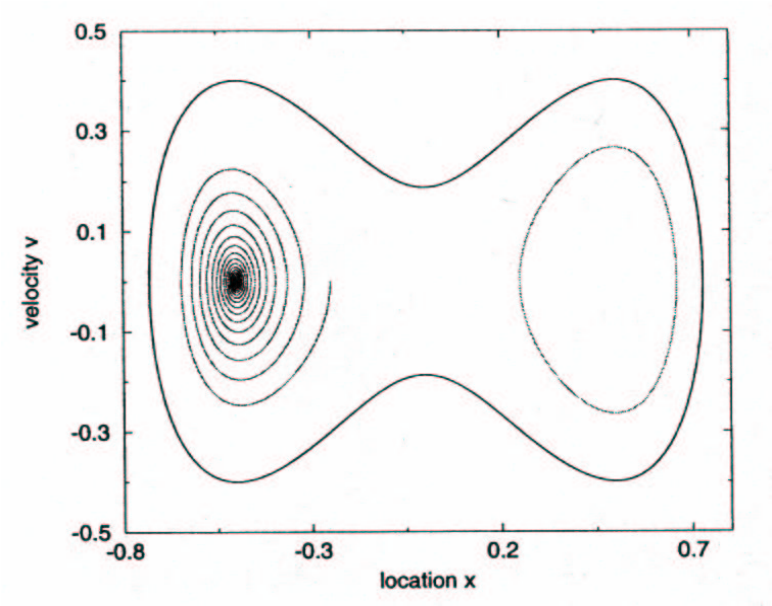

Figure 1.2: Different kinds of solutions in phase space of the nonlinear Duffing oscillator as a result of different initial conditions and parameters. The inner closed curve on the right hand side is the analogy to the undamped harmonic oscillator, whereas the spiral on the left hand side corresponds to the damped case. The enveloping curve is a characteristic example of a nonlinear oscillation.

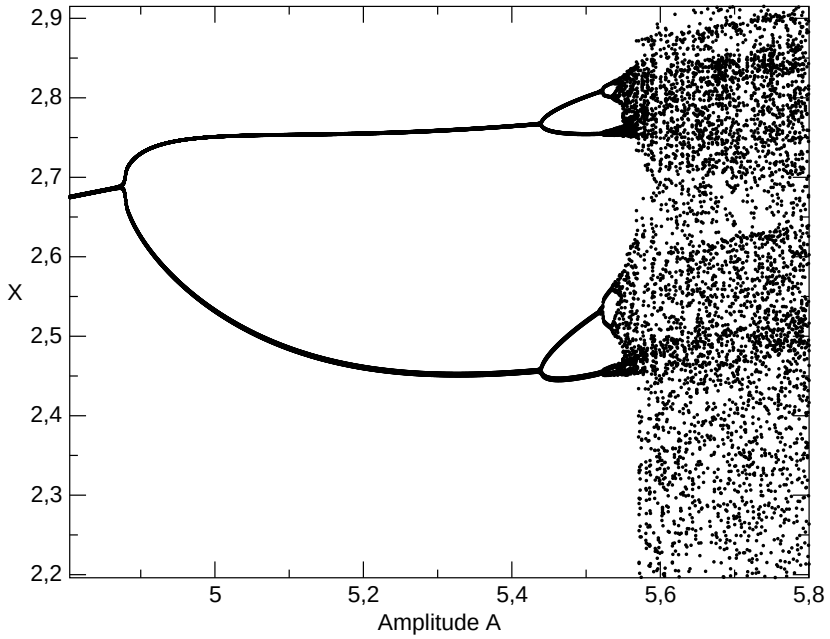

Figure 1.3: Bifurcation diagram of the nonlinear Duffing's oscillator. As a control parameter A is varied, the topology of the state space is changed, leading to qualitatively different types of solutions. The example shows the well studied period-doubling route to chaotic behavior which occurs at a parameter value of about A = 5.57.

Considering three dimensions, quasiperiodic solutions called tori can determine the ultimate destiny of the trajectories and a phenomena known as *chaos* can occur.

In general, chaos is possible in autonomous differential equations if at least three coupled equations are present containing at least one nonlinearity. In case of non-autonomous system already two (!) coupled equations are sufficient to observe chaotic behavior. This emphasizes the importance of the systematic study of complex systems and their specific solutions.

There are several definitions of chaos all having one feature in common: the sensitivity of the systems development to a slight change in the initial conditions, which can be measured by the Ljapunov exponent.

However, chaos does not mean disorder in a stochastic sense. The movement of the trajectory is absolute deterministic, although

the plot of two trajectories starting nearby will reveal an exponential growth of their distance (at least for a while), demonstrating the sensitivity to the initial conditions (see Fig. 1.4). But, in many cases the trajectory will never leave a bounded region and end up in a so called strange attractor (Figs. 1.4 and 1.5).

Although the path of a trajectory might be difficult to predict, the shape of the strange attractor will always be the same, e.g., showing the same *fractal* (self similar) properties as shown in Figs. 1.5 - 1.7.

In parameter space different routes to chaos have been found. One of the most interesting one is the so called period doubling which is displayed in Fig. 1.3. At certain parameter values the system oscillates with a fixed period while changing the parameter suddenly leads to a doubling of this period. This can happen

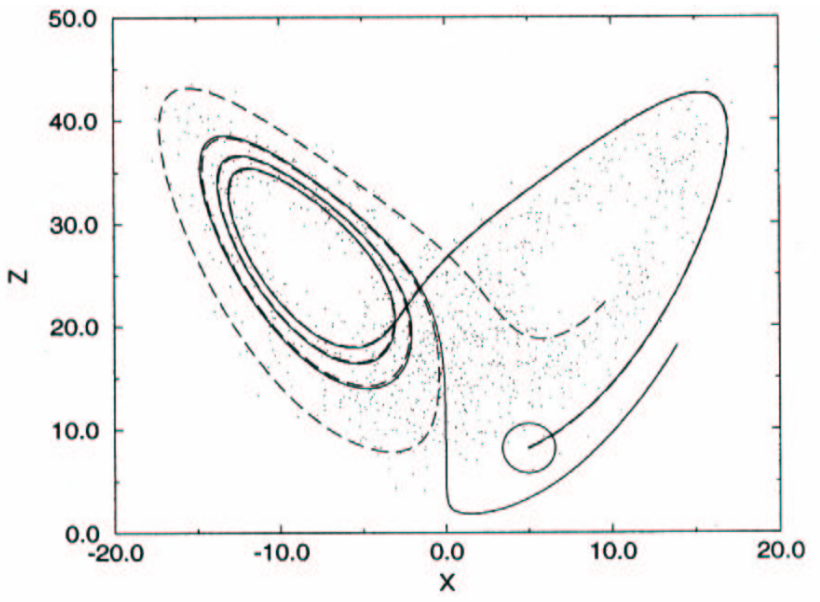

Figure 1.4: The sensitivity of the path of a trajectory in state space to its initial condition is what is called *chaos* in physics. Two trajectories starting very close to each other (her indistinguishable in the small circle), will separate exponentially from each other and finally end up in different regions of the state space. The example, provided here, is taken from the so called strange attractor of the meteorological Lorenz model and suggests the shape of a butterfly. See also Fig. 1.5.

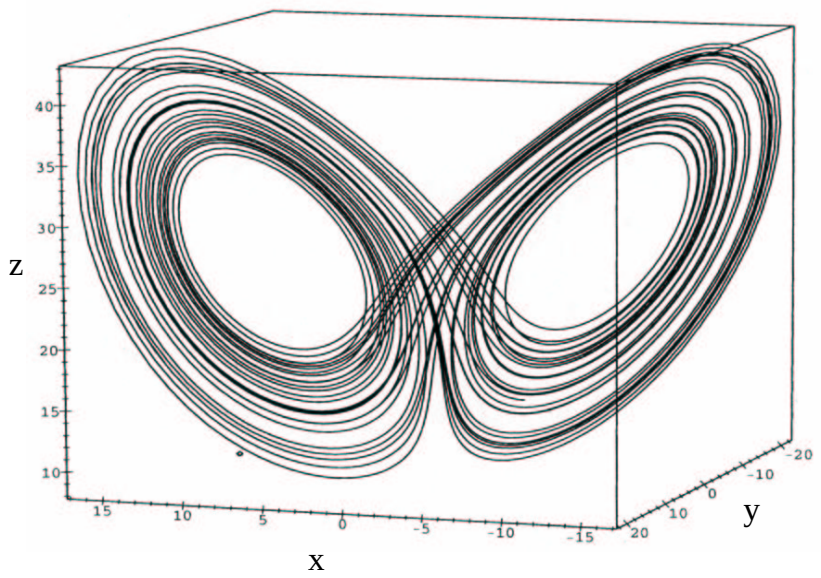

Figure 1.5: The Lorenz attractor as an example of a so called strange attractor. See also Fig. 1.4

when a limit cycle becomes unstable while at the same time two stable limit cycles arise (bifurcation). A further changing of the bifurcation parameter doubles the period again, and so on, until the system ends up in a chaotic region. The ratio of two consecutive parameter values where the period doubles has been found to be a universal scaling constant [4], [5]. If the above mentioned instability continuous as a branch in the parameter space and hits a chaotic region, one dramatically calls this an explosion of chaos or a *crisis*.

Examples of the mentioned (and to be mentioned) mechanisms and phenomena can be found in every field of every scientist.

The study of population dynamics in ecology, i.e., the coupled processes of growth and decay of different species concentrations, has played a key role in the development of the field of complex systems. The spread of epidemics, evolutionary processes, solar systems dynamics or model deduction based on the analysis of time series (such as financial data or electrocardiogram sequences) are further examples.

One important consequence of nonlinearity in coupled differential equations is a principle studied by Hermann Haken in laser

physics; it has been called *slaving principle*. It requires a set of equations (variables) which evolve within different characteristic time scales in a way that the fast varying functions can be eliminated adiabatically. The result is that the time course of one variable (master mode) determines the evolution of the others (slave modes). Thus one can say that the system is "organizing" itself into a certain mode which for this reason is called *self-organization* or *synergetics* [6], [7].

But nonlinear effects are of course not restricted to temporal phenomena only. Considering the well studied reaction-diffusion equation one can observe spatial pattern formations. All what is needed for this observation is a diffusion besides nonlinear terms. A hydrodynamical example is the coupling between convective motion and thermal conduction in a liquid heated from below. At a certain value of a system parameter a hexagonal structure will appear on the surface, indicating a regular cellular structure of the

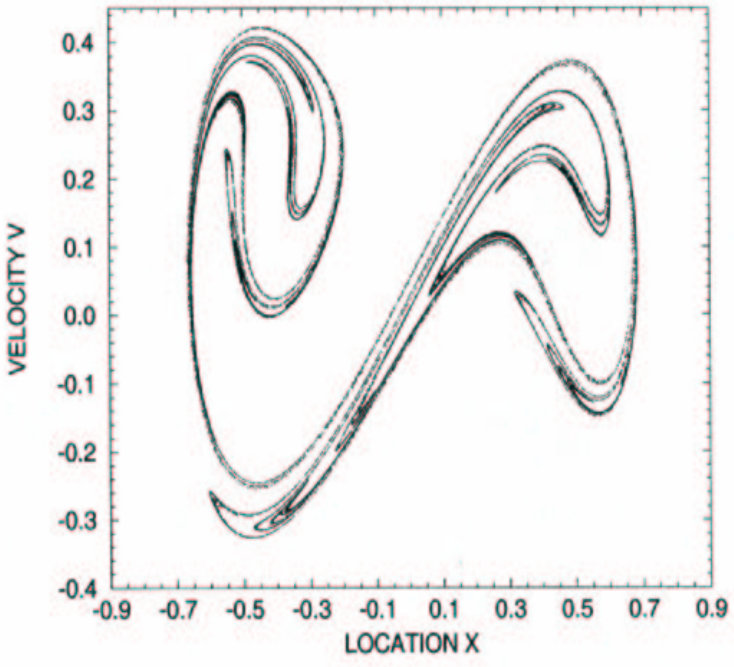

Figure 1.6: A typical example of the properties of a strange attractor. Here, the fractal Poincaré section of the strange attractor of the Duffing oscillator.

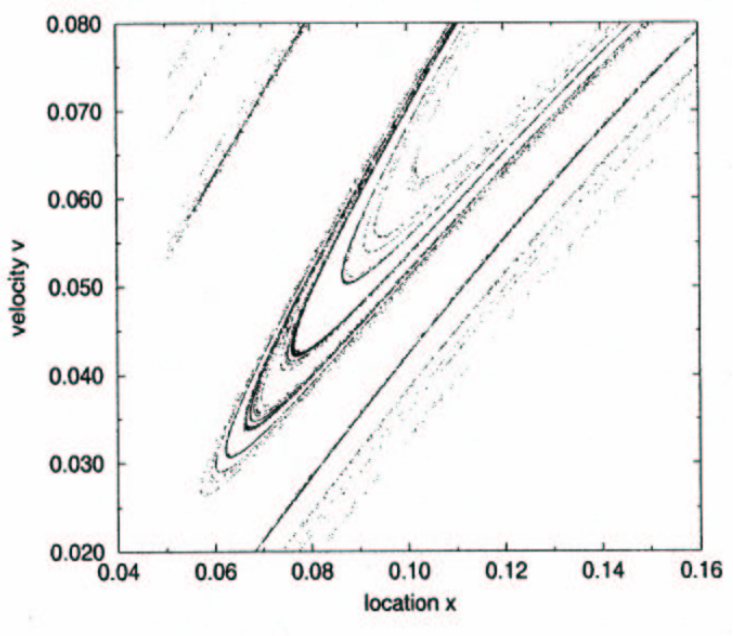

Figure 1.7: Enlargement of the Poincaré section of the strange attractor from Fig. 1.6 shows fractal properties.

heat transportation within the liquid (Rayleigh-Bénard instability [8], Lorenz model [9], Fig. 1.5).

Other examples can be found in plasma physics or chemical reactions such as the Zhabotinsky-Belusov reaction. Here, concentrations in a two dimensional layer vary with space and time, forming wave patterns for example as spirals [10]. Nonlinear waves are very interesting solutions of nonlinear partial differential equations. They do, for example, not show interference, i.e., the superposition principle is not valid here. Nonlinear waves called *solitons* are stable to perturbations and can interact like particles, i.e., with conservation of momenta and energy. Therefore a soliton can travel infinitely long without losing the particular shape.

One of the most simple nonlinear dynamics is given by the free motion of a particle in a bistable double-well potential, providing two stable solutions separated by an unstable one. Depending on the initial condition the particle will come to rest at either of the minima. Contrary, when the particle is forced by deterministic and stochastic forces, unexpected phenomena like dynamic stochastic

resonance can occur, as it is introduced in this thesis in Chapt. 2.1 and 2.4.

1.1.2 Discrete cases

Often the complex behavior of a system can most easily be studied by discretization in space or time. Using the Newton-Raphson method, for example, solutions of nonlinear equations can be found. However, spatially and temporarily discrete problems also arise naturally such as the coupled behavior of single elements often studied as *cellular automata* or the discrete time analysis of iterative expressions such as the logistic equation describing populations of successive generations. The latter one has become famous since despite the simple mathematical formulation a very rich behavior could be found, verifying experimental data such as the periodic variations in the catch reports of the Hudson Bay Company from 1850 to 1930 [11]. Feigenbaum has studied the abstract formulation in great detail discovering periodic and chaotic behavior in the system depending on the parameters. While the parameter is changed, the qualitative behavior changes leading to the Feigenbaum scenario of bifurcations. The universal scaling law, mentioned above, has been observed for the constant ratio of consecutive bifurcation parameter values [4], [5]. Many other maps have been studied such as the Poincare map or the Henon map [12] showing fractal properties in the corresponding attractors.

The fact that already one dimensional problems can give rise to chaotic solutions in case of discrete nonlinear systems underlines the importance of the detailed study of this field.

Simple rules can supply a possibility to create patterns that seem rather complicated. Well known are the fractals of the Cantor-set, the Koch-curve and the Sierpinsky-gasket [13]. Cellular automata in different dimensions show similar behavior. A cellular automata can be understood as a set of elements on a grid whereby the time evolution of the elements depend on the state of the neighbors. Very simple update rules for the next time step can lead to surprisingly complex structures as shown in Fig. 1.8. Examples and applications for the studied models can be found in all kinds of networks.

As mentioned above, a discrete description can arise from the discrete nature of the studied objects. Examples modeled and stud-

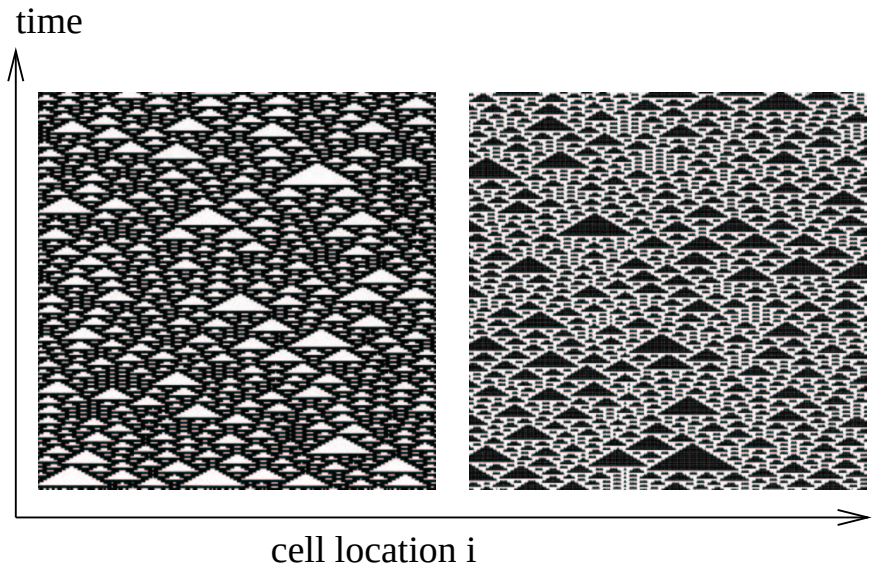

Figure 1.8: An example for a discrete complex system: Spatio-temporal structure formation in a one-dimensional cellular automaton. Very simple interaction rules between adjacent cells can lead to complex and fractal structures.

ied in Chapt. 3.1 of the present thesis are traffic systems of cars and neural spikes which are obviously discrete in their nature.

1.2 Stochastic Processes

1.2.1 Mathematics of stochastic processes

A stochastic process can be defined as a process $Y(X,t)$ depending on a random number X. This is the time dependent case of a more general definition of a random function. As in the previous sections the time dependence can be of discrete or continuous nature. The capital letters X and Y stand for random variables, i.e., an ensemble of their concrete realizations which shall be denoted by x and y. The probability that the realization y eventually will occur is described by a probability distribution function $P(y)$. Often the term probability density $p(y)$ is used. Then $\int_{y_1}^{y_2} p(y)dy$ gives the probability to find a value y within the interval (y_1, y_2) in the

continuous case.

A discrete process Y develops stepwise $(..., y_{n-1}, y_n, y_{n+1}, ...)$ and is described by the probability $P(y_n)$ that y_n appears at time t_n. The dependence of y_n on the previous values of Y is specified by the conditional probability $P(y_n|y_{n-1}, y_{n-2}, y_{n-3}, ..)$, which is the probability that y_n appears at time t_n supposed that the realization of Y at time t_{n-1} was y_{n-1}, at time t_{n-2} was y_{n-2} and so on. Defining the joint probability $P(y_n, y_{n-1})$ as the probability that y_n appears at time t_n and y_{n-1} at time t_{n-1} one can write down the basic expression

$$P(y_n, y_{n-1}) = P(y_n|y_{n-1})P(y_{n-1}) \quad , \tag{1.1}$$

known as Bayes' rule. In case that y_n does not depend on y_{n-1}, i.e., $P(y_n|y_{n-1}) = P(y_n)$, it follows that

$$P(y_n, y_{n-1}) = P(y_n)P(y_{n-1}) \quad , \tag{1.2}$$

which is the most fundamental law in probability theory and means statistical independence of the events y_n and y_{n-1}.

1.2.1.1 Processes without memory

If the state y_n of a process does not depend on the entire past, i.e., only on a finite number k of previous steps this process is called a *Markov process* and the conditional probability reduces according to

$$P(y_n|y_{n-1}, y_{n-2}, y_{n-3}, .., y_{n-\infty}) = P(y_n|y_{n-1}, y_{n-2}, y_{n-3}, .., y_{n-k}). \tag{1.3}$$

Note that this is a general definition and defines a Markov process of kth order. Most common in the literature is a definition which considers only the previous time step, i.e., $k = 1$. This leads to

$$P(y_n|y_{n-1}, y_{n-2}, y_{n-3}, .., y_{n-\infty}) = P(y_n|y_{n-1}) \quad . \tag{1.4}$$

This definition is indeed closer to Markov's original reflections from 1911 [14]. The process is entirely determined by the transition probability $P(y_n|y_{n-1})$ and can successively be constructed. Except for the knowledge of the last step this process has no memory. This is the Markov property and describes the class of stochastic processes which is the most important one in Nature:

Markov Process Examples

- *Radioactive Decay:* The stochastic number of nuclei changes according to the transition probability $P(n, M, t)$ where M and n are the number of pre-reaction nuclei at time 0 and time t respectively. This discrete process does obviously depend on the number of present nuclei only and not on the previous past.

- *Chemical Reactions:* The situation for simple chemical reactions involving the transition between two states is similar to the radio-active decay. Again the transition rate is proportional to the number of pre-reaction atoms or molecules, respectively.

- *Spin Relaxation Model:* Considering a two state system for a single spin, i.e., two possibilities (+ and -) for the directions of a spin one can write down the stationary transition probability and describe a system of spins as it relaxes to the equilibrium.

- *Random Walk:* This is a discrete model useful to describe Brownian motion. Here the direction at each step does not depend on the preceding steps. Brownian motion itself is the most important example of a Markov process in physics.

- *Poisson Process:* This is a point process with independent events on a real (time) axis. The possibilities of application in physics span over a wide range: the counts in a Geiger counter, the arrivals at the anode of a vacuum tube or the energies of cosmic ray particles [15]. Other examples are learning processes in neural networks [16] or stochastic resonance in neuron models [17]. The Poisson process is a special case of a generation-recombination process having a range of integers n which are occupied by the probability p_n. The time evolution of probability density functions is described by so called Master equations. In this case by

$$\dot{p_n} = \nu(p_{n-1} - p_n) \quad . \tag{1.5}$$

Thus the time dependent probability density for the Poisson process is given by

$$p_n(t) = \frac{(\nu t)^n}{n!} \exp(-\nu t) \quad . \tag{1.6}$$

It can be shown that ν is the mean value (rate) of the time gap between successive Poisson events as well as the variance.

As the reader will see later in this treatise, the Poisson process with varying mean rates ν will play a major role in the investigation of a stochastic traffic model.

To describe the time evolution of a stochastic process, two different, but mathematically equivalent, formalisms are common in use. The first is the Fokker-Planck equation [18], which is based on the more general Master equation. The second formalism is based on the Langevin equation. While the Fokker-Planck equation is a partial differential equation for the evolution of the probability density distribution, the Langevin equation is a differential equation for the random variables. Depending on the physical situation, the stochastic variables can enter the equation in additive or multiplicative terms. In this treatise we will see an example of either possibility.

As an example for a the Lagrange equation one can take a look at the equation of motion for a Brownian particle at position x

$$m\ddot{x} = -\alpha\dot{x} + \xi(t) \quad , \tag{1.7}$$

with mass m, friction constant α and the random force $\xi(t)$ having a mean value $< \xi(t) >= 0$.

The two mentioned formalisms are equivalent and suitable for linear problems but have to be handled carefully in nonlinear situations. A major problem is the integration of a stochastic (partial) differential equation since the added stochastic process $\xi(t)$ enters the equations as a random number sequence $y(t = n\epsilon), n \in \mathbb{N}$ of discrete nature [2]. While integrating over a small time interval $(t, t+\epsilon)$, the question arises which value of y should be chosen. There are two main approaches to the problem proposed by Itô ($y(t)$) and Stratonovic ($\frac{1}{2}(y(t) + y(t+\epsilon))$). For an analysis of these problems see [15].

[2]The discrete character is a consequence of the Kramers-Moyal expansion [15] of the corresponding Master equation.

1.2.2 Stochastic processes in physics

Our most fundamental approach to describe Nature, the Quantum-theory, is a probabilistic one containing unpredictability at its deepest level. The stochasticity of the radio-active decay, for example, is a direct consequence of the quantum-mechanical formalism. Although probabilities are the primary quantities which can be determined in Quantum mechanics, the macroscopic laws always appear after integration (averaging) in Hilbert space.

This can be seen in analogy to the ensemble average in systems with many degrees of freedom in classical mechanics, which creates the basis for Statistical Physics[3]. Here one is able to deal with high-dimensional systems with complicated inherent dependencies.

The most famous example is provided by the Brownian motion. The force exerted by a very large number of molecules, acting on a large particle is changing very fast and is practically impossible to calculate using Newton's equation of motion. On the other hand, it is possible to average over small time intervals and reveal the macroscopic properties of the system, such as the validity of the damping law for the average velocity.

This is in fact the basic procedure. Considering different time scales, one can average out the fast varying variables and obtain equations for the remaining slow ones which establishes known macroscopic laws, such as Ohm's law or heat conduction. The interesting feature of Nature is that those laws are described by smooth functions, although they are based on the irregular microscopic motion.

But it is clear that the macroscopic laws do not describe the whole truth since they neglect the intrinsic fluctuations which appear as *noise* in many physical and biological systems [15].

In linear systems which are in equilibrium the random forces act as fluctuations around a certain mean value, only. This has been studied in equilibrium statistical mechanics and is well understood. In contrast, the study of non-equilibrium statistical mechanics is

[3]The average of a high-dimensional system can be the average over an ensemble (many different realizations of the same physical system) or the time average of one of the realizations in case that they are the same. If so, one calls the system ergodic. Ergodicity is the main assumption for equilibrium statistical mechanics.

relatively underdeveloped. A way to describe those systems is possible through the investigation of nonlinear stochastic dynamics, which the central theme of this thesis. Identifying and understanding nonlinear stochastic mechanisms and phenomena is a fruitful challenge and promising source of knowledge for all kind of scientific fields, especially solid state physics.

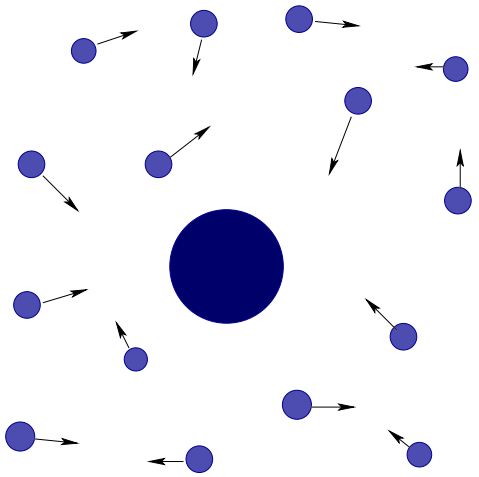

Figure 1.9: Brownian motion in two dimensions: fast varying, irregular, deterministic, microscopic forces acting "as random" on a mesoscopic particle.

1.2.3 The power spectral density of noise

As introduced in subsection 1.2, stochastic processes are often characterized by their probability distribution functions $P(y)$. However, the distribution of energy to the different frequencies $\omega = 2\pi f$ plays a very important role in many physical processes and is described by the power spectral density (PSD) $S(\omega)$. As with any time dependent deterministic function, the Fourier transform can formally be defined for a stochastic process too. Moreover it can be shown quite easily, that the PSD for a stationary process is defined by the Fourier transform $\mathfrak{F}()$ of the autocorrelation function

$$C_{y(t)\,y(t+\tau)}(\tau) \quad = \quad \lim_{T\to\infty} \frac{1}{2T} \int_{-T}^{T} y(t)\, y(t+\tau)\, \mathrm{d}t \quad . \qquad (1.8)$$

Using the relation between the PSD and the Fourier transform

$$S(\omega) = \lim_{T\to\infty} \frac{1}{2T} |\mathfrak{F}(C(\tau))|^2 \quad , \tag{1.9}$$

one can write

$$\begin{aligned} S(\omega) &= \mathfrak{F}(C(\tau)) \\ &= \frac{1}{2\pi} \int_{-\infty}^{\infty} C(\tau)\, \exp(i\omega t) \quad . \end{aligned} \tag{1.10}$$

This is the well-known Wiener-Khintchine Theorem [19], [20].

Returning to the example of Brownian motion one can note that the value of the force, acting on the Brownian particle is independent on the position and velocity. Moreover the value of the force itself is markovian, i.e., does not depend on earlier values. Thus the autocorrelation function is a delta function:

$$\begin{aligned} C_{\xi(t)\,\xi(t+\tau)}(\tau) &= \lim_{T\to\infty} \frac{1}{2T} \int_{-T}^{T} \xi(t)\, \xi(t+\tau)\, \mathrm{d}t \\ &= 2\alpha k T\, \delta(\tau) \quad . \end{aligned} \tag{1.11}$$

The proportionality factor enters for consistency reasons with Eq. (1.7) and the equipartition law

$$< m\frac{\dot{x}^2}{2} >= \frac{3}{2} kT \quad . \tag{1.12}$$

Applying the Wiener-Khintchine theorem (1.10), it is now easy to calculate the power spectral density of the force as

$$S_\xi(\omega) = \frac{\alpha k T}{\pi} \quad . \tag{1.13}$$

Note that $S_\xi(\omega)$ is a constant and does *not* depend on the frequency ω. This means that the energy of the process is uniformly distributed to all frequencies or colors (in analogy to light). Therefore this is called *white noise*. Contrary to this mathematical result, it is clear that there are physical arguments for a cut-off frequency of the uniform spectrum. Otherwise the process would contain an infinite amount of energy.

The result for the white noise is based on the fact that there is no memory in the process and the correlation function of the random

force is a delta function. However, this is not always the case. Considering processes with relaxation times κ, usually containing terms decaying as $\exp(-\kappa t)$, one can find a PSD depending on ω such as

$$S(\omega) \sim \frac{\kappa}{\kappa^2 + \omega^2} \quad . \tag{1.14}$$

This is called a Lorentzian spectrum and is one type of *colored noise* in analogy to white noise.

1.2.3.1 $1/f^k$ noise

One type of noise is of special interest, since it appears surprisingly often in a wide range of systems. This is a noise with a spectrum shaped as

$$S(\omega) = \frac{C}{\omega^k} \quad , \tag{1.15}$$

with C = constant and $\omega = 2\pi f$. In case of $k \approx 1$ it is referred to as *one-over-f-noise*, *flicker noise* or *pink noise*. Figure 1.10 shows several examples of simulated $1/f^k$ noises for different k. The velocity of Brownian motion, for example, corresponds to such noise with $k = 2$.

A general overview of 1/f noise is provided by [21], [22] and [23]. As mentioned above, examples can be found in a lot of physical and *non-physical* systems [4], as in solids [24]; electronic devices [25] - [27]; magnetic systems [28]; traffic flow [29], [172]; network traffic [30]; neuro systems [31], [176] - [178] and financial data [32].

Especially in solid state physics, many theories and models have been developed and proposed to explain the $1/f$-feature of residence fluctuations [33], [34]. Based on a heuristic theory, $1/f$ noise can be explained as the superposition of Lorentzians (Eq. (1.14)). Each Lorentzian is produced by a relaxation process with a certain waiting time distribution $p(\tau)$. In case of a thermally activated process with $\tau = \tau_0 \exp(E/kT)$ the distribution $p(\tau) \sim 1/\tau$ arises naturally and a noise spectrum close to $1/f$ is obtained. The problem consists now of justifying the distribution, which is often assumed to result from charge trapping. Random-walk models in systems containing traps with broad distributions of activation energies have

[4] A nice bibliography on $1/f^k$ noise can be found at http://linkage.rockefeller.edu/wli/1fnoise/

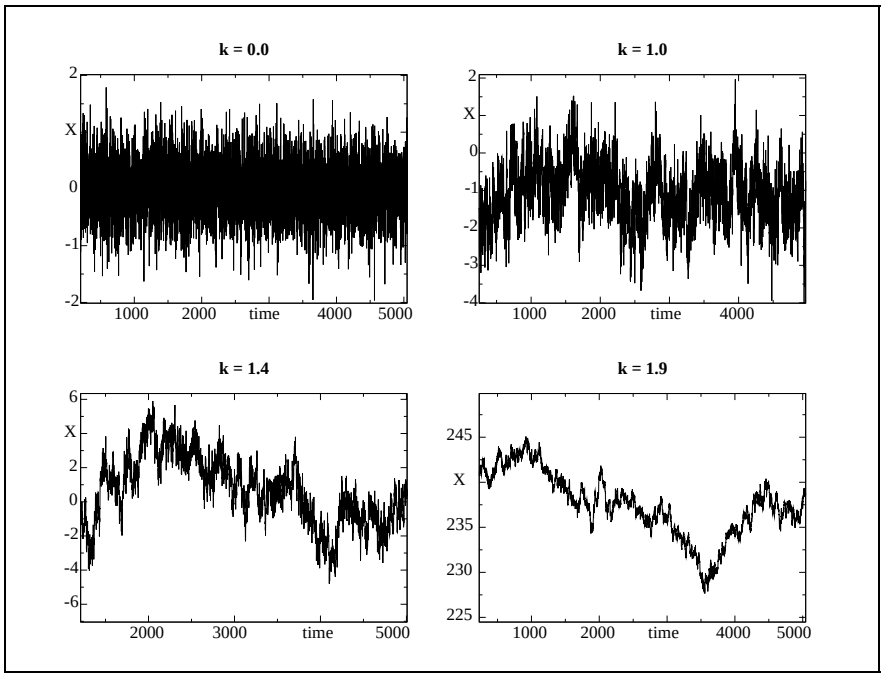

Figure 1.10: Simulated Gaussian noise sequences with different $1/f^k$-shaped spectra.

successfully being used for that investigation [34]. Similar mechanisms might be considered for the explanation of the $1/f$-behavior of other, e.g., non-physical systems.

Chapter 2

STOCHASTIC RESONANCE

Noise-induced order [35] and noise-assisted signal transfer in nonlinear systems are hot topics of today's physics of complex systems. Important examples are noise-induced patterns and front-propagations in excitable media, [36] - [43], noise-induced directed current in ratchet-potentials [44] - [48] and different stochastic resonance (SR) phenomena [48] - [123] (details later on). A proper tuning of the input noise intensity is needed to optimize the transfer of a signal through the stochastic resonator. Characteristic examples on SR have been published in the journals *Nature* [56] - [68] and *Science* [69] - [71]. These examples range from SR in single cells, behavioural SR in the feeding of paddle fishes, neural computing till climate systems and many others.

One of the main motivations is the identification of mechanisms allowing the use of random noise for *beneficial* reasons. This stands in opposition to the every-day experience of a researcher trying to avoid or at least to reduce the noise in the experiment and/or application. On the other hand, one may ask about mechanisms used by Nature exploiting the energy contained in the random motion. This has been done extensively during the last decades and answers where enabled by the enormous increase of computational speed and the development of the theoretical fields of Complex Systems and (Applied) Stochastic Processes.

One example is the Brownian motion in a "ratchet"-potential (see Fig. 2.1). One considers particles affected by (Gaussian) noise

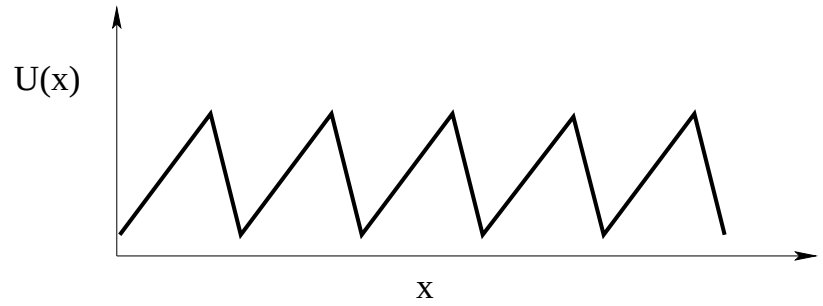

Figure 2.1: The "ratchet"-potential $U(x)$ gives rise to a directed current for particles affected by noise with zero mean value.

in an asymmetric, periodic potential $U(x)$. Although the noise has a zero mean value, the average velocity is non-zero due to the asymmetry, resulting in a directed current of the particles. Depending on the correlation time of the noise and the mass of the particles, current reversals and different mean values for the velocities can be found. This provides the possibility of a mass separation of the particles and therefore a constructive application of the noise [44] - [46]. Further, ratchets can induce a pattern formation process [47] and also show the phenomena of stochastic resonance [48]. While the number of SR-publications per year is increasing in the physical literature (see Fig. 2.2)[1], a continuous process of generalizations of the definition of SR is taking place. Historically two kinds of general SR systems have been considered, dynamical and non-dynamical ones. They will be presented in the following. Further-on in this chapter, modern generalizations and examples are presented demonstrating the wideness and importance of the phenomena of stochastic resonance in Nature.

In Chapt. 2.4 a model of a ferromagnetic domain forced by periodic and stochastic terms is presented, applying the theory of dynamical SR. This example from condensed matter has been published in [82]. In Chapt. 3.1 a discrete stochastic traffic model is studied.

[1]The search criteria at http://prola.aps.org/search has been the appearance of the exact phrase "stochastic resonance" in the full record of all 10 represented APS journals.

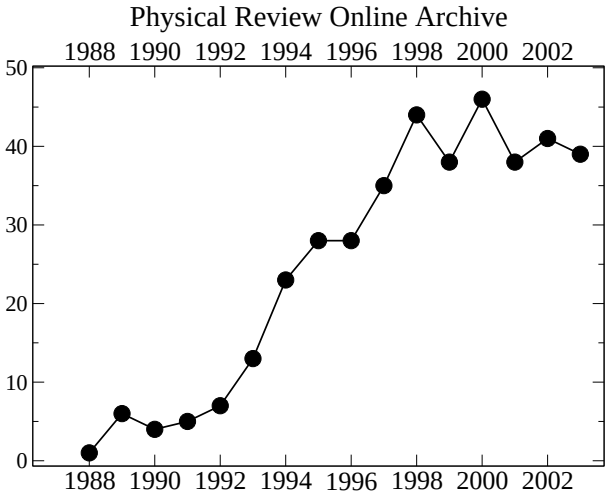

Figure 2.2: The number of publications of SR (vertical axis) per year (horizontal axis) shows an increased interest in the field. The data concern only publications in the Physical Review Online Archive (PROLA) of the American Physical Society (APS). For details see text.

2.1 Dynamical Stochastic Resonance

Historically, SR has first been studied in bistable systems governed by dynamical equations and has therefore been termed *dynamical stochastic resonance*. A generic example demonstrating this kind of SR is provided by the one-dimensional stochastic motion of a periodically forced particle in a double well potential (see Fig. 2.4 and Eq. (2.1)). This can be described by the dynamical Langevin equation

$$\dot{x} = ax - bx^3 + A_0 \cos(\omega_s t + \phi) + \sqrt{2D}\xi(t) \quad . \tag{2.1}$$

Here A_0 denotes the amplitude of the periodic force (signal) with frequency ω_s and phase ϕ. The last term in Eq. (2.1) describes additive, Gaussian white noise $\xi(t)$ with intensity D. Thus it has a zero mean value

$$\langle \xi(t) \rangle = 0 \tag{2.2}$$

and the δ-function as the autocorrelation function

$$\langle \xi(t)\xi(t+\tau) \rangle = \delta(\tau) \quad . \tag{2.3}$$

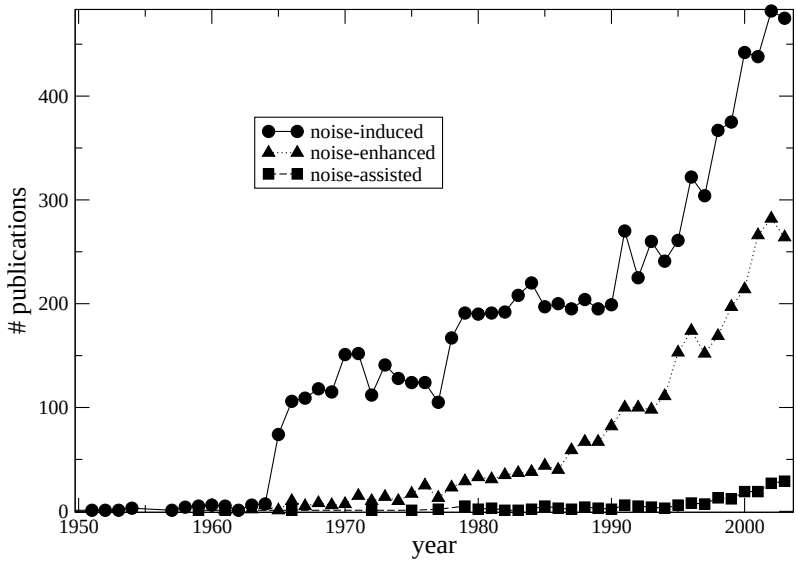

Figure 2.3: Number of publications with search terms given in the legend, gained by the program "scifinder" which exploits several archives like CAPLUS, MEDLINE, and others.

In absence of any forcing the particle would come to rest at one of the two minima $x_{min1,2} = \pm c$ depending on its initial condition (left or right from the bifurcation point). If, however, the particle is forced by a weak periodic signal ($A_0 \ll \Delta U_0$), it will oscillate around the corresponding minimum. Further, if noise is added it will be eventually able to leave the region of the minimum, cross the barrier ΔU and jump to the other side. Figure 2.4 shows the situation in the absence of noise. The periodic force acts as a periodic modulation of the effective potential.

The stochastic motion in absence of the periodic signal is described by the Kramers-rate

$$W_k = \frac{1}{2\pi}[|U''(0)|U''(c)]^{1/2} \exp\left(-\Delta U/D\right) \quad , \tag{2.4}$$

where U'' denotes the second derivative of the potential with respect to the coordinate x. Thus Eq. (2.4) determines a characteristic time $\tau_k = 1/W_k$ for the motion. That is the average time the particle will wait to make its transition (mean first passage time) due to stochastic noise. If that time is equal to half the period of the

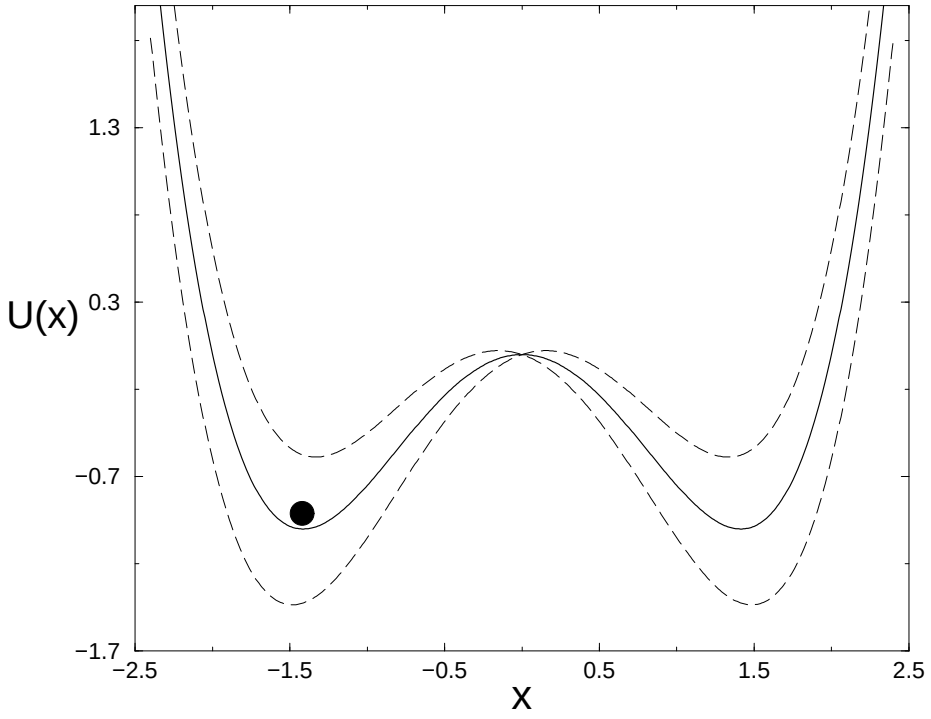

Figure 2.4: Particle in a periodically modulated double well potential $U(x)$: onset for the observation of dynamical stochastic resonance.

periodic signal

$$\tau_k = \pi/\omega_s \quad , \tag{2.5}$$

the stochastic and deterministic signal get synchronized. According to Eq. (2.4) this can be achieved by tuning the noise level D. Since two time scales match, the term "resonance" has been used. But note, τ_k is the rate of a stochastic process and not a frequency of a periodic force.

One can define the response (output) of the system to the input by considering the residence of the particle in either of the minima regions and define a signal-to-noise-ratio (SNR) in the out-

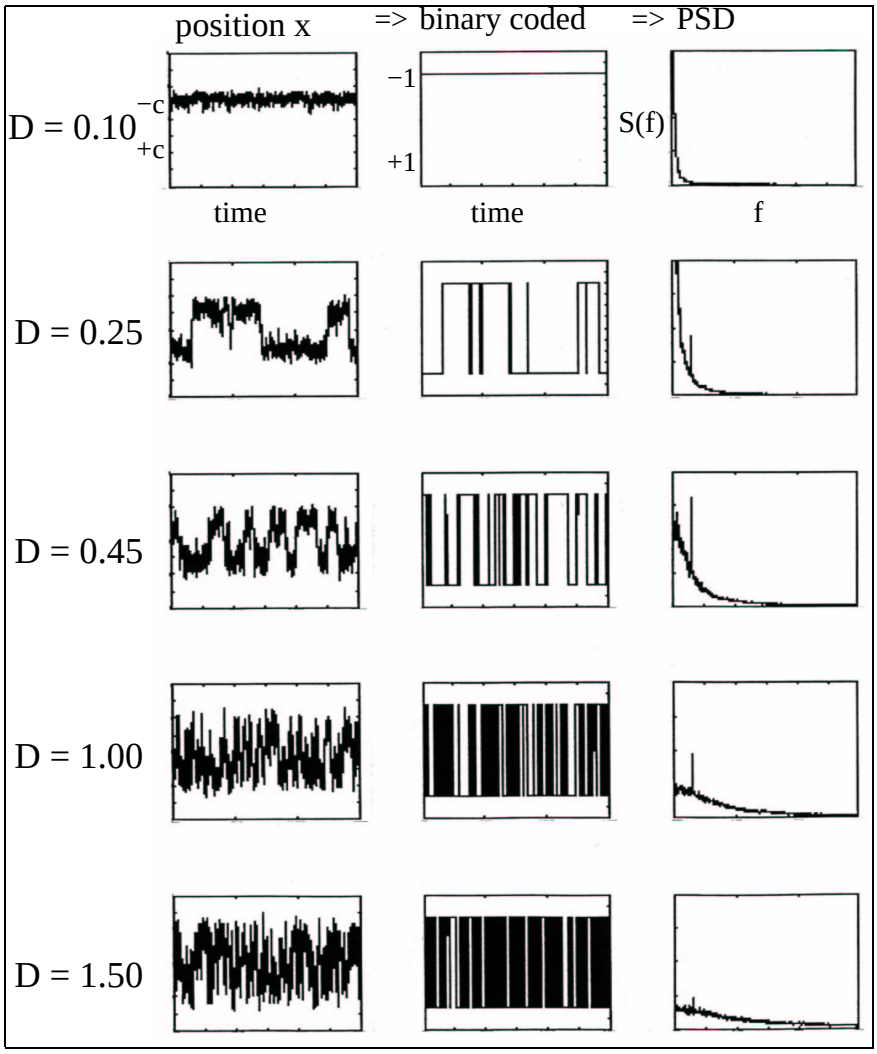

Figure 2.5: Analyzing the output of a stochastic resonator for different noise intensities D: The first coloumn shows the position of the particle in the double-well potential as a function of time. In the second coloumn this position has been "binarised", i.e., the output is either -c in case the particle is located on the negative x-axis or +c if the particle can be found on the positive x-axis. Finally, the third coloumn displays the power spectral density PSD of the binary output. One can clearly detect an inrcease of the signal-to-noise ratio until an optimal noise value is reached.

put's PSD. The SNR is based on the power spectral density of the output and is defined as the height of the peak at the driving frequency ω_s divided by the interpolated value of the background noise spectrum at this frequency. Alternatively in use is the signal-power-amplification (SPA) defined as the ratio of the height of the peak at the driving frequency to the square of the input signal amplitude. Tuning the noise intensity D to the level that fulfills the resonance condition (2.5) will maximize the SNR and SPA. This has been termed "stochastic resonance". Figure 2.5 illustrates the motion of the particle and shows the corresponding PSD. Here one can clearly see an increase of the peak at the driving frequency with increasing noise intensity D. That means the response to the deterministic periodic signal is increased if the noise level is higher. Further noise enhancement will destroy the synchronization which appears as a decreased SNR.

The described effect has mathematically been shown in [72]. This theory of (dynamical) stochastic resonance is based on the Master equation of the process

$$\frac{dn_\pm}{dt} = W_\mp(t)n_\mp - W_\pm(t)n_\pm \quad . \tag{2.6}$$

Here, $n_\pm$ denotes the probability to find the systems in either of the states $\pm$ (i.e., in one of the minima regions). $W_\pm(t)$ are the transition rates between the states and contain the characteristics of the dynamic, i.e., the periodic and stochastic terms. Solving (2.6) (after expansion of the transition rates) yields an expression for the conditional probabilities $n_+(t|x_0, t_0)$. From that any statistical information about the process can be computed, in particular the autocorrelation function. Applying the Wiener-Khintchine theorem (1.10) one can determine the power spectrum density $S(\Omega)$ (see Fig. 2.6) of the process and thus, write down the SNR as a function of the noise intensity D. This indeed shows the maximum behavior of stochastic resonance.

Note that the sketched theory is based on the Master equation and can therefore be applied for all systems with a defined transition rate between two states. The first publication of the theory of SR has been accompanied by applications to the continuous double well potential example (Eq. (2.1)) as well as to a discrete two state example [72].

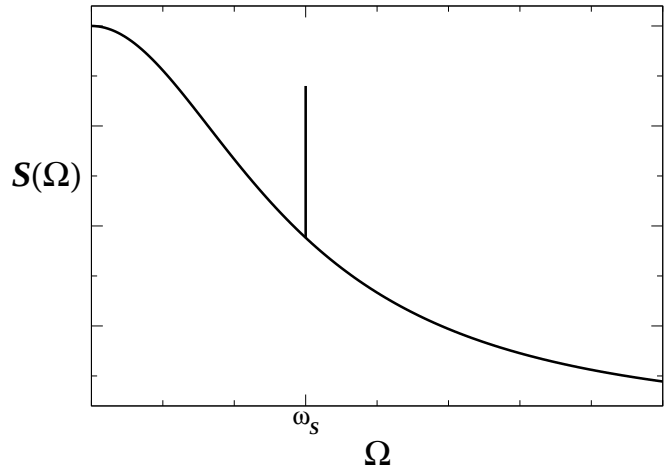

Figure 2.6: The theory of stochastic resonance provides an expression for the power spectrum density $S(\Omega)$ which contains a δ-function at the driving frequency ω_S.

One example for the use of the theory is given in Sec. 2.4 and has been published by the author in [82]. Here, a theory has been developed to describe the forced motion of a ferromagnetic domain in different double well potentials. The mathematical description turns out to be similar to Eq. (2.1) which allows the application of the presented theory of SR.

The beginning of the research on SR was the work of Benzi *et al.* in 1981 [73], [74]. They modeled the global climate as a two state system using a double well potential. The goal was to find a mechanism which was suitable for the explanation of the periodicity of ice ages of about 10^5 years. No periodicity had ever been found to be strong enough for inducing the observed climate changes. Their ground-breaking idea was that additional noise can explain the switch from a warm age to an ice age, and vice versa. According to the idea of Benzi *et al.* the periodic "signal" might be identified as the small periodic deviations of the earth's orbital eccentricity and the noise source could be found in short-term climate fluctuations caused by the varying radiation of the sun.

In 1983 an experiment was carried out demonstrating SR in an

electronic circuit, called Schmitt trigger [75]. This circuit is a proper example for a two state systems since the output can only take the two values V_+ and V_-. The preference for one of those values depends on the input signal which has to cross a threshold V_{T+} or V_{T-}, respectively. Using a subthreshold signal and the addition of white noise, the output peak in the power spectrum passes through a SR effect. The above theory [72] has been applied to this system and fits the results in [75]. Other experimental demonstrations have been given by the study of bistable ring lasers [76] and SQUIDs [54], [64]. Other examples can be found later on as well as an extensive review on SR from 1998 [77].

2.2 Non-Dynamical Stochastic Resonance

Contrary to the examples of the previous section, SR has been shown in a much simpler class of systems which is not governed by dynamic equations. They are often referred to as *threshold systems* and are extremely important for a lot of applications, especially in biological systems, such as neurons. In similarity to the dynamical cases in Sec. 2.4, the requirement for the observation of SR is a subthreshold signal superimposed by noise. Whenever the input (signal + noise) crosses the threshold U_T, the systems responds with a finite pulse (output) of duration τ. Therefore, in the literature, this system is eferred to as a *level-crossing detector* [50]. The situation is illustrated in Fig. 2.7. A periodic signal $A_0 \cos(\omega_s t + \phi)$ remains undetected until the Gaussian noise with intensity D assists the signal to cross the threshold. For vanishing D the detector would be silent for all times and a detection of the signal would be impossible. For non-zero values of D, the probability for a crossing event is larger if the (periodic) signal passes through higher values. Thus the detector output follows more or less the shape of the input signal, depending on the noise intensity. For very large values of the noise intensity $D \gg A_0$ the crossing probability becomes less and less dependent on the shape of the input signal and hence there is an optimal noise level for the detection of the signal. In case of a strict periodic input signal one can describe the detector response to the input signal by quantities based on the Fourier transform. Most common in use are the SNR and SPA, already introduced in

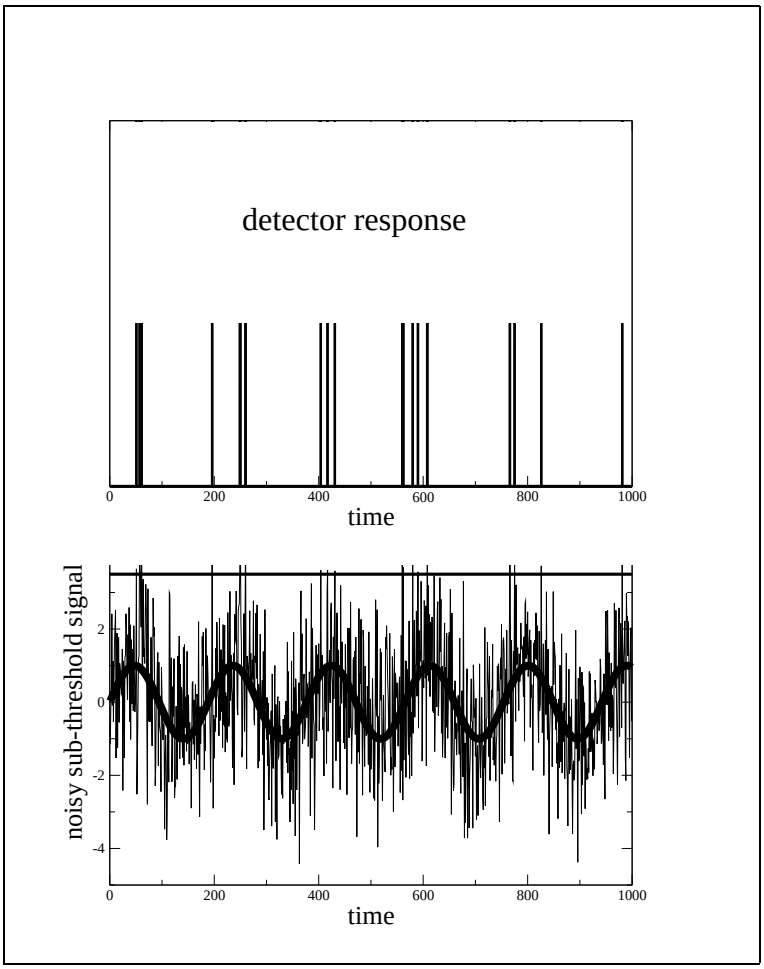

Figure 2.7: Onset of non-dynamical stochastic resonance. Whenever the (periodic) signal with additional noise crosses the threshold, the detector will respond with a finite pulse.

Sec. 2.1.

To calculate the SNR, the system of the noise-modulated periodic subthreshold signal has been viewed as a periodic modulation of the threshold U_T and therefore as a periodic modulation of the mean rate $\nu(t)$ of output pulses, which is a stochastic process $u(t)$ [50]. For white as well as colored noise it is possible to determine the SNR, exploiting Campbell's pulse-noise theorem for the calculation of the spectrum of the output response $u(t)$ for a given ν_0,

which is the mean rate of zero-crossings of the input noise. In order to determine $\nu_0(t)$, the Rice formula [173] has been used and the SNR has been calculated as [50]

$$\mathrm{SNR} = \frac{\nu_0 A_0^2 U_T^2}{D^4} \exp -\frac{1}{2}\left(\frac{U_T}{D}\right)^2 \quad . \tag{2.7}$$

This result shows a maximum of the SNR by variation of the input noise level and consequently the phenomena of SR in a non-dynamical system. Also in [50], this result has been verified for the cases of white noise (Eq. (1.13)), Lorentzian noise (Eq. (1.14)) and 1/f noise (Eq. (1.15)).

An important class of systems showing non-dynamical SR are excitable systems. Unlike dynamical SR only one stable state is needed and SR occurs though the excitation into an unstable state with a short residence time. This can be used to model the rest- and excited states of neurons [78] - [80]. In fact, a major part of the publications on SR in the physical literature describes the effect in real- and model neurons, providing a promising interdisciplinary subject. Further details and examples are found later on as well in the already mentioned extensive review from 1998 [77].

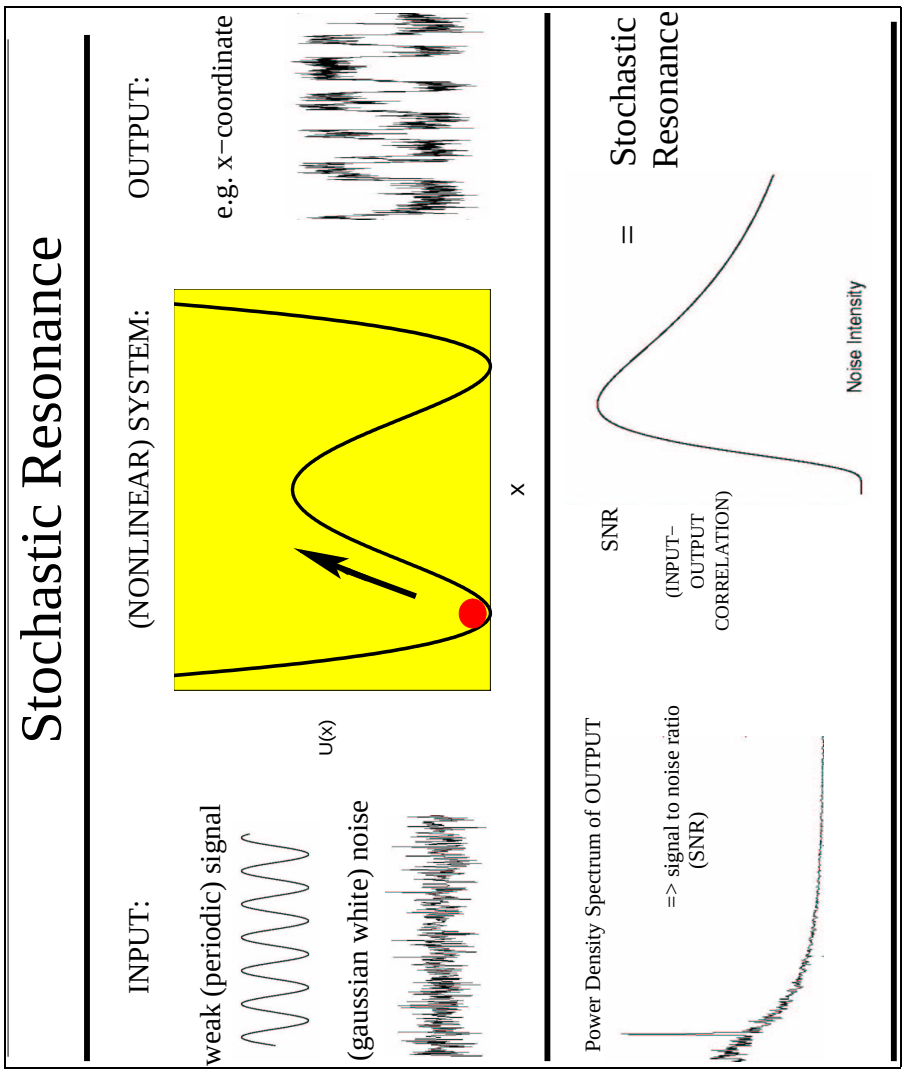

Figure 2.8: The summing-up of stochastic resonance: A two-state system is subjected to a subthreshold signal which itself is unable to change the system's state. Adding Gaussian noise, switches may occur between the states which allows the system to follow the input signal. If the noise intensity D becomes too strong, this input-output correlation will decrease again, which means that there is an optimal noise intensity D_{opt} for which the input-output correlation is maximized.

2.3 Generalizations and Examples

The requirements to find *conventional* SR have been mentioned above: a subthreshold sinusoidal signal and Gaussian white noise. Beyond that, many generalizations and extensions have been made to include a much larger number of systems under the notation of SR.

For instance, there are generalizations concerning the spectral properties of the noise applied to the systems. SR is not restricted to cases of Gaussian white noise and has been demonstrated with colored noise too. General properties of colored noise in dynamical systems and their application to SR problems have been studied in [50], [88] and [90]. The phenomena of SR with colored noise in neurons has been studied theoretically and experimentally for example in [91] and [181].

2.3.1 Quantifiers of stochastic resonance

It is, however, not necessary to restrict SR to sinusoidal signals. SR has been shown using aperiodic signals and termed *aperiodic stochastic resonance* [78], [83]. This is of special relevance, since signals found in Nature are mostly aperiodic. The response of systems to those signals can in most cases not longer be quantified by means of the power spectral density. Other measures, often based on entropies, have been used instead [35], [84], [85]. Those measures include the Shannon entropy and the transinformation (also mutual information). In [49] the information transfer rate has been proposed as the proper SR quantifier for neuron systems. In this example the information channel capacity of neurons has been calculated in the stochastic resonance region using Shannon's formula. It has been shown that the transfered information per unit time (in bits/s) is optimized at a higher noise value as it has been observed for classical measures, such as the SNR or the SPA. In [86] the signal itself has been replaced by colored noise. In certain cases, the power spectral density of this stochastic process has a peak at a certain frequency with a finite width. This is a kind of colored noise favoring one frequency. Therefore it is still possible to apply measures based on the PSD to quantify SR in this special case.

Other popular quantifiers include residence-time-distributions,

distributions of inter-spike intervals, (cross-) correlation measures and response functions [77]. In [87] a distance measure between an input pattern and the corresponding output pattern of an one-dimensional level-crossing detector has been minimized by tuning the noise intensity.

2.3.2 Related phenomena

There are many phenomena which have been covered by the term stochastic resonance or which are seen as SR-like phenomena. Important examples are presented in the following list. Details can be found in the given references.

- Supra-threshold SR [92], [93] (the signal is allowed to cross the threshold even without the noise)
- Multi-threshold SR [93] (Coupled stochastic resonators with individual thresholds.)
- SR without threshold [94] (In noisy nonlinear systems without local maxima (thresholds) signal enhancement can occur depending of the definition of the output.)
- Robust SR [95] (infinite noise variance)
- SR without tuning [57], [96]
- Doubly SR [97] (The noise itself creates a nonlinearity in the system which enable it to enhance the response to a signal.)
- Quantum SR [98], [99] (SR has been found in quantum systems too.)
- SNR improved by symbolic dynamics [100] (The definition of the output can be crucial for the enhancement.)
- Coherence resonance [101] (A case without signal where a dynamical system shows coherent behaviour as an effect of the noisy modulation.)

- System size resonance [102] (A case similar to array anhanced SR where, through the definition of a coupling strength density, the size of an array is varied instead of the coupling strength itself.)
- Noise-enhanced propagation [36], [103] (In spatially extended systems of coupled stochastic resonators, signals can travel through the system even further if noise is present.)
- Noise-enhanced coding in neuronal arrays [104]
- Noise-enhanced temporal association in neural networks [105]

2.3.3 Stochastic resonance and the solid state

The phenomenon of SR has been observed experimentally and theoretically in many physical systems. Important examples in the physics of the solid state are: thin magnetic films, see Chapt. 2.4, [81], [82], [154], Ising spin systems in oscillating magnetic fields, see Fig. 2.11, [106] - [108], electron magnetic resonance [109] - [111], superconductive quantum interference devices (SQUIDs) [64], [112], [113] and tunnel diodes [114], [115].

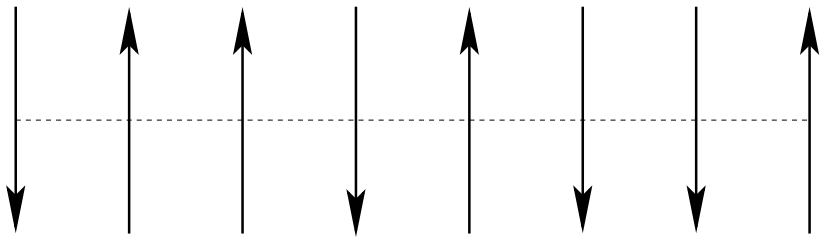

Figure 2.9: Ferromagnetically coupled two-state spins can be viewed as coupled stochastic resonators and, through their interaction enhance the SR-effect.

SR has also been observed in optical devices, such as bidirectional ring lasers [72], [76], lasers with saturable absorbers [116], semiconductor diode lasers [117] and free-electron lasers [118]. Common for all systems is a bistability, a subthreshold signal and a noisy

source. The example of the bidirectional ring laser has been one of the first experimental evidence of SR and proofed the theory of dynamical SR as outlined in Sec. 2.1. In this example, a ring laser which consists of a ring interferometer formed by mirrors can run in two modes. In this two-mode ring laser the light can travel clockwise (cw) or counterclockwise (ccw). The pump mechanism has been modulated by fluctuations and a periodic signal that breaks the symmetry between the two modes. The intensity of the two modes has been extracted from the ring laser and converted to a two-state (cw, ccw) time-series. As a result, the peak of the PSD at the driving frequency shows the maximum behavior which is typical for SR.

The above mentioned examples of magnetic systems have played a key role in the development of SR. Consequently, this can lead to new results in the field of magnetic materials and thus contribute to some cross-fertilization between the fields. Of particular importance are spatially extended systems consisting of coupled stochastic resonators.

The coupling can lead to spatio-temporal patterns (Fig. 2.10) and a further enhancement of SR. This is called *array enhanced stochastic resonance* (AESR). In [108] binary spins have been coupled ferromagnetically, forming a chain. The evolution of the elements is described by the Glauber model and the transition rate $W_i(\sigma_i)$ between the two possible states of the i-th spin σ_i is determined by a transition rate of Arrhenius type $\alpha = \exp(-1/T)$:

$$\begin{aligned} W_i(\sigma_i) = & \frac{\alpha}{2}\left(1 - \frac{\gamma}{2}\sigma_i(\sigma_{i-1} + \sigma_{i+1})\right) - \\ & - \frac{\alpha\delta}{2}\left(\sigma_i - \frac{\gamma}{2}\sigma_i(\sigma_{i-1} + \sigma_{i+1})\right)\cos\left(\omega_s t + \phi\right) \quad , \end{aligned} \tag{2.8}$$

with $\delta = \tanh(A_0/T)$ and the coupling $\gamma = \tanh(2J/T)$.

The chain is forced by the weak external oscillating magnetic field $A_0 \cos(\omega_s t + \phi)$. Tuning the noise intensity, which enters through the temperature T in the exponent of the transition rate, exhibits the SR phenomena for the chain of coupled spins at a fixed value of the ferromagnetic coupling constant J. If, at the optimal temperature T_{opt}, the coupling constant J is tuned, a further enhancement of the SR effect has been observed analytically [108] and numerically. This is the essence of AESR and shown in Figure 2.11 and

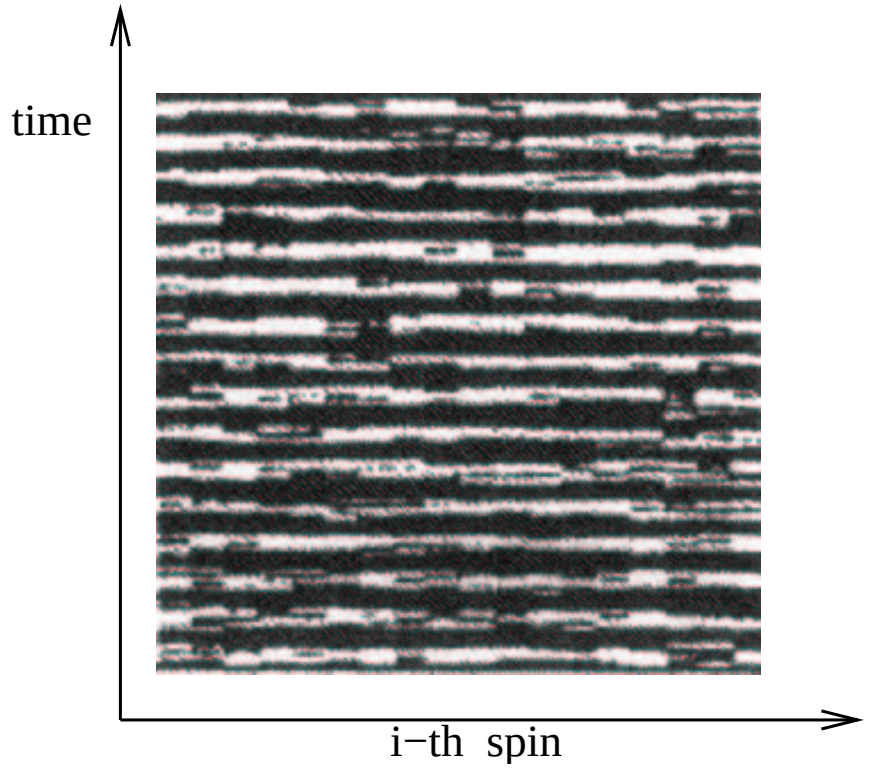

Figure 2.10: Simulated spatio-temporal pattern of an array of 400 ferromagnetically coupled spins due to the interplay between a subthreshold periodic magnetic field and Gaussian magnetic noise. See Figure 2.11 for details. Simulation by the author.

2.12.

The spin chain is an one-dimensional example of coupled zero-dimensional stochastic resonators. Until now, most research on SR has been focused on zero-dimensional systems. Specifically in magnetic materials, SR in uniaxial ferromagnetic single-domain particles and thin epitaxial iron garnet films driven by noisy and periodic external magnetic fields at the uniform magnetization reversal has been observed [119] - [121]. SNR measurements of such systems have been performed and a maximum SNR has been found. SR of a domain wall (DW) motion in one-dimensional nonuniform magnetic media has been studied in [122] and [123]. This phenomenon can be observed experimentally in magnetic nanostructures with

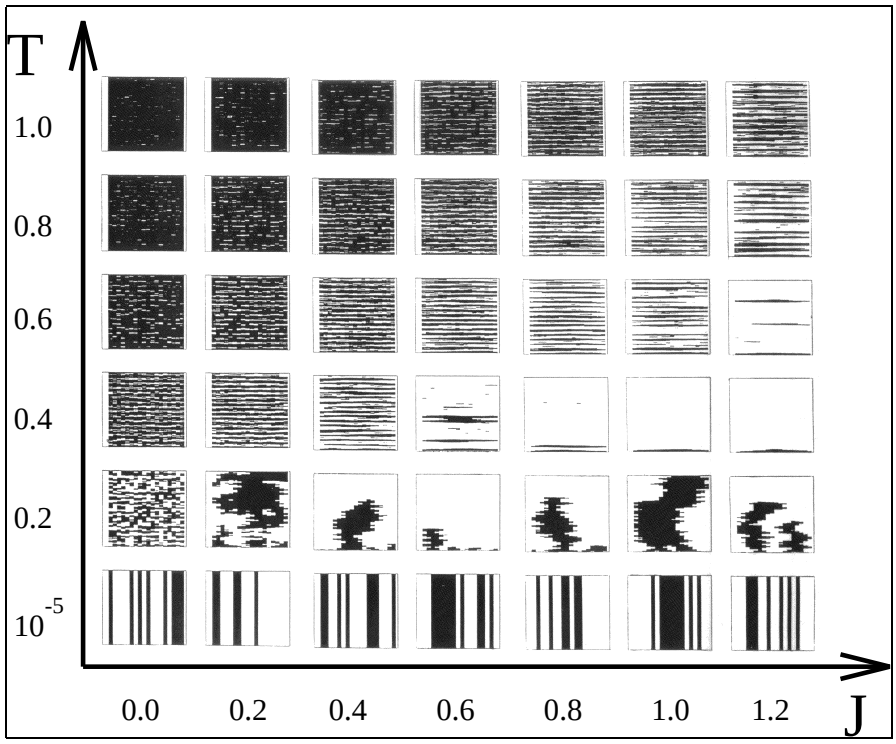

Figure 2.11: Array Enhanced Stochastic Resonance (T = temperature (noise intensity), J = ferromagnetic coupling constant). This is an example for AESR in a model of ferromagnetically coupled spins (horizontal axis in each image; spin up = black dot, spin down = white dot) evolving in time (vertical axis in each image) according to Eq. (2.8). For each value of the coupling constant J there is an optimal synchronization between the ensemble averaged time series and the applied oscillating magnetic field. Further-on there is a global optimum at $T_{opt} \approx 0.6$ and $J_{opt} \approx 0.6$ (dimensionless units). At very low temperatures the initial states are (almost) preserved and the individual spin does (almost) never changes its state. Thus, the individual spin can not follow the applied oscillating magnetic field. At very high values of the temperature, corresponding to a high noise intensities, the periodic component of the dynamic is "washed out" by the noise. Simulations by the author.

a long extension in only one dimension, named nanowires [135] - [138].

There is a good experimental possibility of registering the stochas-

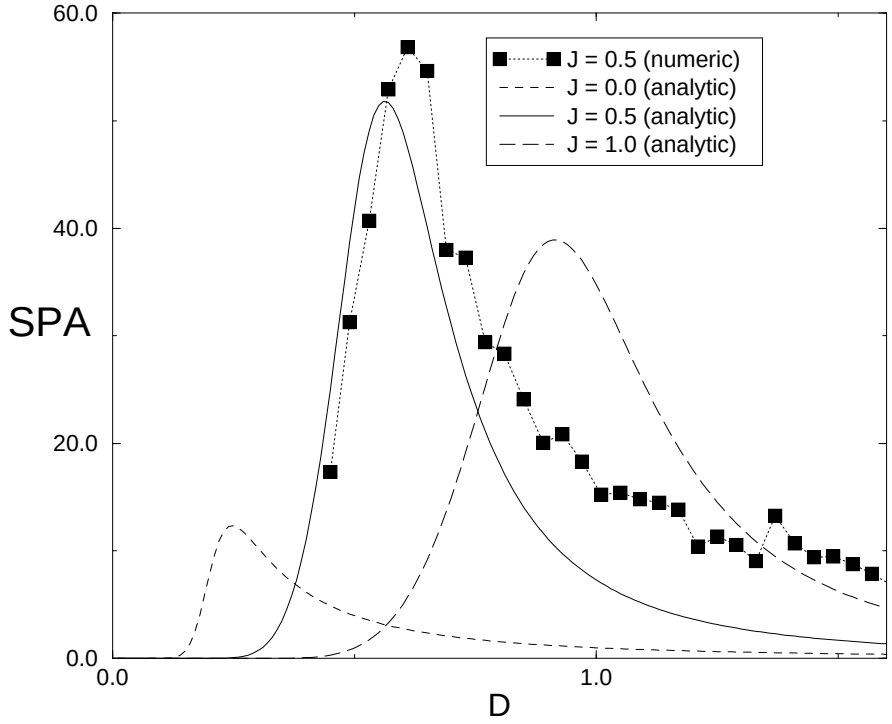

Figure 2.12: Non-monotonic behavior of the spectral power amplification (SPA) as a function of the coupling constant J provides numerical and analytical [108] evidence for AESR in a ferromagnetically coupled spin chain.

tic motion of a DW in the magnetic nanostructures by spin-polarized scanning electron microscopy with high spatial resolution [139], [140], already used successfully for investigation of the spin configuration of such structures [141], [142]. The experimental investigation of DW dynamics in a thin epitaxial ferrite-garnet film has been carried out in [154]. The stochastic motion (Barkhausen jumps) of a DW segment between two nearest pinning centers subjected to some periodic and inhomogeneous magnetic fields and noise has been studied, and measurements of the SNR have been performed. The SNR of the output has shown a clear maximum by increasing the applied noise strength.

The goal in Chapt. 2.4 is to study SR in a model of the mo-

tion of a 1D system subject to deterministic and stochastic forces in bistable, dissipative media. It is shown, analytically and numerically, that SR exist in the model and a experimental verification should be possible. This would possibly provide a new tool to determine system and material parameters, such as the stiffness of the domain. Further-on, many fundamental problems can be analyzed in the framework of this model [81]:

- dynamics of polymers and biomacromolecules [143],
- the motion of dislocations in solids [144],
- the dynamics of flux lines (vortices) in type II superconductors [145], [146],
- domain and domain wall dynamics in thin and ferro-elastic films [149],
- the motion of a front (a wave of transition between the two states dividing the two phases by a narrow moving interface) [42] and
- reaction-diffusion systems [147].

Another possible benefit of the research on SR for solid state physics has been suggested in [148]. The experimental observation of AESR, spatiotemporal synchronization and noise-enhanced propagation in a simple linear array of coupled bistable electronic triggers is reported and an analogy to charge density wave (CDW) like nonlinear conductivity in solids is pointed out.

2.4 Stochastic Resonance in Ferromagnetic Domain Motion

As an example for dynamical stochastic resonance discussed in Sec. 2.1 and an application of the theory sketched there, the motion of a ferromagnetic domain is studied in the following. In particular, the motion of a single stripe domain driven by external deterministic and noisy magnetic fields in an inhomogeneous thin magnetic film has been investigated analytically and numerically. A single

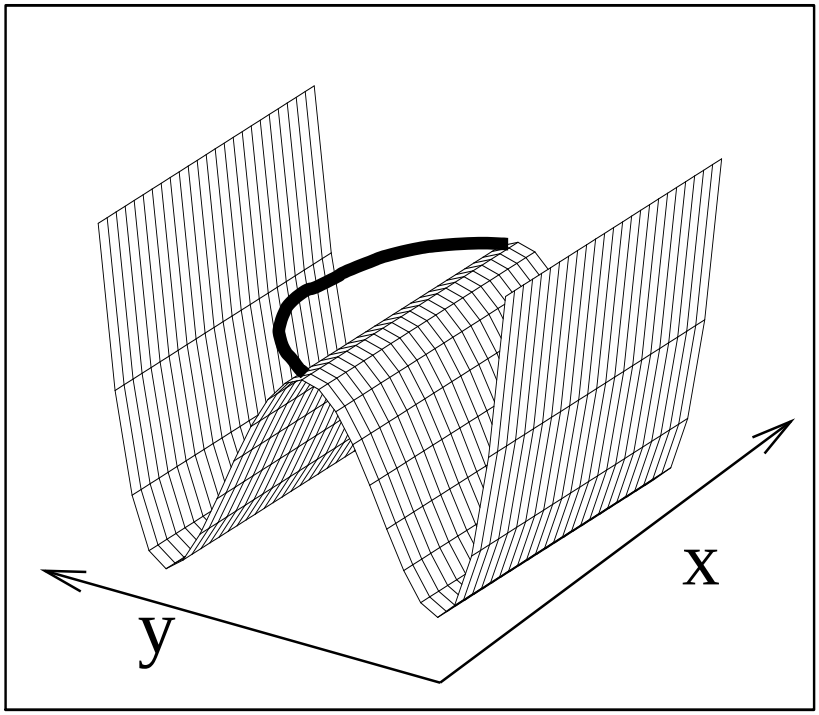

Figure 2.13: A ferromagnetic stripe domain (solid line) in the x-y-plane is subjected to a double-well, time independent magnetic field H_1, here $H_1^{(1)} = -\frac{a}{2}y^2 + \frac{b}{4}y^4$.

stripe domain is an important component of magneto-optic recording devices [149]. Nowadays behavior of a single domain subjected to deterministic uniform and nonuniform magnetic fields has been investigated intensively [150] - [153]. A single stripe domain is a region of a film limited by parallel domain walls and magnetized against the remainder of the film and the bias field. Such domains can be produced by either the system of orthogonal conductors with current on the surface of epitaxial garnet-ferrite film or a pair of centered electromagnets placed on the two sides of the film [153]. A single stripe domain with free ends is unstable and would shrink into a bubble. But, the ends of a domain are able to be fixed in static pinning centers, as, e.g., given by impurities and other de-

fects of a film or the points of the domain intersection with the coil contour [150] - [153]. Thereby, in the case of two pinned ends the stripe domain between them is straight in the presence of an uniform bias field. In the following, stochastic resonance within the

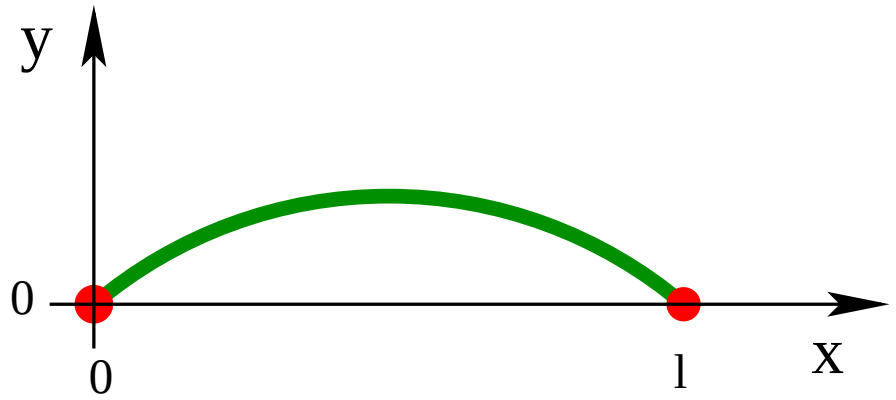

Figure 2.14: The magnetic stripe domain in the x-y plane is pinned at the locations $x = 0$ and $x = l$. The elongation is due to the action of the bistable potential resulting in a force directed perpendicular to the plane.

motion of a single domain placed in a double-well shaped potential and restricted by two pinning points (Fig. 2.13 and 2.14) will be demonstrated. When the noise and the signal are absent, the single domain in the bistable potential will be curved and its profile will have one of two equilibrium configurations which minimizes the total energy of the system.

The domain is driven by external noise and a weak periodic external field. For example, an electromagnetic coil excited by a signal produced by a noise generator can be of use as a source of a noisy magnetic field [154]. Both forces are considered as global actions (time dependent) and do not depend on the position of the domain. "Weak periodic field" means that the external signal never has a sufficiently large amplitude that the system escapes to the second stable configuration without the noise. Otherwise, with the addition of noise the single domain will surmount the barrier between the two equilibrium configurations and switch to the opposite symmetric configuration. Following the predictions of SR one can expect that the action of the weak periodic forces on the hopping

dynamics of the domain will become most coherent to the periodic driving at an optimal noise level.

2.4.1 Lagrangian equation of motion

Let us consider a single stripe domain pinned at the points $x = 0$, $y = 0$ and $x = l$, $y = 0$. The length l is assumed to be large compared with the width w of the front but small with respect to the curvature radius. For this case one can ignore changes of w and of the energy due to deformations of the domain profile besides some geometrical factor. Then, the Lagrangian equation of motion describing the evolution of the stripe domain profile $y(x,t)$ can be derived from the Lagrangian function density

$$L\{y(x,t)\} = T - U \quad . \tag{2.9}$$

Here

$$T = Md_0w\rho\left(\frac{\partial y}{\partial t}\right)^2\sqrt{1+\left(\frac{\partial y}{\partial x}\right)^2} \tag{2.10}$$

stands for the kinetic energy density. Here, $U = E_z + E_m + E_s$ is the potential energy density, M represents the spontaneous magnetization, d_0 the thickness of the thin film and $\rho = m/(2Md_0)$, with m as the effective mass per the unit area of a domain wall.

The contributions to U are the Zeeman (E_z), magnetostatic (E_m), and domain wall surface (E_S) energy densities. The Zeeman contribution is

$$E_z = 2Md_0w(H_b - H(y,t))\sqrt{1+\left(\frac{\partial y}{\partial x}\right)^2}, \tag{2.11}$$

where H_b is the temporally constant and spatially uniform biasing field and $H(y,t)$ stands for spatially inhomogeneous, time dependent periodic and noisy magnetic fields.

The second term of the potential energy density is given by

$$E_m = 2Md_0wH_m\sqrt{1+\left(\frac{\partial y}{\partial x}\right)^2}, \tag{2.12}$$

where H_m is the magnetostatic field.

The expression for the magnetostatic energy density of the infinite straight domain E_m [150] is used as $E_m(w)$ in the case $l \gg w$. Finally, the domain wall surface energy density contribution is

$$E_s = 2w\sigma\sqrt{1+\left(\frac{\partial y}{\partial x}\right)^2}, \tag{2.13}$$

where σ is the domain wall surface energy density. The physics of this term arises from the exchange interaction. In Eqs. (2.10) - (2.13) a geometry factor $\sqrt{1+\left(\frac{\partial y}{\partial x}\right)^2}$ appears in order to replace the energy density for the bow element by the energy density for dx.

Collecting all temporally constant and spatially uniform fields leads to a common parameter

$$H_0 = H_b + \frac{\sigma}{Md_0} + H_m, \tag{2.14}$$

which is a measure for the stiffness of the domain and can be seen as a kind of coupling parameter [149], [155]. Later on it will be one of the central values of the analysis.

Now the Lagrange density (2.9) can be written as

$$L\left(y, \frac{\partial y}{\partial t}, \frac{\partial y}{\partial x}\right) = 2Md_0w\left[\frac{1}{2}\rho\left(\frac{\partial y}{\partial t}\right)^2 - H_0 + H(y,t)\right]\sqrt{1+\left(\frac{\partial y}{\partial x}\right)^2}. \tag{2.15}$$

Since it depends on three variables, the Lagrangian equation of motion has to be used in the form

$$\frac{d}{dt}\frac{\partial L}{\partial(\partial y/\partial t)} - \frac{\partial L}{\partial y} + \frac{\partial}{\partial x}\frac{\partial L}{\partial(\partial y/\partial x)} = -\frac{\partial Q}{\partial(\partial y/\partial t)} \tag{2.16}$$

with a dissipative function

$$Q\left(\frac{\partial y}{\partial t}, \frac{\partial y}{\partial x}\right) = 2Md_0w\rho\lambda\left(\frac{\partial y}{\partial t}\right)^2\sqrt{1+\left(\frac{\partial y}{\partial x}\right)^2}, \tag{2.17}$$

containing $\lambda = \alpha M/(m\gamma\Delta)$ as the viscous attenuation, α is called the Gilbert relaxation constant, Δ as the domain wall width and γ as the gyromagnetic ratio.

In the following, the over-damped dynamics will be considered only. Therefore all terms which have their origin in the kinetic energy density will be neglected. For experimental ferrite-garnet films, the effects associated with the kinetic energy are negligibly small for the sinusoidal driving fields at low-frequency $\Omega \ll 70\text{MHz}$ [149]. In this case the driving field frequency is well below the resonance frequencies of the domain. It is worth noting that the range of low-frequencies is the most interesting for SR observation.

Then, inserting (2.17) and (2.15) into the equation of motion (2.16) leads to the over-damped dynamics

$$2\rho\lambda\frac{\partial y}{\partial t} - \frac{\partial H(y,t)}{\partial y} + \frac{[H(y,t) - H_0]\,\frac{\partial^2 y}{\partial x^2}}{1 + \left(\frac{\partial y}{\partial x}\right)^2} = 0. \tag{2.18}$$

Hereby $H(y,t)$ shall be the sum of two external fields, one bistable temporally constant contribution $H_1(y)$, and $H_2(y,t)$ standing for the temporally periodic and noisy excitations.

Two possibilities of a bistable inhomogeneity have been analyzed. The first one is a sum of a parabolic and a quadric potential

$$H_1^{(1)}(y) = -\frac{a}{2}y^2 + \frac{b}{4}y^4 \quad . \tag{2.19}$$

The second one is the "cusp shaped" potential

$$H_1^{(2)}(y) = -\tilde{a}(\tilde{b}|y| - y^2/2) \quad , \tag{2.20}$$

which corresponds to the combination of gradients and parabolic potentials and has discontinuities in the derivative at $y = 0$. Later on, these potentials will be referred to as the *first* and *second* potential.

Possibly, bistable potentials of such types can be set up by a spatially nonuniform magnetic field of a system of permanent magnets [156] or an effective field of magnetic micro-defects created by the method of synchrotron X-ray lithography [157] or by the laser annealing method [158].

The gradient magnetic field

$$H_2(y,t) = y[A_0 \cos(\Omega_s t + \phi) + \sqrt{2D}\xi(t)] \tag{2.21}$$

consists of a periodic signal field with frequency Ω_s, amplitude A_0 and initial phase ϕ. The force generated by that part is referred

to as signal. The value of ϕ must be treated as a random variable, uniformly distributed over the interval $[0, 2\pi]$ [72]. To make the analysis (theory, experiment and numerics) stationary, results should be averaged over this initial phase.

The second contribution describes a noisy force and we assume Gaussian white noise with mean value 0 and the δ-function as the autocorrelation function:

$$\langle \xi(t) \rangle \ = 0 \ , \quad \langle \xi(t)\xi(t+\tau) \rangle \ = \delta(\tau) \quad . \tag{2.22}$$

D scales the intensity of this noise. The noise will be of "global" type, i.e., it is, as the signal, a function of time only and will therefore have the same value for all $y(x)$.

Eq. (2.18) has been used as the basis for a numerical investigation and for a qualitative theory developed in the following section. Both approaches give evidence for stochastic resonance for the motion of the stripe domain and agree qualitatively (see Figs. 2.16 and 2.17).

The simulated values of the integral $\int_0^l y(x)dx$ of the domain determines the position of the domain. If the integral is negative, the domain is located at a different side of the barrier as it does when the integral is positive. The sign has therefore being used to produce a binary output consisting of the numbers +1 and -1. Therefore, only qualitative results can be expected from the simulation. The numerical investigation has been carried out using simple and fast Euler routines written in C combined with FFT-routines from [184].

2.4.2 Stationary case without temporal forces

According to the described setup an important restriction is made for the motion of the domain. It is assumed that the domain is pinned at two points. Hence, the following boundary conditions should be obeyed

$$y(x=0) \ = \ y(x=l) \ = \ 0 \quad . \tag{2.23}$$

Then, if $H_2(y,t) = 0$, Eq. (2.18) possesses the stationary (time independent) solution

$$y(x) = \pm B \, \mathrm{sn} \left(\frac{x}{x_0}, k \right) \tag{2.24}$$

and

$$y(x) = \pm b \left[1 - \frac{\cosh(\frac{1}{l_0}(\frac{l}{2} - x))}{\cosh(\frac{l}{2l_0})} \right] \tag{2.25}$$

for the first and second potential, respectively.

Here

$$x_0^{-1} = \sqrt{\frac{a+d}{2H_0}},\ B = \sqrt{\frac{a-d}{b}},$$

$$k = \sqrt{\frac{a-d}{a+d}},\ l_0 = \sqrt{\frac{H_0}{a}} \quad . \tag{2.26}$$

sn is the elliptic sine and d is an integration constant.

Using the condition $\partial y(x)/\partial x = 0$ for $x = l/2N, \quad N = 1, 2, ...,$ one can get the equation for the integration constant d for the first potential in the form

$$\frac{l}{2Nx_0} = \mathrm{K}(k) \quad , \tag{2.27}$$

where $\mathrm{K}(k)$ is the complete elliptic integral.

The curve $y(x)$ can have more than one extremum between $x = 0$ and $x = l$. The extrema will be located at $x = \frac{nl}{2N}$ $(n = 1, ..., N)$ because of the symmetry of the system. It is evident that the domain configuration with $N = 1$ has the minimal energy.

It follows from Eqs. (2.24) and (2.25) that the domain configuration depends on the stiffness parameter x_0/l or l_0/l for the first and the second potential, respectively.

The larger H_0 and smaller l and a, the less dangled the domain will become. Approximate expressions of the proposed solutions for the limiting cases of stiff and flexible domains can be found in the Appendix.

Stationary (time independent) configurations of single domains in uniform and inhomomogeneous magnetic fields have been studied experimentally in epitaxial garnet-ferrites [150] - [153]. For these films, doped by Bi, the typical parameters where:

$4\pi M = 160\,\mathrm{G} = 1.6 \times 10^5\,\mathrm{A/m},\ \sigma/(4\pi M^2 d_0) = 0.06,\ d_0 = 8.4 \times 10^{-6}\,\mathrm{m},\ w = 4 \times 10^{-6}\,\mathrm{m},\ H_0 = 4.4 \times 10^3\,\mathrm{A/m},\ \alpha = 0.05\,..\,0.5,\ \gamma = 0.22 \times 10^6\,\mathrm{m/sA},\ \Delta = 1.0 \times 10^{-6}\,\mathrm{m},\ \rho\lambda \approx 3 \times (0.1\,..\,1) \times 10^5\,\mathrm{sA/m^3}$; in inhomogeneous magnetic fields with $\sqrt{a/b} = 2 \times 10^{-6}\,\mathrm{m}$ $(a =$

$3.2 \times 10^{13}\,\mathrm{A/m^3}$ and $b = 2 \times 10^{-6}$ for the first potential, and $a = 0.8 \times 10^{13}\,\mathrm{A/m^3}$ and $b = 2 \times 10^{-6}$ for the second potential), the characteristic length is $l_0 \approx 7.5 \times 10^{-6}\,\mathrm{m}$.

2.4.3 Numerical treatment

The domain can be seen in analogy to a stretched spring which is unable to relax into the state corresponding to a straight line $y = 0$. This is due to the action of the attractive forces arising from the double-well potentials above and below the $y = 0$ axis. Applying temporal noise and temporally periodic forces will drive the "spring" to a flip-flop behavior between the two possible stable configurations. The dynamics of these flippings is dependent on the noise strength and the stiffness of the domain, which will we will see later on. The amplitude A_0 of the periodic force is assumed to be sufficiently small, so that jumps without noise would not occur (subthreshold). Therefore it is required that A_0/D will have a small value. Hence, jumps through the energetically unfavorable state $y = 0$ are initiated by the noise but, as will be seen, are synchronized by the periodic signal. Different snapshots of the flip-flop dynamics of the domain are shown in Fig. 2.15.

Equation (2.18) has been simulated by a fast Euler method taking care of the boundary conditions (2.23). To ensure the reliability of the computer program the convergence to the stationary (time independent) analytic solutions has been tested and was observed. One of these stationary solutions is marked by the dashed line in Fig. 2.15 and perfect agreement with the analytic solutions was found.

Further in the numerical analysis, the stochastic dynamics is reduced to a two state time series with the states +1 and -1 depending on the location of the domain above or below the $y = 0$ axis. The response of the system to the noise and the periodic force, later called output $q(t)$, then reads

$$q(t) = \mathrm{sgn}\left(\sum_{i=1}^{n} y(x_i)\right) = \pm 1 \quad , \tag{2.28}$$

where n is the number of simulated boxes which have been used

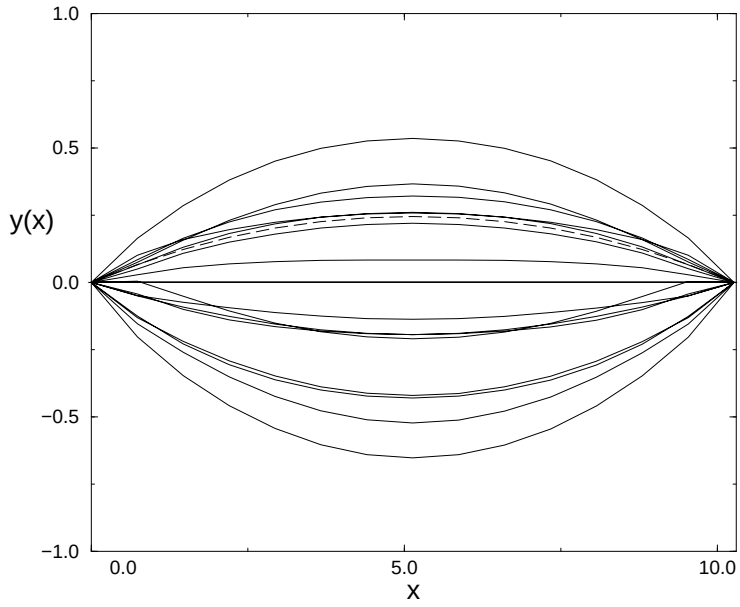

Figure 2.15: The numerical solutions of the dynamics Eq. (2.18) show different snapshots of the vertical jumps of a ferromagnetic stripe domain in a two dimensional plane which is pinned at two points and exposed to a periodic field and Gaussian white noise. The dashed line marks the stationary solution (analytic and numeric) (Numerical units).

according to the necessary discretization of the numerical problem.

The resulting binary time series, e.g.,

$$q(t) = ..., +1, -1, -1, +1, -1, +1, +1, +1, -1, ... \qquad (2.29)$$

can then be processed by Fourier analysis which has been carried out by a fast Fourier transform (FFT) algorithm. To minimize the errors arising from the FFT aliasing problem,a signal frequency Ω_s matching one of the frequencies of the resulting discrete Fourier spectrum has been chosen. The FFT used 4096 sampling points of a total running time of around 2000 time units. A total of 50 spectra with different initial phases had to be averaged in order to get a reliable power spectrum density (PSD).

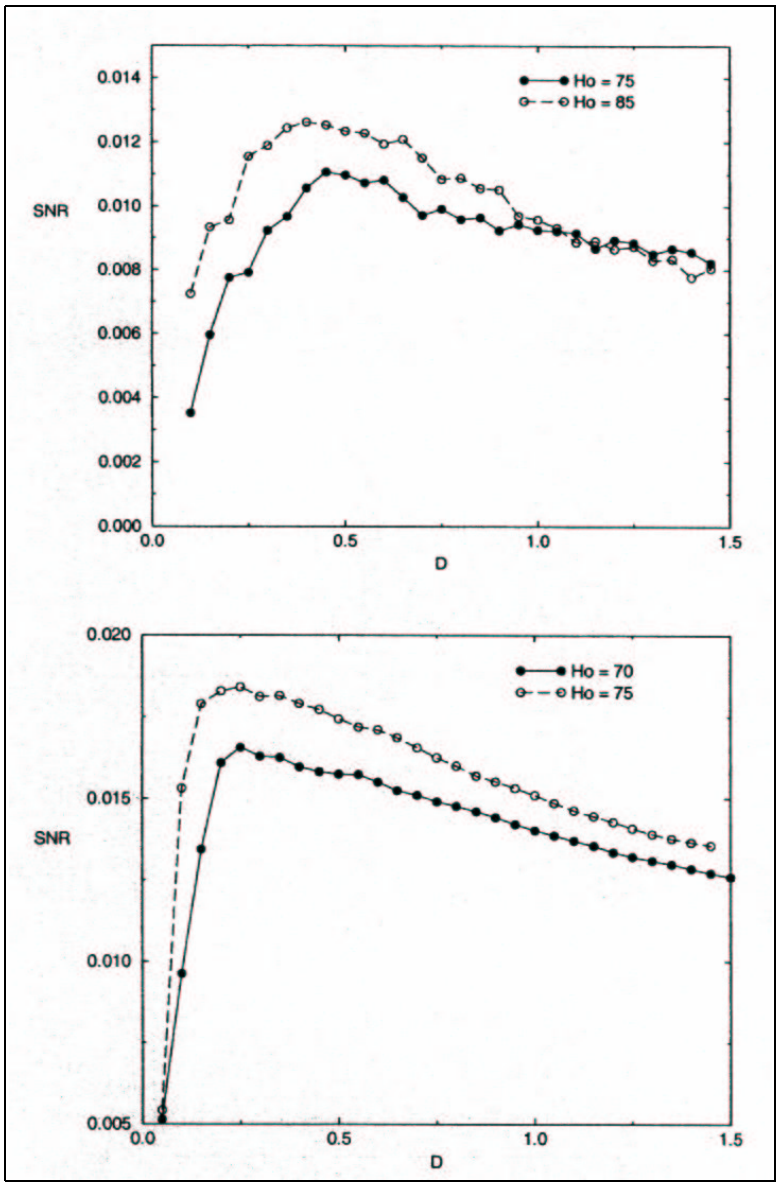

Figure 2.16: Numerical simulation of the SR-effect in the noisy, periodically modulated motion of a ferromagnetic stripe domain in the first (above) and second bistable potential. The signal-to-noise ratio (SNR) shows a maximum behavior as the noise intensity D is increased. The SNR is enhanced even further if the stiffness H_0 of the domain is increased.

The resulting PSD's consists of peaks at Ω_s and its multiples riding on a Lorentzian-like background and is characteristic for many examples of periodically driven stochastic over-damped nonlinear dynamics. To prove stochastic resonance the signal-to-noise ratio (SNR) of the output has been investigated. The SNR has been defined by the height of the first peak at Ω_s divided by the interpolated value of the background noise at this value.

As shown in Fig. 2.16 the SNR shows a clear maximum while tuning the noise intensity D. This maximum behavior is called stochastic resonance. Increasing the intensity of the input noise leads to an increased coherence between the output and the signal. The reasons for this behavior is that tuning noise intensity leads to a change of the stochastic time scale, the flipping time of the domains. For optimally selected noise this time scale can be brought in accordance with the time of the periodic driving. If the mean time for a single flip (mean first passage time (MFPT)) equals the half period of the signal the height of the first peak in the PSD becomes maximal. It means a conformance between two time scale. Therefore the term *resonance* is used.

If the domain is located above $y = 0$ and the periodic force points downwards (towards negative values), the action of this force changes the stochastic time scale so far that the stochastic transition to locations below $y = 0$ becomes nearly a sure event within the time the force acts downwards (half period of the signal). The second ingredient is that the probability of re-hopping upwards during that half period is vanishingly small. Thus the output follows the input signal during a half period with high probability. Since the situation is symmetric with respect to a change of the sign of the force, the domain will follow the signal by subsequent changes for sufficiently low frequencies of the driving.

In addition, Fig. 2.16 shows that the maximum is shifted to larger values of D if the stiffness parameter H_0 of the domain is increased. A way to understand this is given in the next section where a theoretic analytic approach is presented using a picture of an effective potential.

2.4.4 Theoretical approach

As the starting point for a qualitative analysis, Eq. (2.18) for the over-damped dynamic is used again. Although the approximation

$$\left(1+(\frac{\partial y}{\partial x})^2\right)^{-1} \approx 1-(\frac{\partial y}{\partial x})^2 \tag{2.30}$$

for small $\frac{\partial y}{\partial x}$ can be made, it is still hard to solve the equation directly. According to Kantarovich [159], the approximate solution of the variational problem should be sought in the form of finite combination of trial functions with unknown coefficients depending on time. Such an approximation is more adequate than other methods in the present case. In first approximation the ansatzes

$$y(x) = A(t)\left\{B\,\mathrm{sn}\,\left(\frac{x}{x_0},k\right)\right\}, \tag{2.31}$$

$$y(x) = A(t)\left\{b\left[1-\frac{\cosh(\frac{1}{l_0}(\frac{l}{2}-x))}{\cosh(\frac{l}{2l_0})}\right]\right\} \tag{2.32}$$

can be used for the first and second potential, respectively.

The motivation to seek solutions in the above given shape is provided by the stationary solutions which are the factors in (2.31) and (2.32) in the brackets. $A(t)$ will represent an elongation of these solutions and equals ± 1 for the stationary case. The benefit of using this ansatz is that the two-dimensional problem is reduced to a one-dimensional one.

Substituting the ansatzes (2.31) and (2.32) into the Lagrangian (2.9) and the dissipative function Q (2.17) and integrating them with respect to x, one gets the functionals $L[A(t)]$ and $Q[A(t)]$. Considering only small deviations of the domain from the $y=0$ axis, i.e., small elongations $A(t)$, terms with order higher than A^4 and A^2 for the first and second potential, respectively, can be neglected. After carrying out the integration over x this ends up with polynomials in $A(t)$. One gets for the first and second potential

$$L^{(1)}[A(t)] = \frac{S_1}{2}A^2 - \frac{S_2}{4}A^4 + S_3 A[A_0\cos(\Omega_s t+\phi)+\sqrt{2D}\xi(t)] \quad , \tag{2.33}$$

$$Q^{(1)}[A(t)] = (1/2)\Lambda^{(1)}\left(\frac{\partial A}{\partial t}\right)^2 \quad , \tag{2.34}$$

$$L^{(2)}[A(t)] = C_1|A| - \frac{C_2}{2}A^2 + C_3 A[A_0\cos(\Omega_s t + \phi) + \sqrt{2D}\xi(t)] \tag{2.35}$$

and

$$Q^{(2)}[A(t)] = (1/2)\Lambda^{(2)}\left(\frac{\partial A}{\partial t}\right)^2 \quad . \tag{2.36}$$

The coefficients $S_1, S_2, S_3, C_1, C_2, C_3, \Lambda^{(1)}$ and $\Lambda^{(2)}$ can be found in the Appendix.

Considering again the over-damped limit (2.18) of (2.16), one arrives at the reduced equations for the dynamics of the elongations

$$\dot{A}(t) = \tilde{S}_1 A(t) - \tilde{S}_2 A^3(t) + \tilde{S}_3 A_0\cos(\Omega_s t + \phi) + \tilde{S}_3\sqrt{2D}\xi(t) \tag{2.37}$$

and

$$\dot{A}(t) = \tilde{C}_1\mathrm{sign}(A(t)) - \tilde{C}_2 A(t) + \tilde{C}_3 A_0\cos(\Omega_s t + \phi) + \tilde{C}_3\sqrt{2D}\xi(t) \quad , \tag{2.38}$$

with $\tilde{S}_i = S_i/\Lambda^{(1)}$ and $\tilde{C}_i = C_i/\Lambda^{(2)}, i = 1, 2, 3$.

For $S_1, S_2, C_1, C_2 > 0$, Eqs. (2.37) and (2.38) describe nothing else but the stochastic motion of a Brownian particle in modulated double well potentials with rescaled signal amplitudes $A_{0r}^{(1)} = \tilde{S}_3 A_0$ and $A_{0r}^{(2)} = \tilde{C}_3 A_0$ and rescaled noise intensities $D_r^{(1)} = \tilde{S}_3^2 D$ and $D_r^{(2)} = \tilde{C}_3^2 D$.

These are one of the best studied systems in the theory of SR and therefore, former results can be used after rescaling the parameters according to our problem. Of particular use is the theory of dynamical SR outlined in Sec. 2.1. This theory was proven to give sufficiently good results for small amplitudes, especially for a qualitative analysis as in the presented case.

According to Sec. 2.1 (and [72]), the Kramers rate, which corresponds to the inverse MFPT, can now be determined and hence, the PSD. From the corresponding PSD's the signal-to-noise ratios can be extracted and they read

$$\mathrm{SNR}^{(1)} \approx \frac{1}{\sqrt{8}}\frac{\tilde{S}_1^2 A_0^2}{\tilde{S}_2\tilde{S}_3^2 D^2}\; e^{-\frac{\tilde{S}_1^2}{4\tilde{S}_2\tilde{S}_3^2 D}} \tag{2.39}$$

and

$$\mathrm{SNR}^{(2)} \approx \frac{1}{4}\frac{\tilde{C}_1^2 A_0^2}{\tilde{C}_2\tilde{C}_3^2 D^2}\; e^{-\frac{\tilde{C}_1^2}{2\tilde{C}_2\tilde{C}_3^2 D}} \quad , \tag{2.40}$$

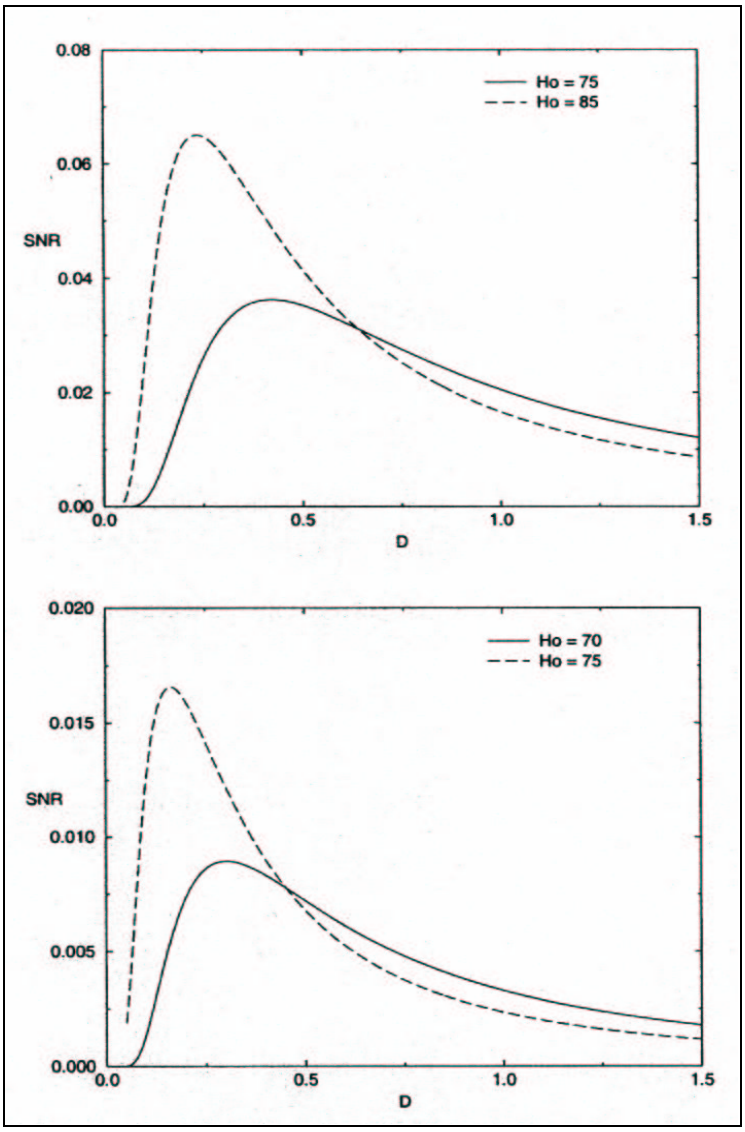

Figure 2.17: Analytical calculation of the SR-effect in the noisy, periodically modulated motion of a ferromagnetic stripe domain in the first (above) and second bistable potential. The signal-to-noise ratio (SNR) shows a maximum behavior as the noise intensity D is increased. The SNR is enhanced even further if the stiffness H_0 of the domain is increased.

respectively.

The SNRs (2.39) and (2.40) are plotted with respect to the noise intensity D in Fig. 2.17 and display the well known bell-shaped curves. Qualitatively they agree with the SNR of the numerical analysis and have maxima with values

$$\mathrm{SNR}^{(1)}_{max} = 8\sqrt{8}\frac{\tilde{S}_2\tilde{S}_3^2}{e^2\tilde{S}_1^2}A_0^2 \tag{2.41}$$

and

$$\mathrm{SNR}^{(2)}_{max} = 4\frac{\tilde{C}_2\tilde{C}_3^2}{e^2\tilde{C}_1^2}A_0^2 \tag{2.42}$$

located at

$$\mathrm{D}^{(1)}_{max} = \frac{1}{8}\frac{\tilde{S}_1^2}{\tilde{S}_2\tilde{S}_3^2} \tag{2.43}$$

and

$$\mathrm{D}^{(2)}_{max} = \frac{1}{4}\frac{\tilde{C}_1^2}{\tilde{C}_2\tilde{C}_3^2} \quad , \tag{2.44}$$

respectively.

From the mathematical point of view these maxima are a consequence of the competition of two tendencies. On the one hand, the noise enters like $\exp(-const/D)$ giving rise to a steep increase with increasing (but still small) D. For large D this factor is no longer dominating but near 1. On the other hand, the SNRs have a D dependent pre-factor, which is a function of a power in D, and thus is unimportant for small D but dominates for $D \to \infty$. It is clear that in this limit, the SNRs should decrease. Hence, one gets a maximum, where the strongly increasing small D branch meets the softly decreasing large D branch.

The calculated SNRs show qualitative agreement with the numerics also in their behavior for increasing H_0, which stands for the domain stiffness. The maxima grow and are shifted to lower values of D with increased stiffness. The coefficients $\tilde{S}_1$, $\tilde{S}_2$ and $\tilde{C}_1$, $\tilde{C}_2$ contain the stiffness parameter x_0/l and l_0/l, respectively. Therefore, the effective potential for the first and second case,

$$U^{(1)}_{eff} = -\frac{S_1}{2}A^2 + \frac{S_2}{4}A^4 \tag{2.45}$$

and

$$U^{(2)}_{eff} = -C_1|A| + \frac{C_2}{2}A^2 \quad , \tag{2.46}$$

will change by varying these parameters. Increased parameters x_0/l and l_0/l flatten the effective potentials (2.45) and (2.46), the domains are pulled towards the $y = 0$ axis and less noise is needed to bring the domain to the other side of the potential barrier. That explains the growth of the SNR maximum and its shift to lower values of D for an increased stiffness H_0. Therefore this system represents a special example of array enhanced SR (AESR) with a shift of the optimal noise strength D only towards smaller values while increasing the coupling strength.

Chapter 3

RANDOM NETWORK SWITCHES

3.1 A Traffic Model of Neuronal and Road Networks

The model, which will be studied in this section has been presented and published in [168] and further developed and discussed by the author in [169] and [170]. It describes neural spike traffic at a junction of neuron channels but can, because of its generality, be used to describe car traffic at highway junctions as well.

Probably, every car driver has experienced a beneficial effect of randomness. In a certain crowded traffic situation, it is not possible to get into a major road from a lower priority road, if the cars are passing the junction periodically with low distance. The gaps between subsequent cars on the main road are not large enough for a waiting car to get into that gap and to accelerate to the required speed. Only a larger gap, which usually occurs randomly in the car flow, makes it possible to enter. Therefore, certain fluctuations, i.e., random noise, can be beneficial for the traffic in certain cases. Similar problems of car traffic including the problem of the gap have been extensively studied in the literature in the last decades [160] - [162].

Road traffic systems, discussed from the viewpoint of statistical physics are traffic jams [163] - [165], time series of single-vehicle data [166] and stabilization of traffic flow due to interaction [167].

However, the questions of an optimal noise and of a possible stochastic resonance have not been addressed yet. In this chapter, the effect of triggering the traffic by various noises, i.e., stochastic processes, is investigated and it is shown that there is an apparent stochastic resonance phenomenon, which concerns the shape of the noise spectrum. This phenomenon can be seen as a type of stochastic resonance effect, where the optimal tuning concerns the shape of the power spectral density $S(f)$ rather than the intensity D of the input noise.

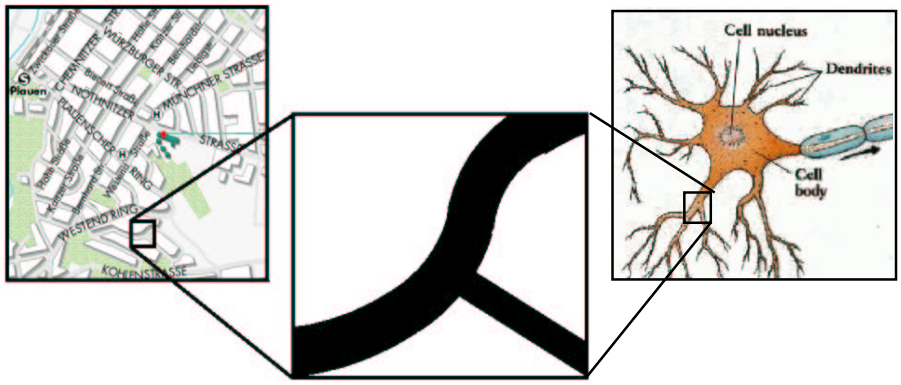

Figure 3.1: The presented junction model can be used to describe signal transfer in neurons as well as car traffic in road networks. See text.

The model considers a single-laned one way main road (channel) with a defined distribution of errant cars (neural spikes). At a junction J a side road is assumed with an infinite number of cars waiting to enter the main road traffic depending on the gap size G_i between two consecutive main road cars. The number N_i of side road cars entering the main road shall be given by the integer function INT() of the ratio between the size of the i-th gap and a minimal gap size G_0, where just a single car could enter (see Fig. 3.2).

$$N_i = \mathrm{INT}\left(\frac{G_i}{G_0}\right) \tag{3.1}$$

The function INT() simply reduces the number to the nearest integer value, i.e., truncates the digits behind the decimal place.

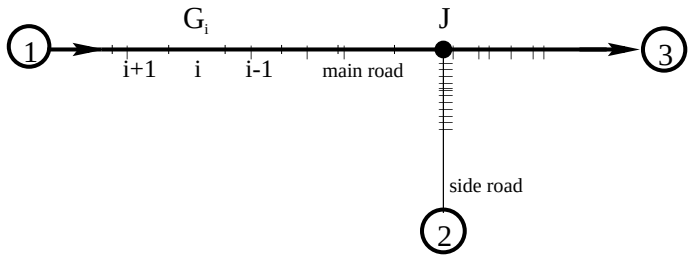

Figure 3.2: The model: Main channel traffic from 1 to 3 reaches the junction J. Side channel traffic is waiting at 2 to enter the main channel depending on the i-th gap size G_i.

To avoid car accidents a minimal gap value could be introduced assuming that the distances G_i and G_0 are measured in conventional length units. Alternatively one can measure G discretely in unit lengths of a car.

To measure the efficiency of the overall traffic (main and side road) the geometric mean $\nu = \sqrt{\nu_{1,3}\nu_{2,3}}$ can be used, where $\nu_{1,3}$ denotes the mean rate of main road traffic before the junction and $\nu_{2,3}$ the mean rate of side road cars entering the main road, respectively. The mean rates are the average number of events (cars, neural spikes) per unit time. The geometric mean yields small values even when only one of the traffic channels performs badly. In particular, zero geometric mean would account for the important situation where information flow through one of the channels is blocked completely. It is clear that the arithmetic mean (as a measure of efficiency) does not have this advantage. The information about traffic efficiency can also be supplied by a $\nu_{2,3}(\nu_{1,3})$ plot. The larger $\nu_{2,3}$ for a given $\nu_{1,3}$, the higher the efficency in the model.

To make the model relevant to neural spike traffic one considers the roads to be neuron channels. As a simplification one can consider both channels to have equal priority. The neuron transfers the spike coming from channel 1 or 2, if the time since the last transferred spike is greater than G_0, where G_0 represents the refractory time of the neuronal junction. This is a simplistic way of modeling a synapsis that connects an axon of one neuron to the dendrite of another one. There has been extensive research over the last 50 years and a lot of knowledge on the anatomy and

the biophysical properties of synapses has been discovered. One of the commonly accepted facts concerns the refractory period of the cell membrane of the synapsis which occurs after a depolarization process. Further-on, it is known that a generated action potential (spike), i.e., the information flow, proceeds only in one direction. That is due to the blocking of the sodium channels which has been passed by the spike. Much less, however, is known about the functional properties of the synapsis. Especially questions about the appropriate measure for the effect of a synapsis, optimizing mechanisms and questions concerning information processing remain to be answered [171].

In the presented model, the frequency of transferred spikes depends on the statistics of spike generation; moreover, the spikes can be lost. Both the output spike frequency and the probability of spike loss influence the efficiency of information transfer, therefore, the question arises about the kind of spike statistics that provides the best efficiency of information transfer. Since neuronal spikes can be lost in contrast to cars, the spike transfer probability and number of output spikes are the relevant measures for the neuronal system.

With this model three different classes of point processes controlling the generation of the spikes (respective car locations) have been investigated: Poisson process, a case with noise but without memory effects; zero crossing events of colored noise processes with $1/f^k$ shaped spectra and periodic traffic, a case with no noise. Further-on the periodic case has been modified by modulation of the phase with Gaussian noise. Here, again the $1/f^k$ spectrum of the noise has been varied by tuning the parameter k.

3.1.1 Noise triggered input

3.1.1.1 Poissonian process

The time moments when cars on the main road pass the junction shall be generated by a Poisson process with rate $\nu_{1,3}^{pois}$. As outlined in 1.2.1.1, the Poisson process is one of the most fundamental Markov processes and occurs in a wide range of natural phenomena. The probability to find exactly M events (cars passing the

junction) during time interval τ is given by

$$P_M(\tau) = \frac{(\nu_{1,3}^{pois}\tau)^M}{M!}\exp\left(-\nu_{1,3}^{pois}\tau\right) \quad . \tag{3.2}$$

To calculate the relationship between mean rates $\nu_{2,3}$ and $\nu_{1,3}$, we can define the moment of a car passing the junction as $t_0 = 0$, and introduce two (positive) observation times t_1 and t_2, such that $t_1 < t_2$. From Eq. (3.2) it follows that the probability to have events (one or more) during time interval $t_1 < t < t_2$ if there were no events at $t < t_1$ is

$$\begin{aligned} P_{M\geq 1,t_1,t_2} &= P_0(t_1) - P_0(t_2) \\ &= \exp\left(\nu_{1,3}^{pois}t_1\right) - \exp\left(\nu_{1,3}^{pois}t_2\right) \quad . \end{aligned} \tag{3.3}$$

In our model this equation gives the probability of accommodating exactly one car from the junction if we put $t_1 = G_0$ and $t_2 = 2G_0$ (one interval of duration G_0 is "clean", but not two). The probability of accommodating exactly two cars is obtained from Eq. (3.3) if $t_1 = 2G_0$ and $t_2 = 3G_0$ (two intervals of duration G_0 are clean, but not three). And so on. The mean number of cars accommodated from the junction per single interval between cars in the main road is given by the sum of these probabilities weighted by the corresponding car numbers

$$\begin{aligned} \langle N\rangle &= \sum_{n=1}^{\infty} n\left[\exp\left(-\nu_{1,3}^{pois}G_0 n\right) - \exp\left(-\nu_{1,3}^{pois}G_0(n+1)\right)\right] \\ &= \frac{\exp\left(-\nu_{1,3}^{pois}G_0\right)}{1-\exp\left(-\nu_{1,3}^{pois}G_0\right)} \quad . \end{aligned} \tag{3.4}$$

Thus the average rate of entering from the junction is

$$\nu_{2,3}^{pois} = \nu_{1,3}^{pois}\langle N\rangle = \frac{\nu_{1,3}^{pois}\exp\left(-\nu_{1,3}^{pois}G_0\right)}{1-\exp\left(-\nu_{1,3}^{pois}G_0\right)} \quad . \tag{3.5}$$

Note that this analytical result is exact and has been plotted together with results of a simulation in Fig. 3.3.

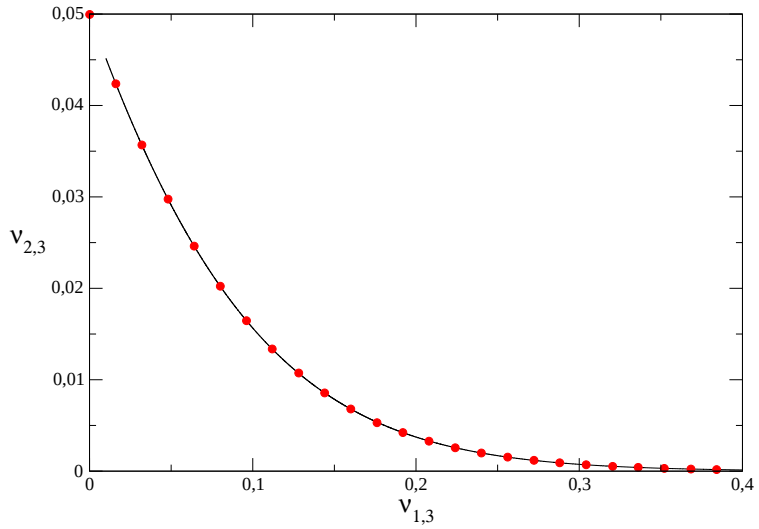

Figure 3.3: Side channel traffic rate $\nu_{2,3}$ as a result of incoming Poisson traffic with rate $\nu_{1,3}$. Plotted is the analytic result of Eq. (3.5) (solid line), which is confirmed by results of a simulation (dots).

3.1.1.2 Colored noise

Now, consider the case when the point process describing the car occurrence on the main road is generated by the zero crossing events of a Gaussian $1/f^k$ noise. When $k > 0$, this noise has a long-range memory. Due to the experimental evidence of occurrence of $1/f^k$-like noise processes in car traffic [172] and neural systems [176]-[178], [181], it is tempting to apply this kind of noises ($0 < k < 2$) to generate the car occurrence. The mean zero crossing rate of a Gaussian noise process is described by the Rice formula [173]

$$\nu_{1,3}^{color} = 2\frac{\sqrt{(\int_0^\infty f^2 S(f)df)}}{\sqrt{(\int_0^\infty S(f)df)}} \quad , \tag{3.6}$$

where f is the frequency and $S(f)$ is the power spectral density of the noise. The value of $\nu_{2,3}$ has not been calculated analytically. The time distribution of the zero crossing events is an unsolved problem [173] - [176].

To compare the different cases of traffic processes, computer simulations have been carried out. The length of the simulation

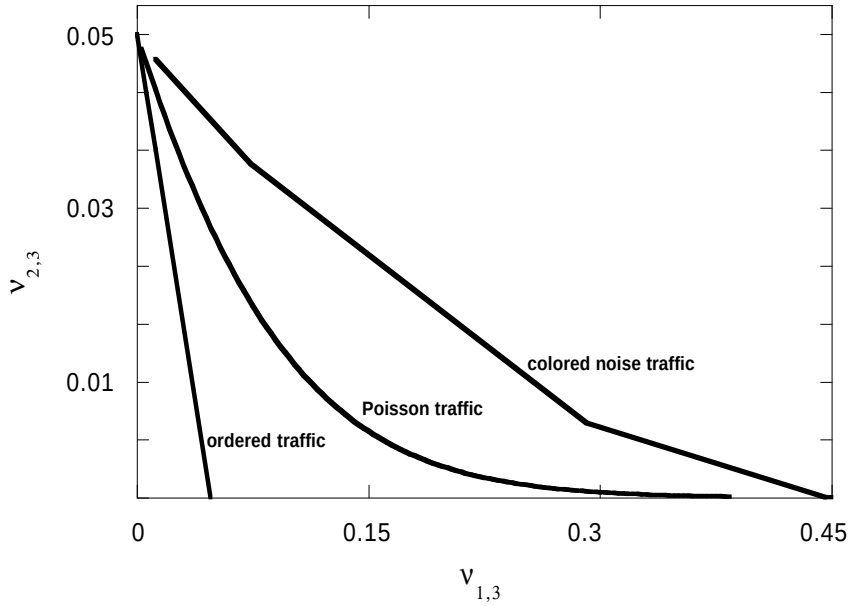

Figure 3.4: Superiority of colored ($1/f^k$ generated) traffic over Poissonian and an example of an inefficient periodic process.

and the point processes describing the car occurrence on the main road were 32768 (2^{15}) and the minimal gap size G_0 was 20. In comparison with a practical highway traffic situation, where the mean distance between the cars is 100 meters, the total process length corresponds to the main traffic road of 160 km. In Fig. 3.4, $\nu_{2,3}$ versus $\nu_{1,3}$ is shown. The results for Poissonian traffic turned out to be in excellent agreement with the predictions of Eq. (3.5) and can be regarded as a test of the simulation accuracy (Fig. 3.3). The frequency range of integration relevant in Eq. (3.6) was determined by the simulation length, so the colored noise traffic was solely controlled by the spectral exponent k. For the results shown in Figure 3.4, the range 0 - 2 was used for k. An example of an ordered traffic with the strictly periodic fragments of $G_i \lesssim G_0$ and regular interruptions with a large G_i to account for $\nu_{1,3} < 1/G_0$ is also given here. It is obvious that this example of periodic traffic gives the smallest $\nu_{2,3}$ and the colored noise traffic gives the largest $\nu_{2,3}$, especially for medium and high $\nu_{1,3}$. It is also apparent that a better compromise between the $\nu_{1,3}$ and $\nu_{2,3}$ is provided by the colored noise traffic compared to the Poissonian case. In the case

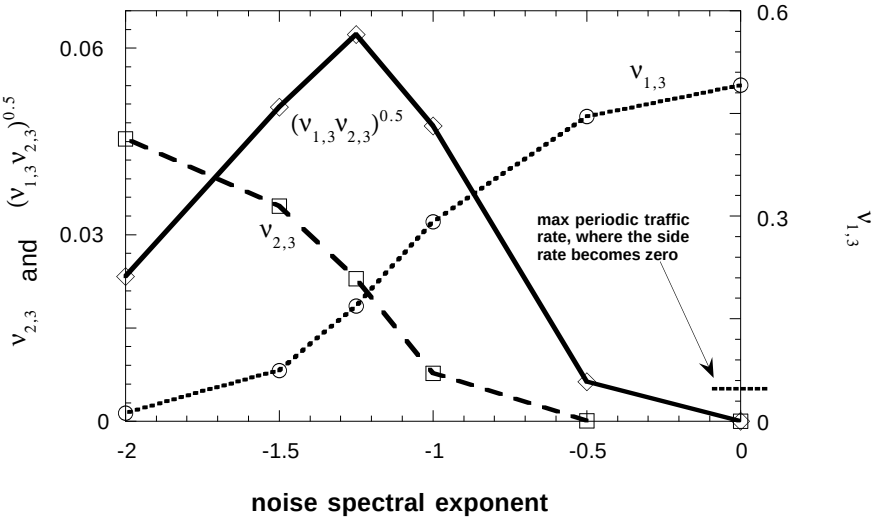

Figure 3.5: Stochastic resonance like peak in the car traffic efficiency $\nu = \sqrt{\nu_{1,3}\nu_{2,3}}$ (solid line) versus the spectral exponent of the colored noise traffic. From L. Kish [168].

of the colored noise generated traffic, the most interesting result is a new kind of SR, spectral stochastic resonance (SSR), which demonstrates the existence of an optimal spectral shape for the highest traffic efficiency, as shown in Fig. 3.5. This new kind of stochastic resonance is similar to the classical effects in the sense that the noise driving is needed to get the optimal performance of the system. On the other hand, instead of the noise intensity, the spectral shape (as described by k) is the SR tuning parameter, which optimizes the performance. Note, that usually, the spectral shape is more related to resonance effects in physics than intensity. Musha and Higuchi [172] reported a $1/f$-like noise in the traffic current of cars on highways, so, it is particularly interesting that the optimal traffic in our model is also found around $k = 1$.

There are also nontrivial features for the neuron traffic model when it is driven by $1/f^k$ noise generated spikes. This time, the introduction of the overall traffic efficiency, as the geometrical mean of the two traffic rates, is not necessary. The mean frequency of the outgoing spikes is a good measure of the variations in the upper limit of information transfer rate through the system. Computer simulations were done in a similar way and with similar conditions as described above. The upper frequency cutoff of the spectrum

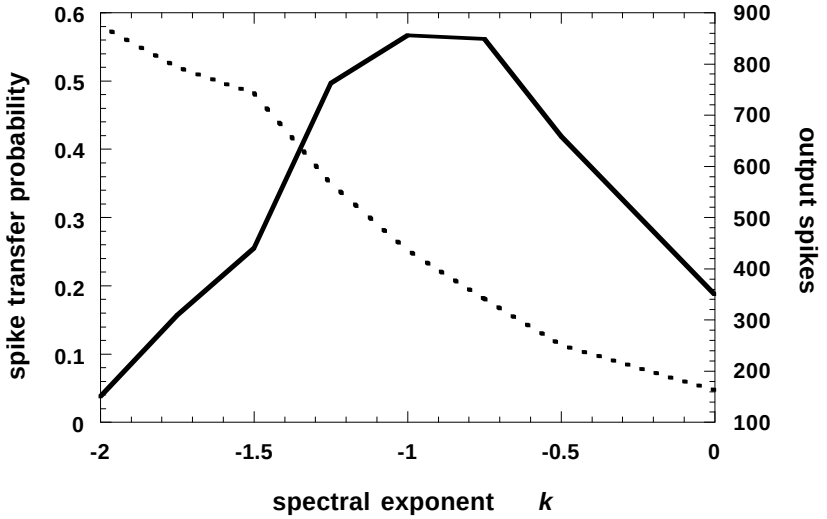

Figure 3.6: Stochastic resonance like peak in the frequency of transferred neural spikes (solid line) versus the spectral exponent of the colored noise traffic. The dotted line shows the probability of spike loss. From L. Kish [168].

was chosen 6000 (compared with the sampling frequency of 32000), which is equivalent to a refractory time of 5.3 (time units), characterizing spike statistics of the sources of spikes. The refractory time of the junction-neuron, which corresponds to the minimal gap size in the car traffic model, was chosen to be 10. In Fig. 3.6, the mean rate of transferred spikes and the probability of spike transfer are shown. The rate of transferred spikes characterizes the highest meaningful bandwidth of information transfer, due to Shannon's sampling theory. Therefore, this quantity is directly related to the information transfer rate.

Here we can also observe a well-pronounced SSR around $k = 1$. This fact is in an interesting coincidence with the general occurrence of $1/f$-like noise phenomena frequently reported in neural activity [176] - [178], [181]. The other quantity, the spike transfer probability characterizes the phenomenon of spike loss. The actual rate of information transfer depends on both quantities as well as on the unknown way of neural coding. The spike loss is the smallest at $1/f^2$ noise (Brownian motion) generated spike train. However, in

this case, the widest meaningful bandwidth of information transfer is one order of magnitude less than it the case of $1/f$ noise. The $1/f$ noise case provides the highest spike propagation rate, though with some compromise in the accuracy of transfer.

3.1.2 Strictly periodic input

Let us now consider a periodic main road traffic *before* the junction, i.e., the cars shall arrive at times $t = i\ G_i v^{-1}$ for $i = 1, 2, ..$ at the junction J (see Fig. 3.7). Here v denotes the unit velocity which shall be set equal 1 for the sake of simplicity. Therefore the mean

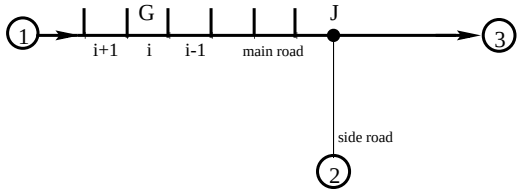

Figure 3.7: Onset for periodic modulated incoming traffic. The incoming main road traffic (1→ 3) is determined by the rate $\nu_{1,3}$ which is now the frequency of a periodic process.

rate of the input is given by the reciprocal of the constant gap size $G = G_1 = G_i$. The number N of cars entering from the side road will then be equal for all G_i, i.e., $N = N_1 = N_2 = .. .$ Hence the mean rate $\nu_{2,3}$ can directly be written down using Eq. (3.2).

$$\nu_{2,3}(\nu_{1,3}) = \frac{N}{G} = \nu_{1,3}\ \mathrm{INT}\left(\frac{1}{\nu_{1,3}\, G_0}\right) \tag{3.7}$$

This equation is the *exact* solution for all processes $\nu_{1,3}$. To discuss the solution it is useful to introduce three lines subdividing the solution space. The three lines correspond to analytic approximations of the INT()-function. The intersections of the solution with the lines are called modes in the following.

1. $\mathrm{INT}\left(\frac{G}{G_0}\right) \approx \frac{G}{G_0}$
2. $\mathrm{INT}\left(\frac{G}{G_0}\right) \approx \frac{G}{G_0} - \frac{1}{2}$

3. INT $\left(\frac{G}{G_0}\right) \approx \frac{G}{G_0} - 1$

1. *first mode: best ordered traffic*; The gap sizes of incoming main road cars are minimal for a certain number of side road cars allowed to enter. There is no waste spacing between consecutive cars which would reduce the overall number of cars passing the junction during a certain time interval and thus impair the overall traffic efficiency.

2. *second mode: medium ordered traffic*; This corresponds to an average over all input rates and can be considered as a critical case as it will be discussed in Sec. 3.1.3.1.

3. *third mode: worst ordered traffic*; The incoming traffic is organized contrarily to mode 1., i.e., the gap sizes G are infinitesimally smaller than multiples of G_0, wasting a spacing of (almost) G_0 each time side road cars enter the main road.

Figure 3.8 illustrates this distinction.

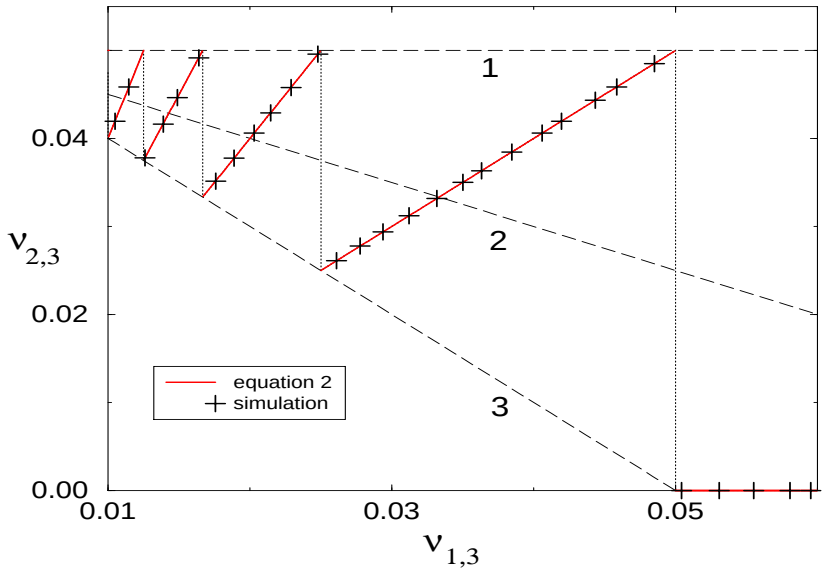

Figure 3.8: Side channel mean rate $\nu_{2,3}$ as a response to periodic main channel traffic with mean rate $\nu_{1,3}$ taken from Eq. (3.7) and simulation ("+" signs). The dashed lines mark the three different modes (approximations) of $\nu_{1,3}$: 1. best, 2. medium and 3. worst ordered traffic.

It has been shown in Sec. 3.1.1 that the third mode of periodic traffic is inferior to the traffic triggered by a Poisson process or the zero crossings of $1/f^k$ noise. Moreover it has been assumed that there are "sites" in the main road flow which follow each other strictly by a distance of G_0. The worst periodic traffic means that these sites are "filled" by cars in a periodic way. So the maximal rate is reached when all sites are filled. The next, lower traffic rate is obtained when every second site is filled. Then the next, lower traffic rate is realized, when every third site is filled, etc. This is a sort of "discrete periodic" case. Further-on it has to be stated that the straight line which contains the single points of mode 3 is a monotonously decreasing function of the main traffic rate. This monotonous decrease holds on up to the main traffic rate where the cross traffic rate smoothly becomes zero. This is a qualitative behavior one can see in practice.

Note that the first mode of ordered periodic traffic can not be exceeded by any other process in the present model. The second mode divides the rate space into two qualitatively different regions. That will be discussed in the next subsection.

3.1.3 Noise modulated periodic input

3.1.3.1 Gaussian white noise

The model has been modified to get a more *realistic* description of the arrival times of the incoming main road traffic at the junction. The modification consists of a random deviation around the strict periodic position according to a Gaussian distribution with variance D (phase noise).

To justify this approach it is worth to take a look at real traffic. Cars pass regulation devices such as traffic lights in an *almost* periodic manner whereas this periodicity gets lost in time due to the individual pattern of behavior or external reasons. $1/f^k$ noise has been observed in traffic flow [182], neuro systems [180] and human coordination [183]. Taking the notations of the previous subsection, a periodic traffic with $(\nu_{1,3}, \nu_{2,3})$ lying between the modes 2 and 3 can be enhanced by applying the noise in the described way. Note

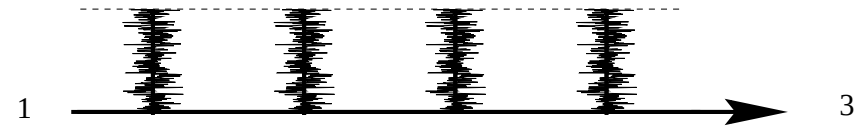

Figure 3.9: The periodic positions of the incoming ($1 \rightarrow 3$) traffic events with rate $\nu_{1,3}$ (see text and Fig. 3.7) are now perturbed by Gaussian (colored) noise. That means it is more likely to find a small deviation from the strictly periodic pattern discussed above, than a large one.

that traffic corresponding to $(\nu_{1,3}, \nu_{2,3})$ between modes 1 and 2 can only be diminished. In this respect, mode 2 is crucial: it separates traffic situations where noise can be beneficial from those where its addition only degrades the system performance.

If point $(\nu_{1,3}, \nu_{2,3})$ is lying between modes 2 and 3, speed modulation devices acting randomly as well as random changes of the speed by the driver present possibilities to increase the overall traffic. In case of $G_i \lesssim G_0$ there would be no side road traffic without the noise at all. This is in agreement with the paradigms of the stochastic resonance effect where a signal is unable to cross a threshold without additional noise. In this way the noise modulated periodic traffic model can be seen as a temporal multi-threshold system with equidistantly distributed thresholds $i\,G_0$ $(i = 1, 2, ..)$.

An increase in the variance (or noise intensity D) leads to a larger total number of cars passing the junction and thus increases the overall traffic efficiency. The physical reason is that the time dependent probability distribution of the events (cars) evolves from a periodic configuration of δ-peaks to an overlap of Gaussian distributions. For large D the probability distribution becomes uniform, which explains the convergence towards mode 2 for *all* possible input rates below *and* above mode 2.

The effect can be viewed in computer simulations presented in Fig. 3.10 where the results of the modulation are plotted together with the results obtained for the un-modulated case ($D = 0$).

3.1.3.2 Gaussian colored noise

How does the shape of the power spectrum of the applied Gaussian noise influence the increase of the overall traffic efficiency?

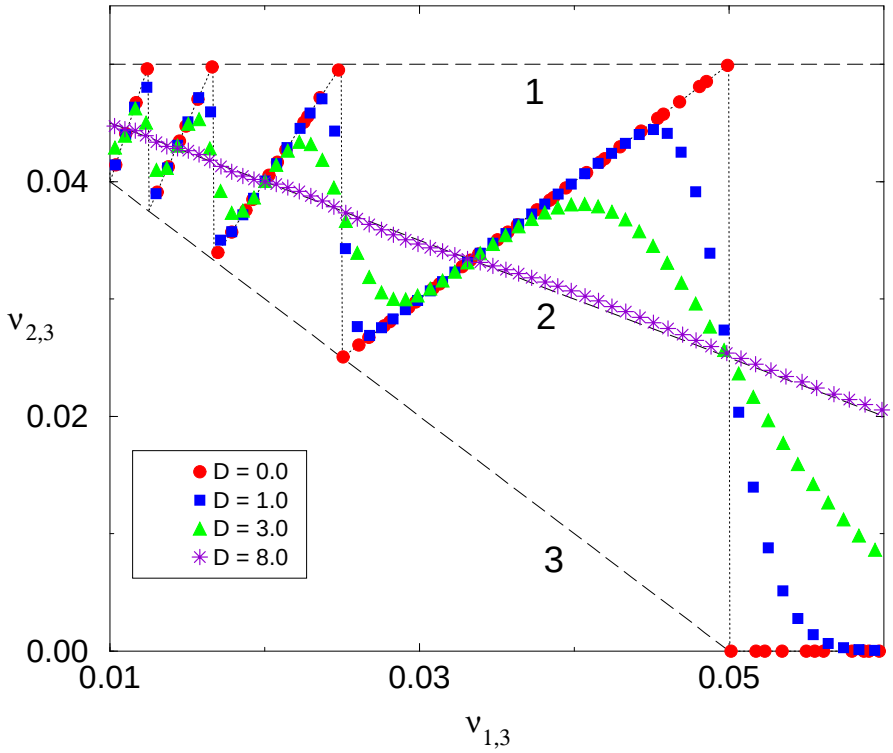

Figure 3.10: Simulated effect of noise modulated periodic main channel traffic. An increased noise strength D smoothes the discrete relation between the rates $\nu_{2,3}$ and $\nu_{1,3}$. For rates $\nu_{1,3}$ below the second mode, a noise enhancement for the overall traffic efficiency occurs. In the high noise limit the curve converges to the second mode from both sides.

To answer this question further simulations have been carried out using long range correlations in the $1/f^k$ noise with $k > 0$. The motivation for introducing $1/f^k$-like noise has been mentioned above and corresponds to a widely discussed occurrence of noise with $1/f^k$ or $1/f^k$-like spectra in various fields.

Figure 3.11 shows the D-dependent increase of the rate $\nu_{2,3}$ for a fixed value of $\nu_{1,3}$ for different values of the spectral exponent k. A faster convergence towards mode 2 for larger values of k, i.e, for longer correlations within the noise, can be observed. Note that a finite number of consecutive values of the generated fractal noise sequences have been averaged, which corresponds to a practical application in real situations.

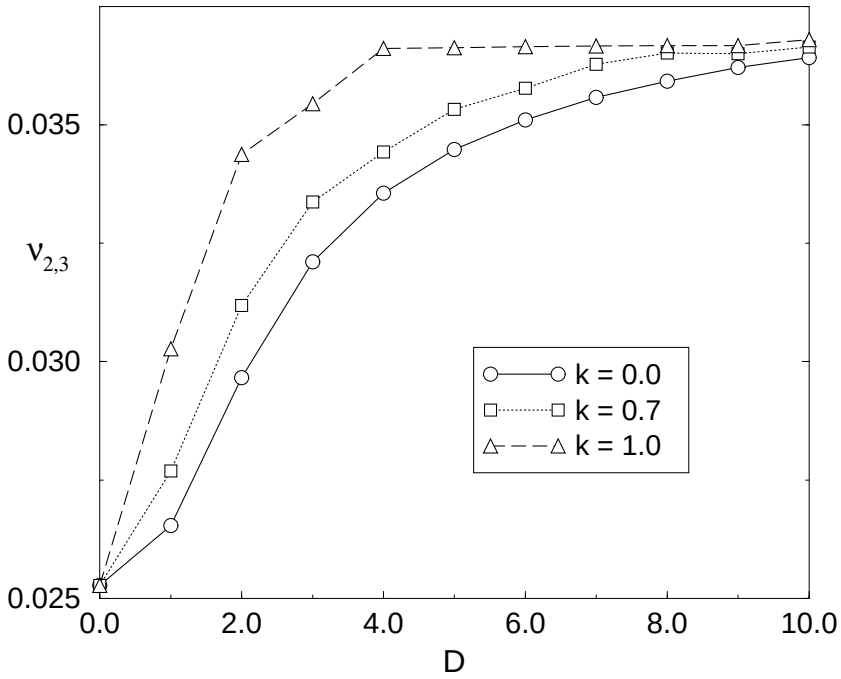

Figure 3.11: Simulated side channel (road) traffic rate $\nu_{2,3}$ as a function of the noise intensity D. The input traffic rate has been fixed at a value $\nu_{1,3} = 1/39 \approx 0.025$. An increased exponent k in the power spectrum of the applied noise leads to a faster growth of the traffic rate $\nu_{2,3}$ within the investigated parameter range. (Numerical units).

3.2 A Stochastic Data Packet Scheduling Algorithm

As an application of the results and ideas gained by the discussed neural spike and road traffic model, a stochastic scheduling algorithm for the flow control in data packet switching networks is suggested in the following. There are similar situations when there is traffic of different priorities as it has been in the previous case by

the introduction of a main and a side channel (road).

In the following an algorithm is developed which controls the flow of data packages of different priorities (or importance) through a network switch or router.

The switch decision between the fixed size data packages of different priorities is left over to stochastic processes with $1/f^k$-like spectral characteristics, in particular to the zero crossing events (ZCE's) of fractal (colored) noise. It will be shown that the tuning of the spectral parameter k allows to optimize the traffic throughput at the switch or router.

3.2.1 Scheduling algorithms

In order to provide "fair" packet scheduling one has to consider the fact that different classes of data traffic have an individual range of different performance requirements in terms of bandwidth, latency, jitter, correlations and others.

Real time video traffic requires higher bandwidth, low latency and low jitter. Voice traffic on the other hand requires lower bandwidth, low latency and low jitter. Interprocess communication in distributed computing handles small amounts of data sets and requires very low delay and small probabilities of data losses. Thus the timing of scheduling a data package has to be dependent on its priority. Some packages have to be allocated higher priorities than others.

All those classes demand their specific compromise between the individual *Quality of Service* (QoS) and an optimal utilization of the available transmission bandwidth. This has to be provided by the scheduling and routing algorithm of the server.

Often, scheduling algorithms are based on hierarchical ordering that allows some connections to receive guaranteed rate performance. One method is the *rate based scheduling* (RBS) procedure proposed in [185].

Rate based scheduling uses tree like structures to store packets awaiting their turn. The transmission to the output link occurs in frames or rounds of fixed size. The packets are queued in each round as singly linked lists and there is an array that points to the packets of each round. One of the round is the active one from

which packets are removed and transmitted. Whenever the server reaches the end of the list it moves on to the next round.

Rate control is achieved by assigning each connection a *service quantum* which fixes the number of packets of that connection to be sent per round. Jitter control is achieved by the fact that the rounds are kept of fixed size. The server will not insert a packet into an earlier round even if the earlier round is not full. This ensures that the jitter is no larger than the service quantum. *Round robin scheduling* is a modification of this method and has been proposed in [186]. It is suitable for the use in networks based on the *asynchronous transfer mode* (ATM). In ATM the data of a file or message to be transmitted are split up into small data packages of fixed size to be served by the switching device. The scheme is known under the name *hierarchical round robin scheduling* (HRRS).

In [186] the function of a round robin server has been described as follows. Data packages of fixed size coming from different connections are stored in corresponding buffers and its *connection identifier* (CID) is registered in a *service list*. The server then reads this list and processes the entries in descending order. Each process has a fixed duration and in case a file or message has not been transfered completely the corresponding CID is returned to the tail of the list. In that way some kind of *fairness* is guaranteed.

If the number of connections increases and the jitter becomes large, i.e., there is a large variation in the arrival of data, the buffer resources will not be fully utilized. Also, this scheme does not correspond to the different individual performance demands in terms of priorities as described above. Common in both, RPS and HRRS, is that data are transmitted in packets or frames of fixed sizes.

Thus it is suggested to additionally sort the data packets by their priorities into different connection buffers. The actual scheduling of the different priorities is then decided by a tunable stochastic process as proposed and described in Sec. 3.2.2.

3.2.2 A stochastic scheduling algorithm

In the HRRS based generic algorithm described above and used in ATM networks periodic, deterministic switching is provided in order to guarantee fairness for different connections of same priority. Using this method while serving connections or buffers with

different priorities, however, would not be adequate. Therefore a probabilistic switching which gives attention to the different priorities is suggested.

In [168] the ZCE's of Gaussian $1/f^k$ noise have been applied to trigger traffic in both neuronal junctions and road structures consisting of a main and a side road. Several stochastic processes have been tested there and it has been shown that, in certain cases, the Gaussian $1/f^k$ noise is superior in terms of maximizing the overall traffic. The optimal spectral exponent k has been found to be around unity. The reasons for applying such type of noise has been motivated by experimental evidence for fractal processes in traffic data of neural spikes and vehicles respectively.

Data packet switching networks like LAN's or the Internet reveal a number of fractal properties. $1/f$-like noise in packet density fluctuations in Internet computer network traffic has been reported, e.g., in [187] over a frequency range of 5 decades. Its importance to the modeling, design and control of broadband networks [188] and the implications to network performance in ATM switches have been discussed [30]. However, no attempt in designing a router scheduling algorithm that is itself based on a fractal stochastic process has been found in the literature.

Thus the author proposes the serving of data packages of different priorities to be triggered by the ZCE's of Gaussian $1/f^k$ noise where the exponent k is to be tuned in order to optimize a performance measure of the algorithm.

The scheduling algorithm works in the following way. Firstly, for the sake of simplicity, it is assumed that the data packages can be sorted into two classes of priorities ($p_1 \leq p_2$), described by priority exponents $p_i, i = 1, 2$, only. In case of a higher number of priority classes, the proposed scheme would have to be applied iteratively, aligning first p_1 to the highest class and p_2 to all the remaining ones and then repeat this scheme within the subclasses of p_2.

In case of equality $p_1 = p_2$, an alternating switching process would obviously be the most efficient one. However, to provide priority biased service the weights have to be different.

The idea is the following: Whenever there was one or more ZCE's during the processing of any package, the next package to be served shall be the one with the higher priority. Thus the (mean)

gap size between consecutive ZCE's will be the crucial value in this scheme. Since processors can do only one job at a time, the ZCE data set is checked after a packet is served. The binary sequence of the logicals of ZCE's (for different k) can to be stored on internal memory of the scheduling device in order to guarantee a fast algorithm. According to different acute network traffic conditions, k can then be adjusted in order to yield maximal performance. This approach is based on the results presented in [168] and has been termed spectral stochastic resonance.

Since we study the optimal throughput we have to assume that the individual buffers (queues) are sufficiently filled with data packets.

3.2.3 Performance measure

To measure the efficiency of the overall traffic the geometric mean has been used in [168]. This measure has the feature to be low in the case that any of the values to be averaged is small. This corresponds to the fairness principles in data switching where the optimal performance can not be achieved by serving only a selected buffer alone. Since we sorted the incoming data traffic by their different priorities it is also necessary to introduce a weighting of the resulting data transmission rates. The performance measure of the router scheduling algorithm with n priorities can hence be defined by

$$E_n \equiv \left(\prod_{i=1}^{n} v_i \right)^{\frac{1}{n}} \tag{3.8}$$

with the weighted rates

$$v_i = w_i^{p_i} \qquad . \tag{3.9}$$

Here, $w_i \leq 1$ are the transmission rates, i.e., the number of transmitted data packages of the priority class i per unit time. The p_i are the priority exponents which increase with the "importance" of the data package. They would be higher for real time video/audio streaming and smaller for, e.g., email transfer.

For the sake of simplicity one can consider the case n = 2 and hence

$$E_2 \equiv \sqrt{(w_1^{p_1} w_2^{p_2})} \qquad . \tag{3.10}$$

The basic properties of "fair" data traffic are satisfied:

$$w_{1/2} \to 0 \quad \Rightarrow \quad E_2 \to 0 \tag{3.11}$$
$$w_{1/2} \to w_{2/1} \quad \Rightarrow \quad E_2 < \mathrm{MAX}(E_2) \tag{3.12}$$
$$v_{1/2} \to v_{2/1} \quad \Rightarrow \quad E_2 \to \mathrm{MAX}(E_2) \quad . \tag{3.13}$$

Without the loss of generality we set $p_1 = 2$ and $p_2 = 1$ and assign a value of L time units for the processing of one package. Assuming sufficiently filled buffers, the maximal data transmission rate w_{max} then reads

$$w_{max} = w_1 + w_2 = 1/L \quad , \tag{3.14}$$

yielding a maximal performance

$$E_{max} = \sqrt{\frac{4}{27L^3}} \tag{3.15}$$

in our example at $w_1 = \frac{2}{3L}$ and $w_2 = \frac{1}{3L}$.

Alternatively, one may define a performance measure E_{alt} ranging from 0 (lowest performance) to 1 (highest performance) as the ratio of the geometric mean to the arithmetic one

$$E_{alt} \equiv \frac{(\prod_{i=1}^{n} v_i)^{\frac{1}{n}}}{\frac{1}{n}\sum_{i=1}^{n} v_i} \leq 1 \quad , \tag{3.16}$$

which, again, yields its maximum in the case that all weighted rates v_i are equal

$$v_1 = v_2 = .. = v_i = .. = v_n \quad . \tag{3.17}$$

This follows from the fact that the geometric mean is always less than or equal to the arithmetic mean.

3.2.4 Simulations and discussion

Numerical simulations have been carried out to study the setup described above. Sequences of Gaussian $1/f^k$ noise have been generated by utilizing the Fourier transform.

Firstly, uncorrelated sequences of (pseudo) random numbers (PRN's) have been produced by the linear congruential method

combined with a shuffling procedure that breaks up serial correlations to a considerable extent. The period of the PRN's was in the order of 10^{18}. Applying the Box-Muller method [184] to those uniformly distributed PRN's yielded Gaussian distributed uncorrelated PRN's modeling Gaussian white noise. Transforming the sequences to the Fourier space allowed us to manipulate the power spectral density by multiplying the sequences by the desired function. Applying the inverse Fourier transform using the (inverse) fast Fourier transform algorithm finally provided the Gaussian distributed correlated PRN's modeling Gaussian $1/f^k$ noise to be exploited by the algorithm.

Those sequences have then been analyzed in order to extract the discrete sequences of logicals consisting of 1's (ZCE) and 0's (no ZCE). These relatively small data sets would have to be stored on the local memory allowing a fast access for the switching decision to be made.

10 different logical sequences of 5×10^5 unit time steps each for 18 values of k equally spaced in the interval [0, 1.7] have been evaluated and the corresponding results of the performance measure Eq. 3.10 have been averaged. The plot $E(k)$ reveals a non-monotonous behavior of the performance while varying the spectral exponent k (see Fig. 3.12). The optimum occurs around $k = 0.8$ and is dependent on the data package size L, which can be scaled additionally. Thus, after defining the package length (respectively the unit time step), k can in practice be adjusted to maximize the efficiency of the algorithm and hence assist to optimize the network performance. A similar effect has been termed spectral stochastic resonance [168].

The plot in Fig. 3.12 displays a monotonous increase of the efficiency value up to an maximum of about $E = 0.0344$ and an asymptotic decrease towards the zero line for higher values of k. This simulation result very well agrees with the calculation of the maximal efficiency in Eq. 3.15. For large values of k, transmission of the packages of higher priority is more and more favored, leading to a disappearance of lower priority data packages and therewith a diminution of the overall efficiency.

The reason for this behavior is an interaction between the dependency of the gap size between consecutive ZCE's on the correlated noise process and the nonlinearity of Eq. 3.8. Fig. 3.13 displays

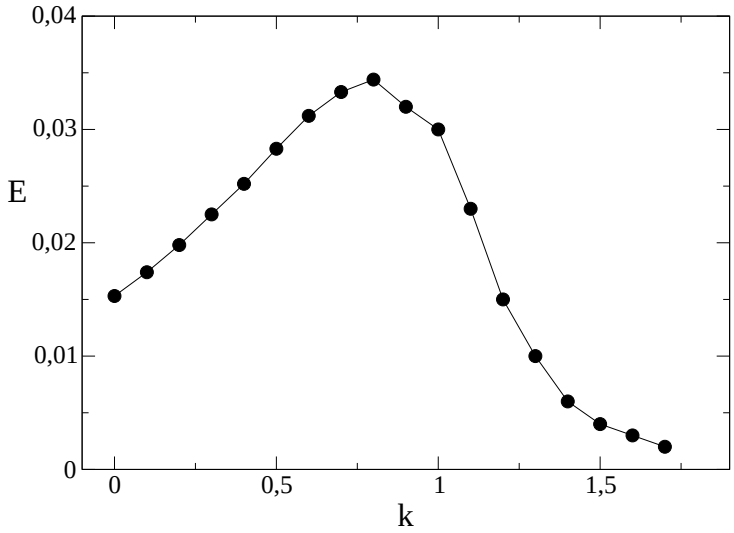

Figure 3.12: Simulated traffic efficiency E as a function of the spectral exponent k of the applied $1/f^k$ noise. An optimal switching decision of the algorithm is made around $k = 0.8$.

the simulated gap size distribution between two successive ZCE's for different values of k. Within the investigated interval, the gap size distribution of the ZCE's of the fractal noises seems to follow power laws. However, an analytic solution of the time distribution of the ZCE's for arbitrary k values is still an unsolved problem. The plot also reveals a higher probability for a fixed gap size to appear in case of larger values of the spectral exponent k. It implies a bigger mean gap size, i.e., a lower mean zero crossing rate for larger k. This can be seen in Fig. 3.14. The mean gap size between two consecutive ZCE's has been found to be a monotonously increasing function of the spectral exponent in the interval $0 < k < 1.7$ as a results of numerical simulations. Here one has to note that the finite simulations run into difficulties for $k > \approx 1.2$ due to the fractal character of the noise. This implies that the standard deviation of the statistics gained by averaging 50 mean gap values for each value of k advances to the same order of magnitude as the mean value itself (see Fig 3.14 B).

An investigation of higher k values became meaningless. In Fig. 3.14 A, the mean gap size including its standard deviation is plotted against k. As k is tuned towards larger values, the standard

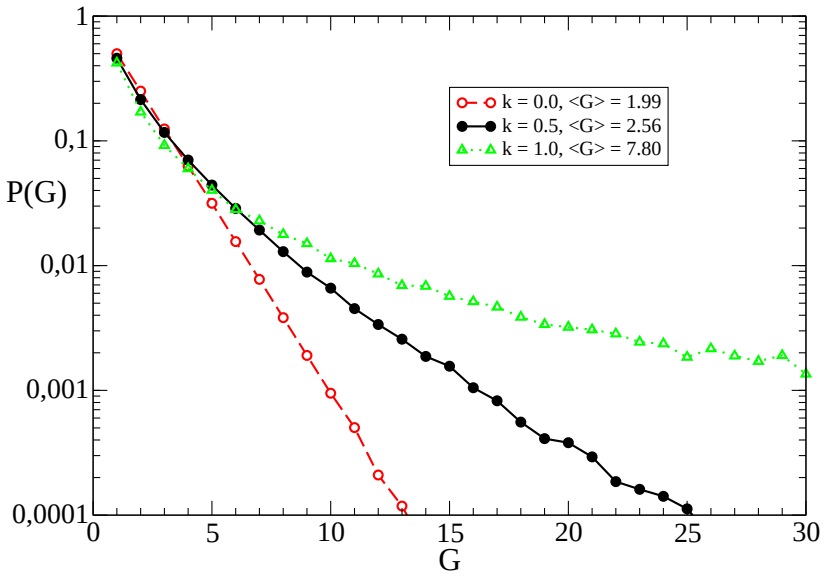

Figure 3.13: Probability distribution $P(G)$ of distance (gap size) G between consecutive zero crossing events of $1/f^k$ noise for selected values of k. The legend gives the respective mean values. For numerical parameter values see text.

deviation increases, as the mean gap size does. The noise reveals its fractal character more explicitly and approaches the zero line more seldom. These are the underlying reasons why this kind of stochastic processes can be used to trigger the scheduling in a correlated way and optimizes the presented algorithm.

There are publications on probabilistic and stochastic routing considering path selection [189] or the connectivity between edges in a complex computer network [190] often aiming at congestion studies and control. But no suggestions has been found to trigger the scheduling of a router as the traffic switching unit in a network by colored noise processes which embody the same fractal properties as the network and data packet traffic itself. The difficulty hereby is to identify the exact mechanisms leading to the fractal network properties and in finding the appropriate way of adjusting the switching units to it in order to optimize the efficiency and supply the required *Quality of Service*. For that, more detailed measures of the efficiency would have to be defined in further studies,

considering not only the different priorities of the individual data packages, but also the correlations between them. This method has a good scope for generalization. One can design stochastic engines which can be plugged into nonlinear decision making systems like routers and servers for maximizing some efficiency index. Thus it is worth investigating the introduction of correlated randomness in the multitasking decision making process.

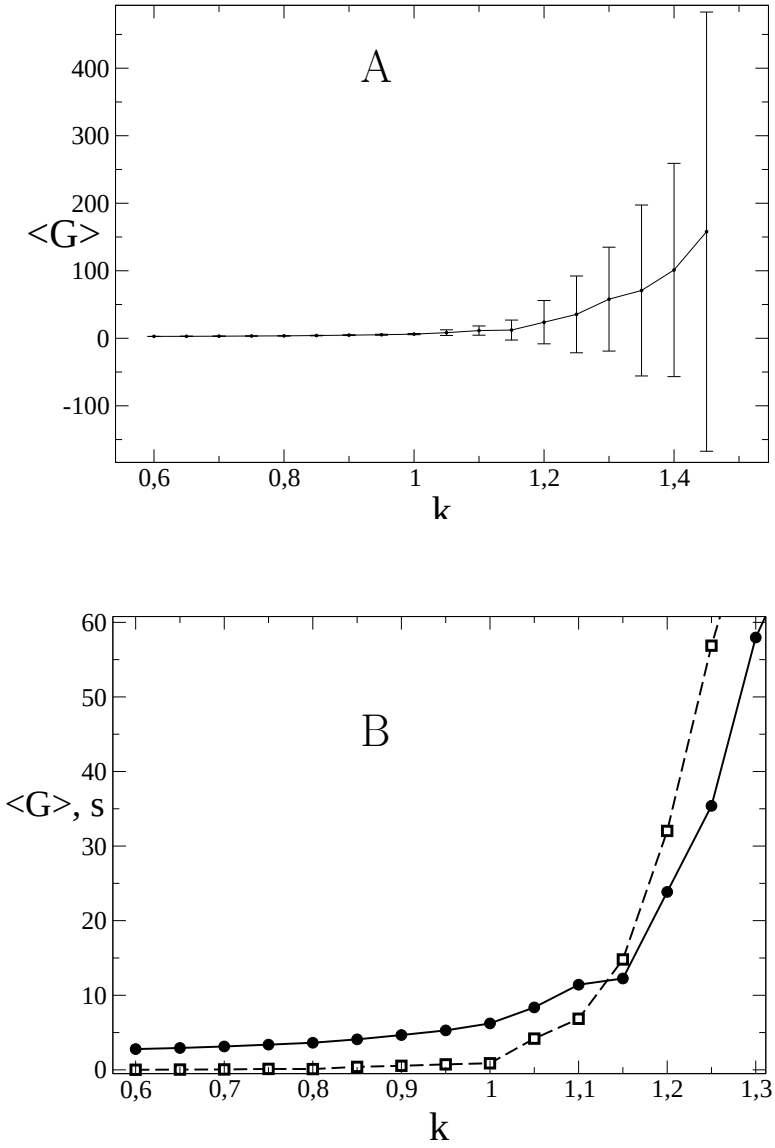

Figure 3.14: Mean gap size $\langle G \rangle$ (including standard deviation s) between consecutive zero crossing events of $1/f^k$ noise in dependence on the spectral parameter k. The standard deviation of the numerical statistics increase dramatically while increasing k and approaches the same value as the mean gap at $k \approx 1.1$, i.e., the dashed line indicating the standard deviation crosses the plot of the mean gap values itself (Fig. 3.14 B).

Chapter 4

SUMMARY & OUTLOOK

In this thesis, the question about *beneficial* properties of noise and fluctuations in Nature has been asked and positively answered in various kinds of systems, such as ferromagnetically coupled magnetic moments and domains or network switches like neuronal and road junctions and data network router algorithms. All systems have in common that they are nonlinear and that parameter variation of the applied noise, which is modeled as stochastic processes, enhances the quality of a transmitted signal.

In case of ferromagnetically coupled Ising spins, which are exposed to a weak, subthreshold periodic magnetic field and, additionally, Gaussian white magnetic noise, the phenomenon of array enhanced stochastic resonance has been demonstrated through numerical simulations. This phenomenon implies the possibility of an enhancement of the individual stochastic resonance (SR) effect through next-neighbors interaction of ferromagnetic type. The individual SR effect is evident through an increase of the signal-to-noise ratio (SNR) and the spectral power amplification of the power spectral density of the time dependent magnetic moment or spin value. Enhancing the bath temperature until an optimal temperature T_{opt}, as a measure of the noise intensity, synchronizes the dynamics of the individual spin with the periodic subthreshold signal. A further increase of the temperature above T_{opt} only annihilates this synchronization. But, through coupling of the above mentioned type, a further enhancement is still possible by tuning the coupling strength J until an optimal value J_{opt} is reached. It has been graphically and visually shown that for every value of J exists an T_{opt} and

for every value of T there exists an J_{opt}.

A similar effect has been demonstrated in the dynamic of a ferromagnetic stripe domain of a thin inhomogeneous magnetic film through numerical simulations and analytical calculations. The stripe domain is pinned at two locations and committed to a magnetic double-well potential. Further, the domain is driven by external magnetic Gaussian white noise and weak periodic magnetic fields. Thus the conditions for SR are given and the corresponding maximum behavior of the SNR has been shown both, numerically and analytically for two different types of double-well potentials.

The position of the maximum of the signal-to-noise ratio is shifted towards smaller noise values if the stiffness of the domain is increased. This is due to the fact that the barriers of the effective potential (2.45) gets smaller. This effect might be used for a measuring tool for the system's parameters.

An experimental verification of the results in Bi-doped epitaxial garnet-ferrite films should be possible. The parameters for such an investigation are provided in the thesis.

A future work could also focus on the application of colored noise to the ferromagnetic domain and a possible enhancement of the SR effect. The investigation may have impact on magnetic storage devices and/or the detection of weak magnetic signals.

Further-on, it is shown that noise, i.e., random fluctuations, can enhance the traffic flow in a model of a junction of neural and/or road traffic. Periodic arrangements do not always provide the optimal throughput efficiency, but stochastic triggering or modulation can be essential. This might provide the possibility to enhance the traffic efficiency in real networks which can be described by the presented model.

It is shown that traffic flows generated by $1/f^k$ noises have superior properties over Poissonian noise and, in certain cases, over periodic cases too. The best properties are achieved around $k = 1$. This fact is in an intriguing coincidence with the general occurrence of $1/f$-like noise phenomena in neural activity, highway car traffic and other complex networks.

Although this model favors this kind of noise in terms of efficiency, the question about the reasons of its appearance in real net-

works like neural or road systems is still an open one. A complete analysis of the "microscopic" mechanisms in both neural activity and car traffic which should reveal the reasons for the macroscopically observed $1/f$-like spectra remains to be done.

As a potential application of the traffic results, a stochastic scheduling algorithm for data network switches has been proposed. The algorithm is based on the stochastic process of zero crossings of $1/f^k$-noise. Thus the switch decision is not deterministic anymore, but based on similar random and fractal properties as the network topology itself reveals. For an efficiency measure, which includes the rate of transmitted data packages only, a tuning of the spectral parameter k is shown to optimize the throughput of the switch.

A future work could aim to apply the ideas to existing network algorithm which would have to consider other performance measures as well.

ACKNOWLEDGMENTS

I would like to express my thanks to all the people having supported me in my research. Above all of them my supervisors Prof. Laszlo B. Kish, Prof. Claes-Göran Granqvist and Prof. Lutz Schimansky-Geier for their kind support and their scientific inspiration. I am deeply grateful for the aid I have received from the Division of Solid State Physics of the Department of Engineering Sciences of Uppsala University.

I would also like to thank the Swedish Research Council (formerly Naturvetenskapliga Forskningsrådet (NFR), now Vetenskapsrådet) for financial support of our project with the title: "Stochastic Resonance and Signal Transfer in Systems of Coupled Neurons" ("Stokastisk resonans och signalöverföringar i system av kopplade neuroner"), grant number (dnr): 2524/1999.

Peter S. Hammerstein

BIBLIOGRAPHY

[1] R.C. Hilborn and N.B. Tufillaro, in *Resource Letter: ND-1: Nonlinear Dynamics*, edited by R.H. Stuewer, Am. J. Phys. **65**, 822 (1997).

[2] G. Duffing, *Erzwungene Schwingungen bei Veränderlicher Eigenfrequenz* (Vieweg & Sohn, Braunschweig, 1918).

[3] B. van der Pol, Philos. Mag. **7**, 978 (1926).

[4] M. Feigenbaum, J. Stat. Phys. **19**, 25 (1978).

[5] M. Feigenbaum, J. Stat. Phys. **21**, 669 (1979).

[6] H. Haken and R. Graham, Umschau **6**, 191 (1971).

[7] H. Haken, *Synergetics. An Introduction. Nonequilibrium Phase Transitions in Physics, Chemistry and Biology* (Springer, Berlin, 1978).

[8] M. H. Jensen, L. Kadanoff, A. Libchaber, I. Proccacia, and J. Stavans, Phys. Rev. Lett. **55**, 2798 (1985).

[9] E.N. Lorenz, J. Atmos. Sci **20**, 130 (1963).

[10] A. M. Zhabotinsky, Chaos **1**, 379 (1991).

[11] E.P. Odum, *Fundamentals of Ecology* (Saunders, 1953).

[12] R. Devaney, *An Introduction to Chaotic Dynamical Systems* (Addison Wesley, Redwood City, 1989).

[13] H. Peitgen, H. Jürgens, and D. Saupe, *Chaos and Fractals: New Frontiers of Science* (Springer, 1992).

[14] A.A. Markoff, *Wahrscheinlichkeitsrechnung* (Teubner, Leipzig and Berlin, 1912).

[15] N.G. van Kampen, *Stochastic Processes in Physics and Chemistry* (North-Holland, Amsterdam, 1981).

[16] T.M. Heskes and B. Kappen, Phys. Rev. A **44**, 2726 (1991).

[17] F. Chapeau-Blondeau, X. Godivier, and N. Chambet, Phys. Rev. E **53**, 1273 (1995).

[18] H. Risken, *The Fokker-Planck Equation: Methods of Solution and Applications* (Springer, 1996).

[19] N. Wiener, Acta Math. **55**, 117 (1930).

[20] A. Khintchine, Math. Ann **109**, 604 (1934).

[21] B.B. Mandelbrot, *Multifractals and 1/f Noise: Wild Self-Affinity in Physics* (Springer, 1999).

[22] L.B. Kiss, Rev. Solid State Science **2**, 659 (1988).

[23] M.S. Keshner, Proc. IEEE **70**, 212 (1982).

[24] Sh. M. Kogan, Sov. Phys. Usp. **26**, 170 (1985).

[25] A.P. Dmitriev, E. Borovitskaya, M.E. Levinshtein, S.L. Rumyantsev, and M.S. Shur, J. Appl. Phys. **90**, 301 (2001).

[26] M.E. Levinshtein, Physica Scripta **69**, 79 (1997).

[27] Sh. Kogan, *Electronic Noise and Fluctuations in Solid* (Cambridge University Press, Cambridge, 1996).

[28] P. Refregier, M. Ocio, and H. Bouchiat, Europhys. Lett. **3**, 503, (1987).

[29] H. Hayakawa and K. Nakanishi, Progress of Theor. Phys. (suppl.) **130**, 57 (1998).

[30] Z. Sahinoglu and S. Tekinay, IEEE Comm. Mag. **37**, 48 (1999).

[31] H. Fujii, K. Aya, and K. Shima, Medical and Biological Engineering and Computing, (suppl.) **29**, 1103 (1991).

[32] B.J.W. Fleming, D. Yu, R.G. Harrison, and D. Jubb, Eur. Phys. J. B **20**, 543 (2001).

[33] L.B. Kiss and J. Hajdu, Solid State Commun. **72**, 799 (1989).

[34] J. Machta, M. Nelkin, Th.M. Nieuwenhuizen, and M.H. Ernst, Phys. Rev. B **31**, 7636 (1985).

[35] L. Schimansky-Geier, J. Freund, A. Neiman, and B. Shulgin, Intern. Journal of Bifurc. and Chaos **8**, 869 (1998).

[36] A.A. Zaikin, J. Garcia-Ojalvo, L. Schimansky-Geier, and J. Kurths, Phys. Rev. Lett. **88**, 010601 (2002).

[37] L.Q. Zhou, X. Jia, and Q. Ouyang, Phys. Rev. Lett. **88**, 138301 (2002).

[38] H. Hempel, L. Schimansky-Geier, and J.Garcia-Ojalvo, Phys. Rev. Lett **82**, 3718 (1999).

[39] M.A. Santos and J.M Sancho, Phys. Rev E **59**, 98 (1999).

[40] H. Zhonghuai, Y. Lingfa, X. Zuo, and X. Houwen, Phys. Rev. Lett. **81**, 2854 (1998).

[41] A.A. Zaikin and L. Schimansky-Geier, Phys. Rev. E **58**, 4355 (1998).

[42] M. Santos, Ch. Zuelicke, and L. Schimansky-Geier, Phys. Lett. A **290**, 270 (2001).

[43] S. Kadar, J. Wang, and K. Showalter, Nature **391**, 770 (1998).

[44] B. Lindner, L. Schimansky-Geier, P. Reimann, and P. Hänggi APS Conf. Proc. **411**, "Applied Nonlinear Dynamics and Stochastic Systems Near the Millennium", edited by J.B. Kadtke and A. Bulsara, pp. 309-314 (AIP, Woodbury, New York, 1997).

[45] R. Bartussek, P. Hänggi, B. Lindner, and L. Schimansky-Geier, Physica D **109**, 17 (1997).

[46] B. Lindner, L. Schimansky-Geier, P. Reimann, P. Hänggi, and M. Nagaoka, Phys. Rev. E **59**, 1417 (1999).

[47] L. Schimansky-Geier, S. Seefeld, and V. Buchholtz, Ann. Phys. **9**, 705 (2000).

[48] J.-D. Bao, Phys. Lett A **265**, 244 (2000).

[49] L.B. Kish, G.P. Harmer, and D. Abbott, Fluct. Noise Lett. **1**, 13 (2001).

[50] Z. Gingl, L.B. Kiss, and F. Moss, Europhys. Lett. **29**, 191 (1995).

[51] S.M. Bezrukov and I. Vodyanoy, Nature **385**, 319 (1997).

[52] D.G. Luchinsky and P.V.E. McClintock, Nature **389**, 463 (1997).

[53] J.M.G. Vilar, G. Gomila, and J.M. Rubi, Phys. Rev. Lett. **81**, 14 (1998).

[54] M.E. Inchiosa, A.R. Bulsara, A.D. Hibbs, and B.R. Whitecotton, Phys. Rev. Lett. **80**, 1381 (1998).

[55] M. DeWeese and W.Z. Bialek, Nuovo Cimento **17D**, 733 (1995).

[56] P.N. Narins, Nature **410**, 644 (2001).

[57] J.J. Collins, C.C. Chow, and T.T. Imhoff, Nature **376**, 236 (1995).

[58] J.J. Collins, Nature **402**, 241 (1999).

[59] D.F. Russell, L.A. Wilkens, and F. Moss, Nature **402**, 291 (1999).

[60] B. Suki, A.M. Alencar, M.K. Sujeer, K.R. Lutchen, J.J. Collins, J.S. Andrade, E.P. Ingenito, S. Zapperi, and H.E. Stanley, Nature **393**, 127 (1998).

[61] M.I. Dykman and P.V.E. McClintock, Nature **391**, 344 (1998).

[62] R.D. Astumian, R.K. Adair, and J.C. Weaver, Nature **388**, 632 (1997).

[63] S.M. Bezrukov and I. Vodyanoy, Nature **378**, 362 (1995).

[64] K. Wiesenfeld and F. Moss, Nature **373**, 33 (1995).

[65] C.V. Rao, D.M. Wolff, and A.P. Arkin, Nature 420, 231 (2002).

[66] H. Liljenström, Neuropsychopharmacology **28**, 64 (2003).

[67] M.T. Huber, H.A. Braun, and J.-C. Krieg, Neuropsychopharmacology **28**, 13 (2003).

[68] F. Moss and J.G. Milton, Nature **425**, 911 (2003).

[69] M. Volgushev and U.T. Eysel, Science **290**, 1908 (2000).

[70] R.A. Kerr, Science **290**, 697 (2000).

[71] J. Glanz, Science **277**, 1759 (1997).

[72] B. McNamara and K. Wiesenfeld, Phys. Rev. A **39**, 4854 (1989).

[73] R. Benzi, A. Sutera, and A. Vulpiani, J. Phys. A **14**, 453 (1981).

[74] R. Benzi, G. Parisi, A. Sutera, and A. Vulpiani, Tellus **34**, 10 (1982).

[75] S. Fauve and F. Heslot, Phys. Lett. A **97**, 5 (1983).

[76] B. McNamara, K. Wiesenfeld, and R. Roy, Phys. Rev. Lett. **60**, 2626 (1988).

[77] L. Gammaitoni, P. Hänggi, P. Jung, and F. Marchesoni, Rev. Mod. Phys. **70**, 223 (1998).

[78] J.J. Collins, C.C. Chow, and T.T. Imhoff, Phys. Rev. E **52**, R3321 (1995).

[79] K. Loerincz, Z. Gingl, and L.B. Kiss, Phys. Lett. A **224**, 1 (1996).

[80] F. Chapeau-Blondeau and X. Godivier, Phys. Rev. E **55**, 1478 (1997).

[81] I.E. Dikshtein, N.I. Polzikova, D.V. Kuznetsov, and L. Schimansky-Geier, J. Appl. Phys. **90**, 5425 (2001).

[82] P. Ruszczynski[1] L. Schimansky-Geier, and I. Dikshtein, Eur. Phys. J. B **14**, 569 (2000).

[83] A. Neiman, L. Schimansky-Geier, and F. Moss, Phys. Rev. E **56**, R9 (1997).

[84] A.R. Bulsara and A. Zador, Phys. Rev. E **54**, R2185 (1996).

[85] A. Neiman, F. Moss, L. Schimansky-Geier, and W. Ebeling APS Conf. Proc. **411**, "Applied Nonlinear Dynamics and Stochastic Systems Near the Millennium", edited by J.B. Kadtke and A. Bulsara, pp. 151-156 (AIP, Woodbury, New York, 1997).

[86] A. Neiman and L. Schimansky-Geier, Phys. Rev. Lett. **72**, 2988 (1994).

[87] P. Ruszczynski[1], *Pattern Analysis with Stochastic Resonance* (in German) Diplomathesis, supervisor: L. Schimansky-Geier, (Library of the Institute of Physics, Humboldt University of Berlin, Germany, 1998).

[88] C. Berghaus, A. Hilgers, and J. Schnakenberg, Z. Phys. B **100**, 157 (1996).

[89] P. Hänggi, P. Jung, C. Zerbe, and F. Moss, J. Stat. Phys. **70**, 25 (1993).

[90] P. Makra, Z. Gingl, and T. Fülei, Phys. Lett. A **317**, 228 (2003).

[91] D. Nozaki and Y. Yamamoto, Phys. Lett A **243**, 281 (1998).

[92] F. Apostolico, L. Gammaitoni, F. Marchesoni, and S. Santucci, Phys. Rev. E **55**, 36 (1997).

[1] now: Hammerstein

[93] N.G. Stocks, Phys. Rev. Lett. **84**, 2310 (2000).

[94] S. Bezrukov and I. Vodyanoy, in *Unsolved Problems of Noise and Fluctuations*, edited by D. Abbott and L. Kiss, AIP Conf. Proc. No. 511 (AIP, New York, 1999).

[95] B. Kosko and S. Mitaim, Phys. Rev. E **64**, 051110 (2001).

[96] D.R. Chivalo, A. Longtin, and L. Müller-Gerking, Phys. Rev. E **55**, 1798 (1997).

[97] A.A. Zaikin, K. Murali, and J. Kurths, Phys. Rev. E **63**, 020103 (2001).

[98] R. Löfstedt and S.N. Coppersmith, Phys. Rev. Lett. **72**, 1947 (1994).

[99] H.H. Adamyan, S.B. Manvelyan, and G.Yu. Kryuchkyan, Phys. Rev. A **63**, 022102 (2001).

[100] P. beim Graben, Phys. Rev. E **64**, 051104 (2001).

[101] Z. Liu and Y.-C. Lai, Phys. Rev. Lett. **86**, 4737 (2001).

[102] A. Pikovsky, A. Zaikin, and M.A. de la Casa, Phys. Rev. Lett. **88**, 050601 (2002).

[103] J.F. Lindner, S. Chandramouli, A.R. Bulsara, M. Löcher, and W.L. Ditto, Phys. Rev. Lett. **81**, 5048 (1998).

[104] N.G. Stocks and R. Mannella, Phys. Rev. E **64**, 030902 (2001).

[105] Y. Shim, H. Hong, and M.Y. Choi, Phys. Rev. E **65**, 036114 (2002).

[106] Z. Neda, Phys. Rev. E **51**, 5315 (1995).

[107] S.W. Sides, P.A. Rikvold, and M.A. Novotny, Phys. Rev. E **57**, 6512 (1998).

[108] U. Siewert and L. Schimansky-Geier, Phys. Rev. E **58**, 2843 (1998).

[109] L. Gammaitoni, M. Martinilli, L. Pardi, and S. Santucci, Phys. Rev. Lett. **67**, 1799 (1991).

[110] L. Gammaitoni, F. Marchesoni, M. Martinelli, L. Pardi, and S. Santucci, Phys. Lett. A **158**, 449 (1991).

[111] D. Gourier and D. Gerbault, Phys. Rev. B **57**, 2679 (1998).

[112] A.B. Hibbs, A.L. Singsaas, E.W. Jacobs, A.R. Bulsara, J.J. Bekkedahl, and F. Moss, J. Appl. Phys. **77**, 2582 (1995).

[113] R. Rouse, S. Han, and J.E. Lukens, Appl. Phys. Lett. **66**, 108 (1995).

[114] R.N. Mantegna and B. Spagnolo, Phys. Rev. E **49**, R1792 (1994).

[115] R.N. Mantegna, B. Spagnolo, and M. Trapanese, Phys. Rev. E **63**, 011101 (2000).

[116] A. Fioretti, L. Guidoni, R. Mannella, and E. Arimondo, J. Stat. Phys. **70**, 403 (1993).

[117] J.M. Iannelli, A. Yariv, T.R. Chen, and Y.H. Zhuang, Appl. Phys. Lett. **65**, 1983 (1994).

[118] O.G. Calderón, Phys. Rev. E **63**, 016502 (2000).

[119] A.N. Grigorenko and P.I. Nikitin, JETP Lett. **52**, 593 (1990).

[120] A.N. Grigorenko, P.I. Nikitin, A.N. Slavin, and P.Y. Zhou, J. Appl. Phys. **76**, 6335 (1994).

[121] A.N. Grigorenko and P.I. Nikitin, Appl. Surf. Sci. **92**, 466 (1996).

[122] I. Dikshtein, A. Neiman, and L. Schimansky-Geier, JMMM **188**, 301 (1998).

[123] I. Dikshtein, A. Neiman, and L. Schimansky-Geier, Phys. Lett. A **246**, 259 (1998).

[124] D. Rousseau, J.R. Varela, and F. Chapeau-Blondeau, Phys. Rev. E **67**, 021104 (2003).

[125] H. Busch and F. Kaiser, Phys. Rev. E **67**, 041105 (2003).

[126] J.P. Sharpe, N. Sungar, M. Swaney, K. Carrigan, and S. Wheeler, Phys. Rev. E **67**, 056222 (2003).

[127] R. Stoop, J. Buchli, G. Keller, and W.-H. Steeb, Phys. Rev. E **67**, 061918 (2003).

[128] D. Rousseau, F. Duan, and F. Chapeau-Blondeau, Phys. Rev. E **68**, 031107 (2003).

[129] I. Rabbiosi, A.J. Scroggie, and G. L. Oppo, Phys. Rev E **68**, 036602 (2003).

[130] A. Krawiecki and T. Stemler, Phys. Rev. E **68**, 061101 (2003).

[131] P. Chvosta and P. Reinecker, Phys. Rev. E **68**, 066109 (2003).

[132] F. Duan, D. Rousseau, and F. Chapeau-Blondeau, Phys. Rev. E **69**, 011109 (2004).

[133] I. Goychuk and P. Hänggi, Phys. Rev. **69**, 021107 (2004).

[134] A. Samoletov, M. Chaplain, and V. Levi, Phys. Rev. E **69**, 045102 (2004).

[135] F.J. Himpsel, Y. W. Mo, T. Jung, J. E. Ortega, G. J. Mankey, and R. F. Willis, Superlattices Microstruct. **15**, 237 (1994).

[136] H.J. Elmers J. Hauschild, H. Höche, U. Gradmann, H. Bethge, D. Heuer, and U. Köhler, Phys. Rev. Lett. **73**, 898 (1994).

[137] H.J. Elmers, J. Hauschild, and U. Gradmann, *Conference Digest of 15th International Colloquium on Magnetic Films and Surfaces (ICMFS'97)*, (Queensland, Australia, 1997).

[138] S.A. Gusev, N.A. Korotkova, D.B. Rozenstein, and A.A. Fraerman, J. Appl. Phys. **76**, 6671 (1994).

[139] K. Koike, H. Matsuyama, and K. Hayakawa, Scanning Microsc. Suppl. **1**, 241 (1987).

[140] M.R. Scheinfein, J. Unguris, M.H. Kelley, D.T. Piers, and R.J. Cellota, Rev. Sci. Instrum. **61**, 2501 (1990).

[141] H. Siegmann, J. Phys. Cond. Matter **4**, 8395 (1992).

[142] D.P. Pappas, K.-P. Kamper, B.P. Miller, H. Hopster, D.E. Fowler, C.R. Brundle, A.C. Luntz, and Z.-X. Shen, Phys. Rev. Lett. **66**, 504 (1991).

[143] M. Doi and S.F. Edwards, *The Theory of Polymer Dynamics* (Clarendon, Oxford, 1986).

[144] J. Friedel, *Dislocations* (Addison-Wesley, 1964).

[145] G. Blatter, M.V. Feigelman, V.B. Geshkenbein, A.I. Larkin, and V.M. Vinokur, Rev. Mod. Phys. **66**, 1125 (1994).

[146] E.H. Brandt, Rep. Prog. Phys. **58**, 1465 (1995).

[147] A.S. Mikhailov, L. Schimansky-Geier, and W. Ebeling, Phys. Lett. A **96**, 453 (1983).

[148] A.C.H. Rowe and P. Etchegoin, Phys. Rev. E **64**, 031106 (2001).

[149] A.P. Malozemoff and J.C. Slonczewski, *Magnetic Domain Walls in Bubble Materials* (Acad. Press, 1979).

[150] A.M. Bobeck, Bell System Tech. J. **46**, 1901 (1967).

[151] G.J. Zimmer, L. Gal, and F.B. Hamphry, J. App. Phys **48**, 362 (1977).

[152] V.L. Dorman, V.L. Sobolev, A.L. Sukstanskii, and N.E. Shishkova, Sov. Tech. Phys. Lett. **11**, 1058 (1085).

[153] V.D. Stasovskii, *Digest of 17th All-Union Conference on Physics of Magnetic Phenomena* (Donetsk, 1985).

[154] A.N. Grigorenko, P.I. Nikitin, and G.V. Roshchepkin, Zh. Eksp. Teor. Fiz. **112**, 628 (1997).

[155] T.H. O'Dell, *Ferromagnetodynamics* (Maximillian Press, 1981).

[156] S.V. Gerus, F.V. Lisovskii, and E.G. Mansvetova, Sov. Microelectronics **10**, 506 (1981).

[157] F. Rousseaux, D. Decanini, F. Carcecae, E. Cambril, M.F. Ravet, C. Chappert, N. Bardou, B. Bartenlian, and P. Vallet, J. Vac. Sci. Technol. B **13**, 2787 (1995).

[158] J.P. Omaggio and P.E. Wigen, J. Appl. Phys. **50**, 2264 (1979).

[159] L.E. El'sgoltz, *Differential Equations and Variational Calculus*, in Russian (Nauka, Moscow, 1969).

[160] G.H. Weiss and A.A. Maradudin, Operations Research **10**, 74 (1962).

[161] D.C. Gazis (editor), *Traffic Science* (John Wiley & Sons, 1974).

[162] D.W. Harwood, J.M. Mason, and R.E. Brydia, Transportation-Research **33A**, 199 (1999).

[163] K. Konishi, H. Kokame, and K. Hirata, Phys. Rev. E **60**, 4 (1999).

[164] D. Chowdhury and A. Schadschneider, Phys. Rev. E **59**, 2 (1999).

[165] T. Nagatami, Phys. Rev. E **61**, 4 (2000).

[166] L. Neubert, L. Santen, A. Schadschneider, and M. Schreckenberg, Phys. Rev. E **60**, 6480 (1999).

[167] T. Nagatami, Phys. Rev. E **60**, 6395 (1999).

[168] L.B. Kish and S.M. Bezrukov, Phys. Lett. A **266**, 271 (2000).

[169] P.S. Ruszczynski[1] and L.B. Kish, Phys. Lett. A **267**, 187 (2000).

[170] P.S. Ruszczynski[1], L.B. Kish, and S.M. Bezrukov, Chaos **11**, 581 (2001).

[1] now: Hammerstein

[171] M. London, A. Schreibman, M. Häusser, M.E. Larkum, and I. Segev, Nature *Neuroscience* **5**, 332 (2002).

[172] T. Musha and H. Higuchi, Jpn. J. Appl. Phys. **15**, 1271 (1976).

[173] S.O. Rice, Bell. Syst. Tech. J. **23**, 282 (1944).

[174] S.O. Rice, Bell. Syst. Tech. J. **24**, 46 (1945).

[175] B. Kedem, *Time Series Analysis by Higher Order Crossings* (IEEE, New York, 1994).

[176] Ch.R. Doering, in *Unsolved Problems of Noise*, edited by Ch.R. Doering, L.B. Kiss, and M.F. Shlesinger (World Scientific, New York, 1997).

[177] S.M. Bezrukov, same as [176].

[178] T. Musha and M. Yamamoto, in *Noise in Physical Systems and 1/f Fluctuations*, edited by V. Bareikis and R. Katilius (World Scientific, New York, 1995).

[179] M. Nakao, T. Takahashi, Y. Mizutani, and M. Yamamoto, Biol. Cybernetics **63**, 243 (1990).

[180] M. Usher, M. Stemmler, and Z. Olami, Phys. Rev. Lett. **74**, 326 (1995).

[181] D. Nozaki, J.J. Collins, and Y. Yamamoto, Phys. Rev. E **60**, 4 (1999).

[182] P. Wagner and J. Peinke, Zeitschrift für Naturforschung (A: Physical Sciences) **52**, 8 (1997).

[183] Y.Q. Chen, M.Z. Ding, and J.A.S. Kelso, Phys. Rev. Lett. **79**, 22 (1997).

[184] *Numerical Recipes in C: The Art of Scientific Computing*, (Cambridge University Press, 1992).

[185] H. Kanakia, AT&T Bell Laboratories internal memorandum, (see also [186]).

[186] C.R. Kalmanek, H. Kanakia, and S. Keshav, IEEE GLOBECOM'90 **1**, 12 (1990).

[187] M. Takayasu, H. Takayasu, and S. Takamitsu, Physica A **233**, 824 (1996).

[188] B. Tsybakov and N.D. Georganas, IEEE/ACM Transactions on Networking **5**, 397 (1997).

[189] T. Ohira and R. Sawatari, Phys. Rev E **58**, 193 (1998).

[190] K.-I. Goh and D. Kim, Phys. Rev. Lett **88**, 108701-1 (2002).

APPENDIX

A.1 Stiff and flexible ferromagnetic stripe domains

The stationary solutions (2.24) and (2.25) can be substantially simplified in the limiting cases of flexible of stiff domains.

a) In the case of the first potential, we have

$$y(x) = \pm B \begin{cases} \tanh(\frac{x}{x_0}) & \text{for } 0 < x < l/2 \\ \tanh(\frac{l-x}{x_0}) & \text{for } l/2 < x < l \end{cases} \tag{4.1}$$

with

$$B = \sqrt{\frac{a}{b}} \left[1 - 4 \exp\left(-\frac{l}{\tilde{x}_0} \right) \right] \tag{4.2}$$

and the other parameters given by

$$\begin{aligned} k &= 1 - 8 \exp\left(-\frac{l}{\tilde{x}_0} \right) \ , \\ d &= 8a \exp\left(-\frac{l}{\tilde{x}_0} \right) \ , \\ x_0 &= \tilde{x}_0 \left[1 - 4 \exp\left(-\frac{l}{\tilde{x}_0} \right) \right] \end{aligned}$$

for a flexible domain

$$l \gg \tilde{x}_0 \equiv \sqrt{\frac{2H_0}{a}}$$

and N = 1. For a stiff domain

$$l \cong x_{c1} \equiv \pi \sqrt{\frac{H_0}{a}}$$

one gets

$$y(x) = \pm B \sin\left(\frac{x}{x_0}\right) \quad , \tag{4.3}$$

with

$$B = \sqrt{\frac{2a}{b}} k \left(1 - \frac{k^2}{2}\right) \quad ,$$

whereby

$$k = \sqrt{\frac{4}{3}\left(\frac{l}{x_{cl}} - 1\right)} \left[1 - \frac{1}{8}\left(\frac{l}{x_{c1}} - 1\right)\right] \quad ,$$

$$d = a(1 - 2k^2 + 2k^4)$$

and

$$x_0 = \frac{l}{\pi}\left(1 - \frac{k^2}{4} - \frac{5}{64}k^4\right) \quad .$$

In this case, a domain can become curved for $l \geq x_{c1}$, only.

b) In the case of the second potential, the stationary solution can be approximated by

$$y(x) = \pm b \begin{cases} \frac{x}{l_0}\left[1 - \frac{x}{2l_0} - 2\exp\left(-\frac{l}{l_0}\right)\right] & \text{(a)} \quad , \\ 1 - \exp\left(-\frac{x}{l_0}\right) - \exp\left(-\frac{l-x}{l_0}\right) & \text{(b)} \quad , \\ \frac{l-x}{l_0}\left[1 - \frac{l-x}{2l_0} - 2\exp\left(-\frac{l}{l_0}\right)\right] & \text{(c)} \quad , \end{cases} \tag{4.4}$$

for a flexible domain ($l \gg l_0$) and where the three cases are for (a): $x < l_0$, (b): $x > l_0$ and $l - x > l_0$ and (c): $l - x < l_0$, respectively.

For a stiff domain ($l \ll l_0$) we get

$$y(x) = \pm bx(l - x)/l_0^2 \quad . \tag{4.5}$$

A.2 Coefficients for Section 2.4.4

1. For the first potential we have obtained

$$\begin{aligned} S_1 &= \frac{2aB^2l}{3k^2}\left[\frac{2+k^2}{1+k^2} - \frac{4x_0}{l}E(k)\right] \quad , \\ S_2 &= \frac{bB^4l}{3k^4}\left[2+k^2 - \frac{4x_0}{l}(l+k^2)E(k)\right] \quad , \\ S_3 &= \frac{x_0B}{k}\ln\frac{1+k}{1-k} \quad , \\ \Lambda^{(1)} &= 2\rho\lambda\frac{B^2l}{k^2}\left(1 - \frac{2x_0}{l}E(k)\right) \end{aligned} \tag{4.6}$$

with $E(k)$ being the complete elliptic function.

2. For the second potential we have obtained

$$\begin{aligned} C_1 &= C_2 = ab^2l\left(1 - \frac{2l_0}{l}\tanh\left(\frac{l}{2l_0}\right)\right) \quad , \\ C_3 &= \frac{C_1}{ab} \quad , \\ \Lambda^{(2)} &= 2\rho\lambda b^2l\left(1 + \frac{1}{2}\mathrm{sech}^2\left(\frac{l}{2l_0}\right) - \frac{3l_0}{l}\tanh\left(\frac{l}{2l_0}\right)\right) \quad . \end{aligned}$$

A.3 SNRs in the limit of stiff and flexible domains

With the estimations given in the Appendix, corresponding limiting values of the SNR can be estimated.

It follows from Eqs. (2.41) and (2.42) that in the large stiffness limit ($l \to x_s \mathrm{or} l \ll l_0$), the maximal values of the SNRs and their

corresponding noise intensities behave as

$$\begin{aligned} S^{(1)}_{max} &\propto k^{-4} \propto \left(\frac{l}{x_s} - 1\right)^{-2} \quad , \\ D^{(1)}_{max} &\propto k^{4} \propto \left(\frac{l}{x_s} - 1\right)^{2} \quad , \\ S^{(2)}_{max} &\propto \left(\frac{l_0}{l}\right)^{2} \text{ and} \\ D^{(2)}_{max} &\propto \left(\frac{l}{l_0}\right)^{2} \quad . \end{aligned}$$

On the other hand for flexible domains $l/x_0 \to \infty$ or $l/l_0 \to \infty$ the $S^{(1,2)}_{max}$ and $D^{(1,2)}_{max}$ approach constants, in particular

$$\begin{aligned} S^{(1)}_{max} &= 8\sqrt{2}\frac{A^2 b}{e^2 \rho \lambda a^2} \quad , \\ D^{(1)}_{max} &= \frac{\rho \lambda a^2}{4b} \quad , \\ S^{(2)}_{max} &= 4\frac{A^2}{e^2 \rho \lambda a b^2} \text{ and} \\ D^{(2)}_{max} &= \frac{\rho \lambda a b^2}{2} \end{aligned}$$